3.5 Rectangular permeable breakwaters

3.5.1 General

When computational domain contains a permeable breakwater, we have to set the inertia and drag coefficient in the simulation method in order to model the fluid resistance. Very little is known about these two parameters for the permeable breakwater. We experimentally determine these values by applying the simulation model. In this section, numerical simulation is carried out and compared with the experimental results to examine the interaction between waves and permeable breakwaters. The mechanism of the wave reflection and transmission is investigated numerically related to two components of the wave force.

3.5.2 Experiments

Experiments were performed by using a two-dimensional wave flume (76.5m long, 0.9m wide and 1.2m deep). The surface displacements were measured to obtain the incident wave height, the wave reflection and transmission coefficients. The reflection coefficient was estimated by using the method for resolving of the incident and reflected waves proposed by Goda and Suzuki(1976). The displacements of the transmission wave were measured at five locations in order to examine fluctuation of the transmitted waves through the permeable breakwater. The averaged values of the transmitted wave heights are used in the following analysis. The reflection and transmission coefficients are defined by Eqs.(3.59) and (3.60), respectively:

$$K_R = \frac{H_R}{H_I}, \tag{3.59}$$

$$K_T = \frac{H_T}{H_I}, \tag{3.60}$$

where H_I, H_R and H_T are the incident, reflected and transmitted wave heights, respectively.

The energy dissipation rate ΔE is defined by Eq. (3.61):

$$\Delta E = (1 - K_R^2 - K_T^2). \tag{3.61}$$

Surface displacements between rectangular wire-screen cribs of which the permeable breakwater consisted were also measured at two locations to investigate the local wave

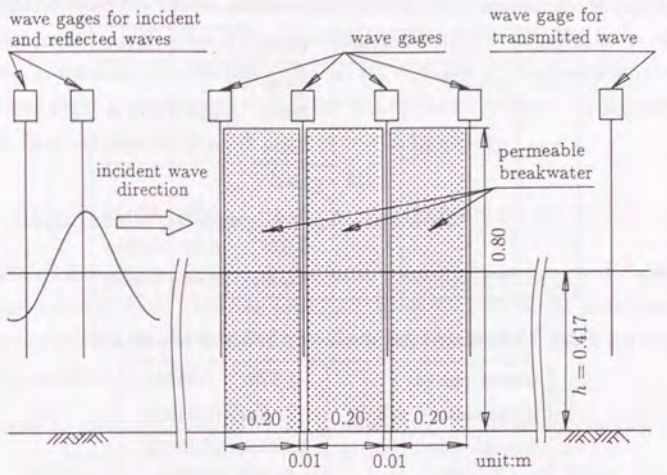

Fig.3.11 Experimental setup of rectangular permeable breakwater

transformation such as the wave length and the wave damping in the permeable breakwater. The time lag of the wave propagation between two wave gages was estimated by the cross spectrum analysis and was used to evaluate the wave length and the wave celerity.

A rectangular permeable breakwater used in the experiment was constructed in an uniform water depth as shown in Fig. 3.11. It consisted of three rectangular wire-screen cribs. They were placed with the spacing of 0.01m to install wave gages among them. The surface displacements in the permeable breakwater were also measured at two locations.

The experimental condition is shown in Table 3.3. The monochromatic waves with the period ranging from 1.0s to 2.5s and various wave heights were used under nonbreaking wave condition. The height of the model breakwater was sufficient to prevent overtopping by the highest waves. Two sizes of Tetrapod and three sizes of gravel were contained in turns in the wire-screen cribs. The resultant values of the porosity of Tetrapod were quite close to each other (the porosity ε=0.57 of W=0.45kg and ε=0.55 of W=0.054kg). The size of the pore of smaller Tetrapod is nearly a half of that of larger Tetrapod. The values of the porosity of gravel are ε=0.50 for W=0.54kg, ε=0.52 for W=0.074kg and ε=0.44 for W=0.0064kg. The value of the porosity of the smallest gravel was quite different from the rest of two.

Table 3.3 Experimental conditions (Wave transformation due to rectangular breakwater)

T(s)	H(m)	h(m)	W(kg)	ε	R(m)
1.0	0.015–0.14		Tetrapod		
			0.45	0.57	0.0123
1.5	0.017–0.18		0.054	0.55	0.0056
		0.417	gravel		
2.0	0.018–0.18		0.54	0.50	0.0121
			0.074	0.52	0.0058
2.5	0.018–0.19		0.0064	0.44	0.0022

Table 3.4 Experimental conditions(Sollitt and Cross,1972)

Gravel size (d)	1.37in	(0.0348m)
Breakwater width (w)	21.6in	(0.549m)
breadth (b)	29.75in	(0.756m)
weight (W)	1126.5lb	(510kg)
In situ porosity(ε)	0.437	
Water depth (h)	21.6in	(0.549m)

The experimental condition by Sollitt and Cross(1976) is also shown in Table 3.4. The comparison between the present method and the linear wave theory by Sollitt and Cross(1976) is made under their experimental conditions.

3.5.3 Wave reflection and transmission

An effect of the wave force on the wave reflection and transmission is numerically investigated to comprehend the mechanism of wave transformation due to the permeable breakwater. Fig. 3.12 shows the dependence of the reflection and transmission coefficients on the inertia coefficient while the drag coefficient is constant(C_D =10). As the inertia coefficient C_M increases, the reflection coefficient K_R slightly increases, on the other hand, the transmission coefficient K_T decreases. The energy dissipation ΔE obtained from the calculated results ranges from ΔE =0.63 at C_M =0 to ΔE =0.61 at C_M =2.0. It keeps almost constant as long as the drag coefficient is constant. It is confirmed that inertial resistance does not contribute to the wave energy dissipation.

Fig. 3.13 shows the dependence of the reflection and transmission coefficients on the

drag coefficient when the inertia coefficient is constant(C_M =0 and 1.0). When the drag coefficient is equal to null, $K_R^2 + K_T^2$ =1 is satisfied for both C_M =0 and 1.0. As the drag coefficient C_D increases, the reflection coefficient K_R decreases at the small drag coefficient and increases slightly. On the other hand, the transmission coefficient K_T decreases. As expected, the energy dissipation ΔE depends on the drag force.

3.5.4 Simulation of wave transformation

The first numerical simulation of the wave transformation due to the permeable breakwater was carried out under the experimental condition by Sollitt and Cross(1972) to compare with their results obtained with the linear wave theory. Table 3.5 shows the calculation condition.

Table 3.5 Calculation condition for breakwater by Sollitt and Cross(1972)

H(m)	T(s)	h(m)	L(m)	$\Delta x/L$	$\Delta z/h$	$\Delta t/T$	cal. region
0.048	1.7	0.549	3.45	1/50.3	1/20	1/200	$L \times 6.2$

Fig. 3.14(a) shows the simulated result of the free surface displacement in and near the permeable breakwater. Fig. 3.14(b) shows the maximum, minimum and mean water levels. Fluctuation of the surface displacement is seen just near the region on the windward and leeward sides of the breakwater. It is considered that this fluctuation is due to the discontinuous change of the porosity. Propagation of the transmitted wave is reasonably simulated. It is seen in Fig. 3.14(b) the mean water level is below the still water level in the leeward side. On the windward side, because the partial standing wave system occurs, the mean water level fluctuates. It is slightly higher than the still water level. It seems that the mass transport was prevented by the permeable breakwater.

Fig. 3.15 shows the comparison between the calculated and experimental results of the reflection and transmission coefficients. The unknown parameters,C_D and C_M were chosen so that the reflection and transmission coefficients obtained by the computation agreed with those by the experiments, respectively. In this figure, the calculated results estimated on the basis of the linear wave theory by Sollitt and Cross(1972) are also drawn with a broken line for the transmission coefficient K_T and a dash-dotted line for the reflection coefficient K_R. It is confirmed that the present simulation method can better reproduce the experimental results than the analytical solution based on the linear theory.

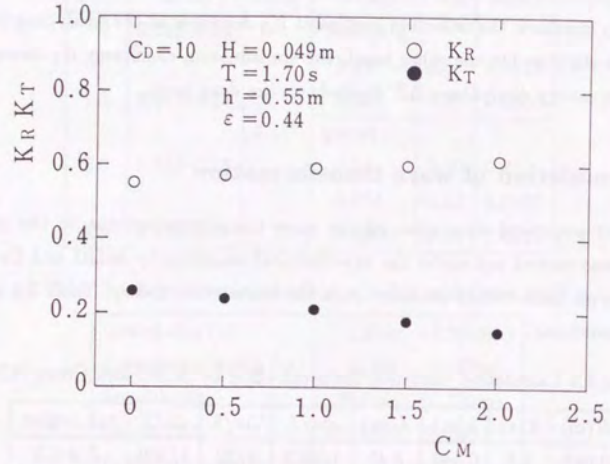

Fig.3.12 Reflection and transmission coefficients depending on inertia coefficient

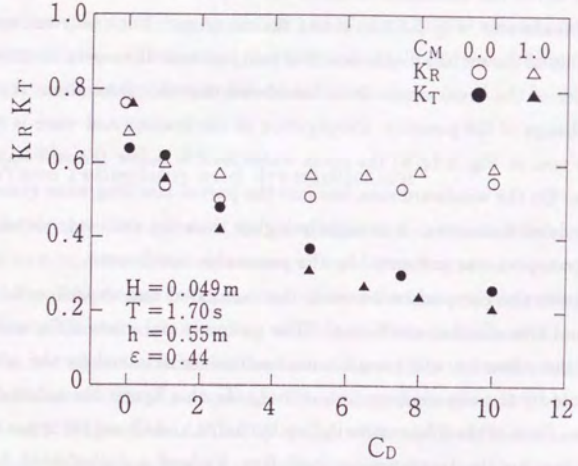

Fig.3.13 Reflection and transmission coefficients depending on drag coefficient

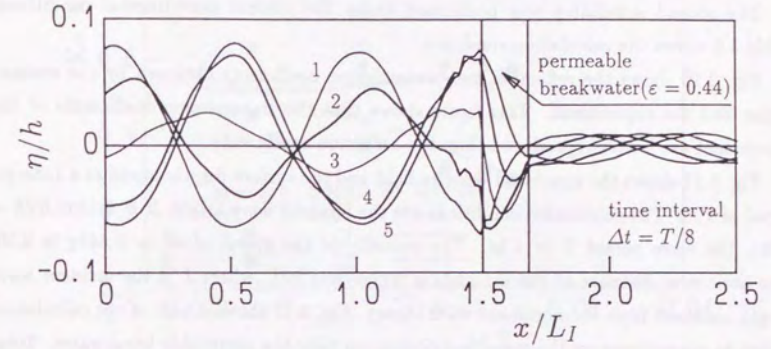

(a) Sequential surface displacement

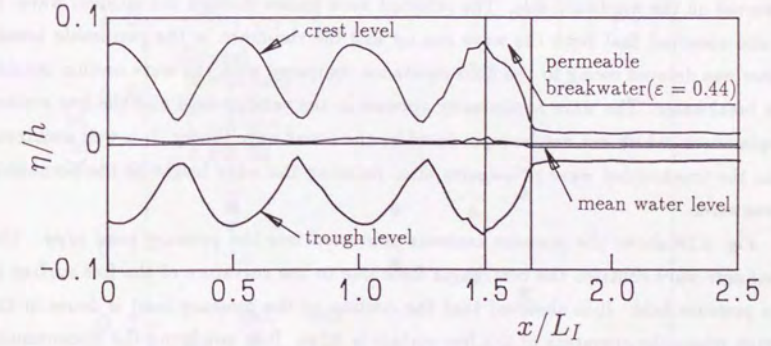

(b) Crest, trough and mean water levels

Fig.3.14 Simulated results of wave transformation in and near permeable breakwater

Table 3.6 Calculation condition for rectangular permeable breakwater

H(m)	T(s)	h(m)	L(m)	$\Delta x/L$	$\Delta z/h$	$\Delta t/T$	cal. region
0.107	1.5	0.417	2.68	1/53.6	1/15	1/200	$L \times 10$

The second simulation was performed under the present experimental conditions. Table 3.6 shows the calculation condition.

Fig. 3.16 shows the reflection and transmission coefficients obtained by the computation and the experiment. This figure shows that the transmission coefficients of the experiment are better reproduced than the reflection coefficients.

Fig. 3.17 shows the simulated velocity field and the surface displacement at a time interval of $T/8$. The calculation conditions are the incident wave height $H = 0.15\text{m}(H/h = 0.36)$, the wave period $T = 1.5\text{s}$. The porosity of the gravel of $W = 0.54\text{kg}$ is 0.50. The horizontal distance of the calculation region was $10L$, where L is the incident wave length obtained from the nonlinear wave theory. Fig. 3.17 shows a part of the calculation region to concentrate on the wave transformation near the permeable breakwater. Total time step was 3200 steps for $16T(\Delta T = T/200)$ to reach the steady state of wave motion near the breakwater. From these sequential figures, the partial standing wave motion is observed on the windward side. The reflected wave passes through the incident wave. It is also observed that both the wave run-up and the run-down in the permeable breakwater was delayed owing to the fluid resistance compared with the wave motion outside the breakwater. The wave nonlinearity appears in the velocity field and the free surface displacement which can not be reproduced by the linear wave theory. It is well simulated that the transmitted wave propagates after reducing the wave height in the permeable breakwater.

Fig. 3.18 shows the pressure contours converted into the pressure head $p/\rho g$. The nonlinear wave contains the centrifugal force due to the curvature of the free surface in the pressure field. It is observed that the contour of the pressure head is dense in the region where the curvature of the free surface is large. It is not found the discontinuity of the pressure near the free surface at the boundaries between inside the permeable breakwater and outside it.

Fig. 3.19 shows the successive profiles of the net wave pressure directed onshore acting on the permeable breakwater assuming that it is a rigid body. The profiles are similar those of the perfect standing wave shown in Fig. 3.10. The difference is the levels where the maximum wave pressure occurs. The maximum wave pressure of the perfect standing

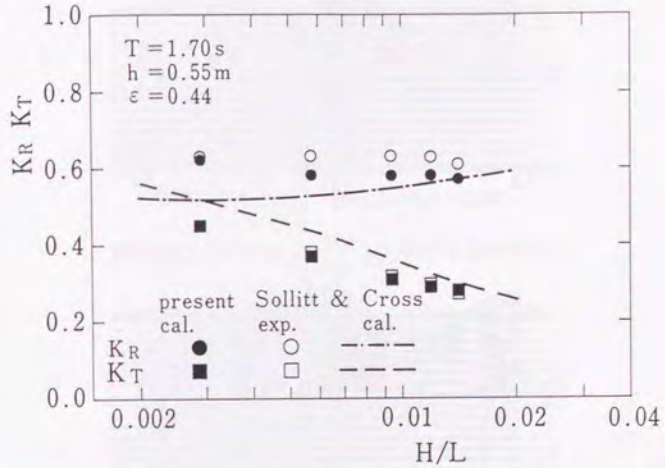

Fig.3.15 Comparison of calculated K_R and K_T with experimental results of Sollitt and Cross(1976)

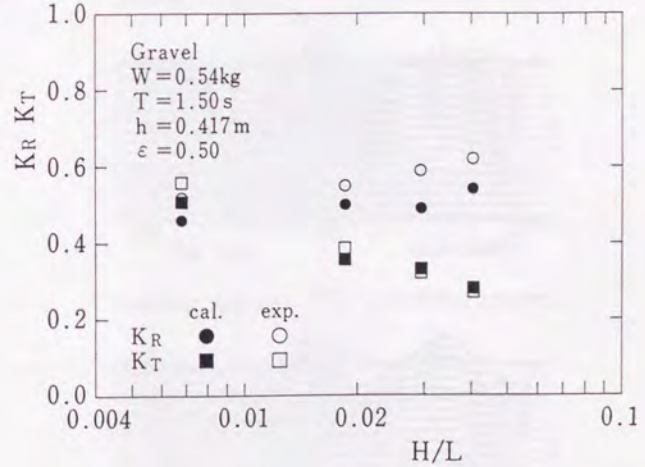

Fig.3.16 Comparison of calculated K_R and K_T with present experimental results

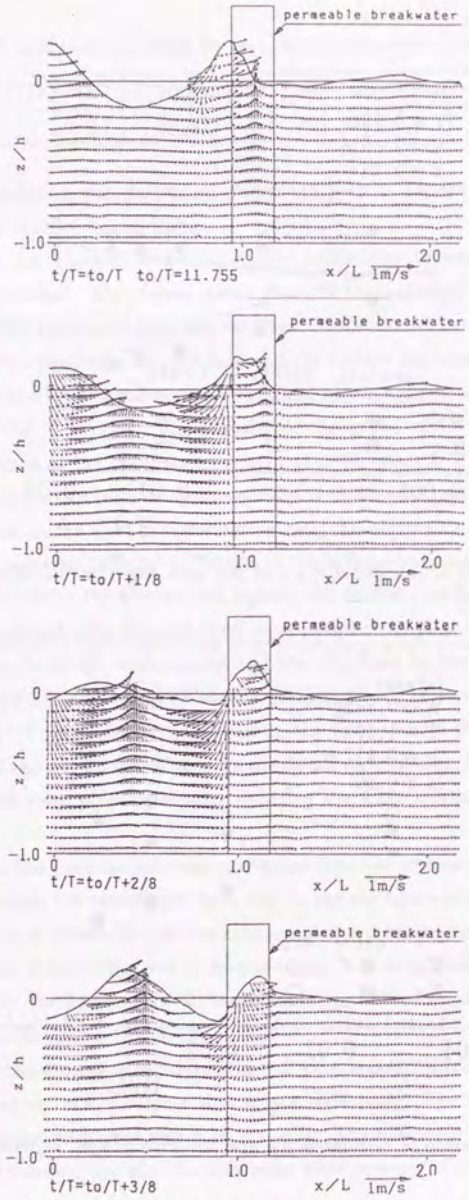

Fig.3.17 Simulated results of velocity vector and surface displacement-1-

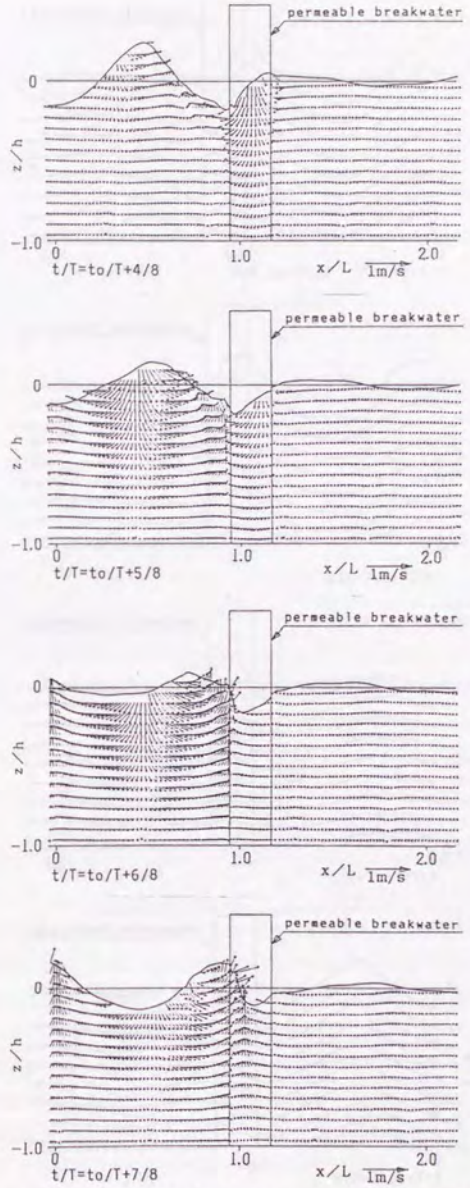

Fig.3.17 Simulated results of velocity vector and surface displacement-2-

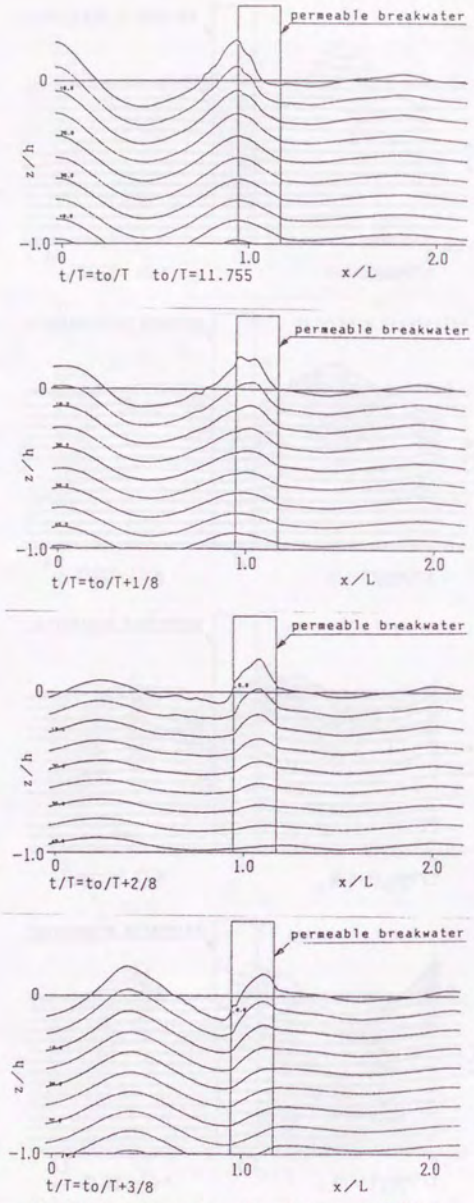

Fig.3.18 Simulated results of pressure field–1–

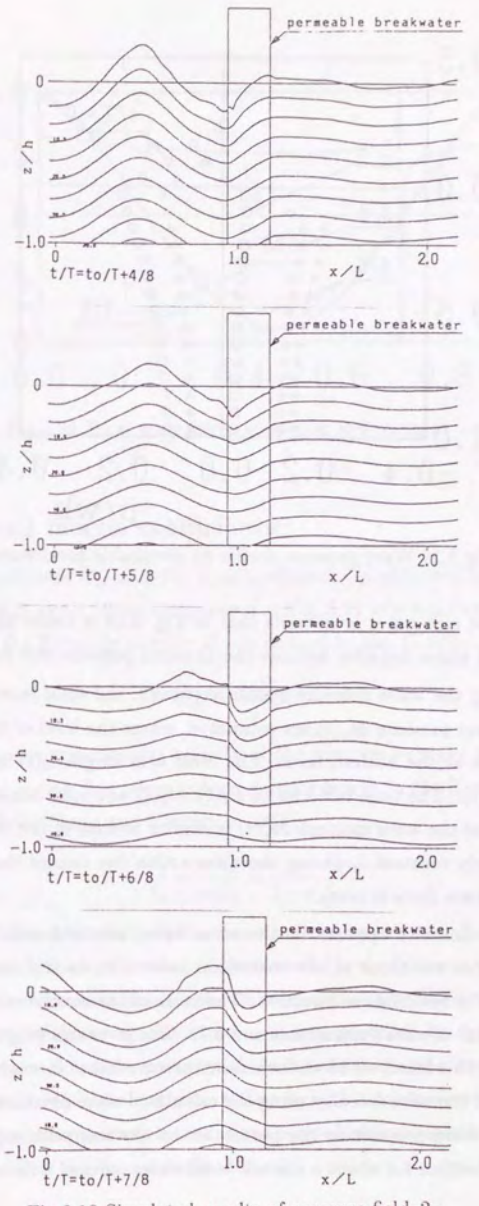

Fig.3.18 Simulated results of pressure field–2–

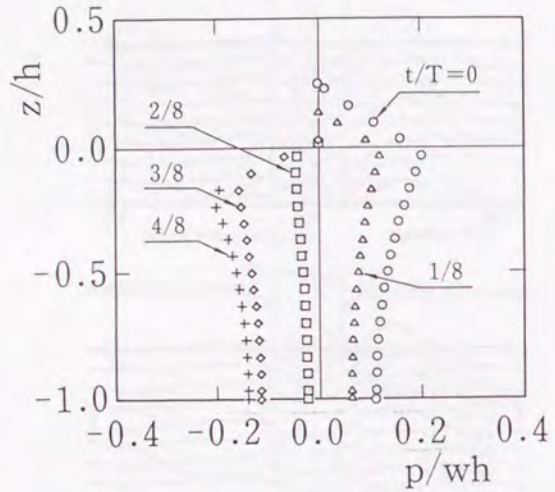

Fig.3.19 Wave pressure profile on permeable breakwater

wave occurs at the still water level while that in Fig. 3.19 is below the still water level when positive and above negative because the dynamic pressure was reduced.

By integrating the wave pressure profile vertically, the total wave force $F_x(t)$ and the moment of wave pressure $M_y(t)$ are estimated, where the level of the moment center of $M_y(t)$ is chosen at the bottom level. The lever arm length $l_z(t)$ is also obtained as $l_z(t) = M_y(t)/F_x(t)$. The time histories of $F_x(t), M_y(t)$ and $l_z(t)$ are shown in Fig.3.20. The time history of the wave moment $M_y(t)$ is similar to that of the total wave force. It results in the nearly constant l_z during the wave action (we cannot define the lever arm length when the wave force is zero).

The wave nonlinearity appears in the wave force, moment and lever arm length. The following ratios are those of the maximum value *i.e.*, in the onshore-direction to the minimum one in the offshore-direction. The ratio of the maximum wave force to the minimum is 0.9, that of wave pressure moment 0.75. The lever arm length at the maximum wave force is l_z=0.6h while l_z=0.5h at the minimum wave force. It was demonstrated that the nonlinearity of the wave force by using the calculated wave pressure. The comparison of the calculated wave pressure in the permeable breakwater with experimental results will be shown in Section 4.4 about a caisson breakwater covered with armor units.

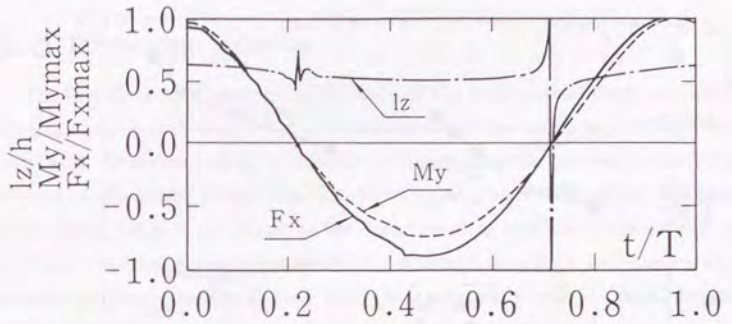

Fig.3.20 Total wave force, lever arm and moment

3.5.5 Drag and inertia coefficients

The inertia coefficient C_M and the drag coefficient C_D obtained in the calculation and shown in Figs.3.15 and 3.16 are summarized in Fig. 3.21 as a function of the Reynolds number R_{eR}. Here the Reynolds number R_{eR} is defined by Eq. (3.62):

$$R_{eR} = \frac{u_c R}{\nu}, \tag{3.62}$$

where u_c is the maximum horizontal velocity of the progressive wave at the still water level. The hydraulic radius R is taken as the reference length in the Reynolds number as expressed by Eq. (3.63)(Shuto and Hashimoto,1970):

$$R = \frac{V_f}{S_t} = \frac{\varepsilon V_b}{m S_S} = \frac{\varepsilon}{1-\varepsilon}\frac{V_S}{S_S}, \tag{3.63}$$

where V_f is the volume of the fluid, V_b the volume of the breakwater, S_t the total surface area of the material, S_S the surface area of the material, ε the porosity, m the number of the material in the breakwater. Because the number of the material in the breakwater is given by $m = (1-\varepsilon)V/V_S$ the hydraulic radius R is represented by the right hand side of Eq. (3.63) as a function of the porosity of the breakwater and the surface area, the volume of the material. With the hydraulic radius R, both a relative quantity(the volume porosity) and an absolute quantity(the size of the pore which is proportional to the armor unit size) are included in the Reynolds number.

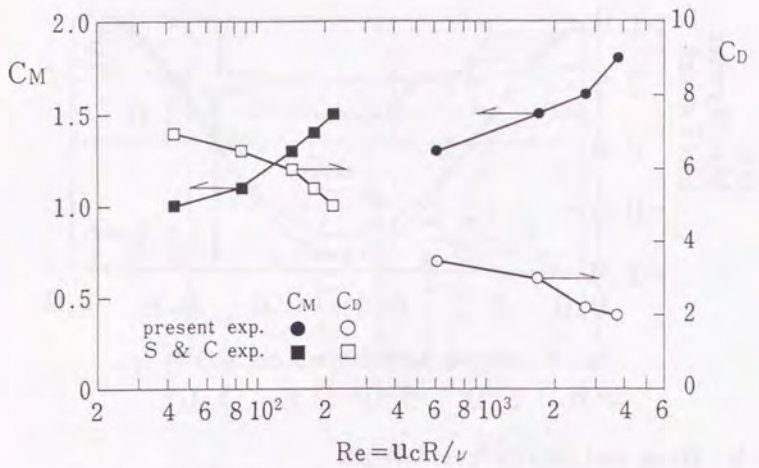

Fig.3.21 Drag and inertia coefficients depending on Reynolds number

It is found in Fig. 3.21 that as the Reynolds number R_{eR} increases, the inertia coefficient C_M increases while the drag coefficient C_D decreases. The value of the inertia coefficient ranges from 1 to nearly 2. The relationships between these coefficients and the Reynolds number agree with the result obtained by Tabuchi and Takigawa(1978) and that obtained in Chapter 2. On the other hand, a linearized friction factor increases as the Reynolds number increases. The trend of the relationship between the Reynolds number and the nonlinear drag coefficient or the linearized friction factor which is equivalent to the linearized drag coefficient depends on the definition of the drag force.

Primary factor of the wave reflection is the reduction of the area through which the fluid flows. Secondary factor is the wave condition such as the wave steepness. The reflection coefficient changes slightly as the wave steepness increases. The wave transmission is described by the rest of the energy after subtracting the reflected wave and the amount of the energy dissipation in the breakwater from the total wave energy. The amount of the wave energy dissipation is related to the drag force. The above mechanisms of the occurrence of the wave reflection and transmission can be taken into the present numerical simulation method through the porosity as a geometrical condition and the inertia and drag coefficients as a function of the Reynolds number.

3.6 Linear wave theory in permeable breakwater

3.6.1 Dispersion relation

The first theoretical analysis on the basis of the linear wave theory to estimate the wave transmission and reflection of a permeable breakwater was presented by Sollitt and Cross(1972). To obtain a solution, a number of assumptions are involved in the derivation. For instance, convective terms are neglected and the drag force is linearized. The linearized friction factor which is equivalent to the linearized drag coefficient is evaluated so that the rates of the energy dissipation due to the nonlinear drag force over one wave cycle is equivalent to that of the linear drag force. It is commonly called Lorentz' condition of equivalent work.

The dispersion relation on the wave in the permeable breakwater is given by the following equation:

$$\sigma^2[\varepsilon + C_M(1-\varepsilon) - if_p] = g\mathrm{k}\tanh \mathrm{k}h, \tag{3.64}$$

where $\sigma = 2\pi/T$ is the angular wave frequency, f_p the linearized friction factor, k the complex wave number. The real part of the complex wave number denoted by k_r is the wave number which gives the wave length L of the definition $k_r = 2\pi/L$. The imaginary part of that denoted by k_i gives the the wave damping coefficient. It is assumed that the wave height attenuates exponentially in the permeable breakwater:

$$H(x) = H(0)\exp(-k_i x). \tag{3.65}$$

In order to determine the complex wave number, it is necessary to know in advance the values of the linearized friction factor and the inertia coefficient as functions of a wave condition. To the contrary, in order to determine the values of C_M and f_p by experiments, it is required that a set of C_M and f_p satisfy the dispersion relation with the wave number and the wave damping coefficient obtained by the experiments. So far, solutions of the dispersion relation given by Eq. (3.64) are not compared with experimental results. In this section, solutions of the complex wave number of the dispersion relation are examined with those of the experimental results.

The wave number in the permeable breakwater is estimated from the experimentally determined wave length L by using a pair of wave gages in the permeable breakwater. The wave damping coefficient k_i is evaluated on the assumption that the wave attenuates only in the permeable breakwater. We have the following equation to estimate the wave

damping coefficient:

$$H_T = H_I \exp(-k_i B), \tag{3.66}$$

where H_I is the incident wave height, the transmitted wave height H_T obtained by the experiments and B is the breadth of the rectangular permeable breakwater.

Fig. 3.22 shows the characteristics of the solution of the dispersion relation equation. It is expressed as the relationship between L_r/L_a and the inertia coefficient C_M, where $L_a = 2\pi/k_a$ the wave length of the pure water wave obtained by the dispersion relation in the pure water:

$$\sigma^2 = g k_a \tanh k_a h. \tag{3.67}$$

The additional conditions in the dispersion relation are the wave period T =2.5s, the water depth h =0.417m and the porosity ε =0.57.

When $C_M = 1$ and $f_p = 0$ are introduced into the dispersion relation, Eq. (3.64) completely agrees with Eq. (3.67) for any value of the porosity. Therefore, the wave length in the permeable breakwater become equal to that in the pure water. With null fluid resistance and any value of the porosity($C_M = f_p = 0, \varepsilon \neq 0$), the left hand side of Eq. (3.64) is less than σ^2 because the porosity is normally less than unity. The wave length under such an idealized condition becomes longer than that in the pure water. As

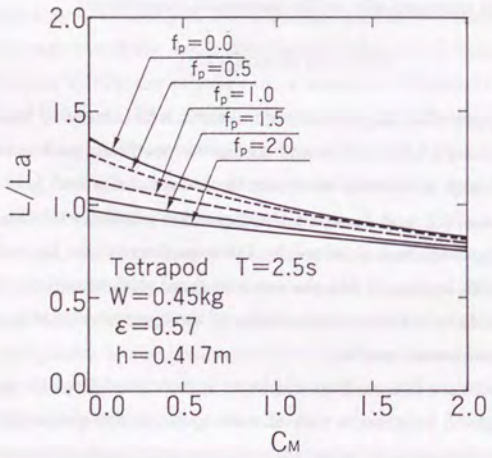

Fig.3.22 Solution of dispersion relation

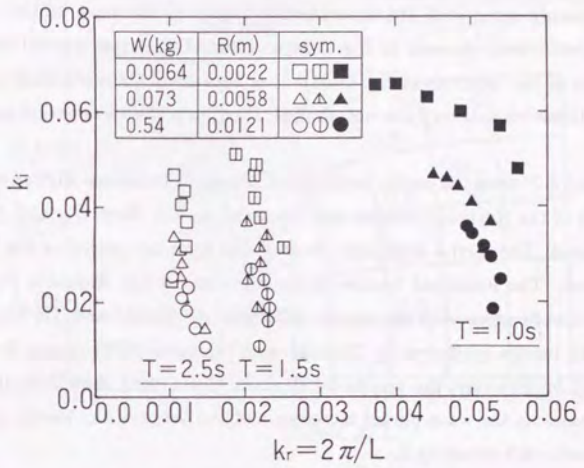

Fig.3.23 Complex wave number depending on hydraulic radius

the inertia coefficient increases, the wave length in the permeable breakwater decreases. When C_M is less than unity, the wave length in the permeable breakwater is smaller than that in the pure water. It is also found that the wave length decreases as the linearized friction factor f_p increases.

Fig. 3.23 shows the experimental results of the relationship between the wave number k_r and the wave damping coefficient k_i for three kinds of gravel. It is natural that the wave damping coefficient k_i increases as the hydraulic radius R decreases. Both the wave number and the wave damping coefficient are depending on the wave height. As the wave height increases, the wave number decreases while the wave damping coefficient increases.

3.6.2 Inertia and linearized friction factor

Fig. 3.24 shows the comparison of the wave number and the wave damping coefficient between the experimental results and the solutions of the dispersion relation given by Eq. (3.64). Izumiya and *et al.*(1990) determined the linearized friction factor, neglecting

the effect of the inertia coefficient *i.g.*, they assumed that the inertia coefficient was constant. In order to determine values of C_M and f_p, it is necessary to obtain them which simultaneously agree with the experimental results of the wave number and the wave damping coefficient. As seen in Fig. 3.24(b) some of the experimental results are not in the region of the solutions of Eq. (3.64). It is because of the wave nonlinearity. It shows that the linear wave theory can not applied when both the wave period and height increase.

Figs. 3.25 and 3.26 show the inertia coefficient C_M and the linearized friction coefficient f_p as a function of the Reynolds number and the wave period. Both C_M and f_p depend on the wave period. The inertia coefficient decreases as the wave period or the Reynolds number increases. The linearized friction factor increases as the Reynolds number increases. These trends agree with the results obtained by Tabuchi and Takikawa(1978). The value of the inertia coefficient by Tabuchi and Takikawa(1978) ranges from about -0.5 to nearly 2.5. However, the results by Deguchi *et al.*(1988) show that the inertia coefficient increases as the wave period increases and the value of the inertia coefficient ranges from about -0.5 to nearly 2.

In the linear wave theory, the frictional coefficient f_p is linearized so that the formulation is analytically treated. However, the drag force is essentially proportional to the velocity squared. The relationship between the linearized friction factor and the Reynolds number shows the different trend from that between the drag coefficient and the Reynolds number shown in Fig. 3.21. It is because the linearized friction factor contains a part of fraction which is proportional to the velocity squared in the drag force.

It is better that the fluid resistance is modeled so that the model reflects the real mechanism. Although the drag force is proportional to the velocity squared, it is linearized in the linear wave theory. It should be noted that the characteristic of the linearized friction factor is different from that of the nonlinear one. The nonlinear model of the fluid resistance is better than the linear one to comprehend the real mechanism which appears in the inertia and drag coefficients as functions of the Reynolds number.

Although the numerical simulation and the analytical treatment make a progress, data of the coefficients included in the model of the fluid resistance are not sufficient. In order to predict the wave transformation by using either the linear wave theory or the present numerical simulation method, further experiments are required to obtain the the inertia and drag coefficients as functions of wave conditions and the material of a permeable breakwater.

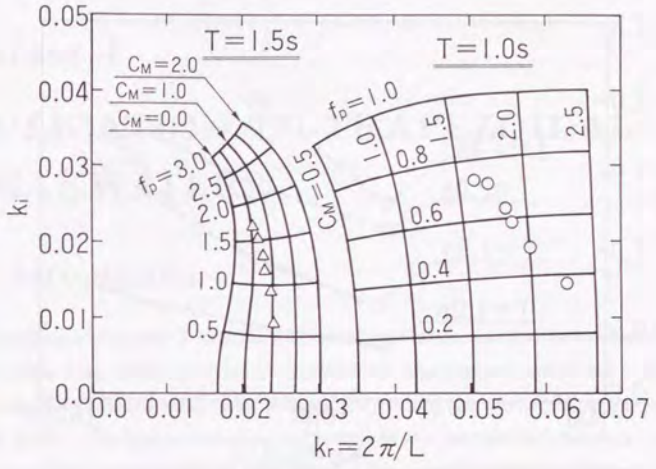

(a) T=1.0s and T=1.5s

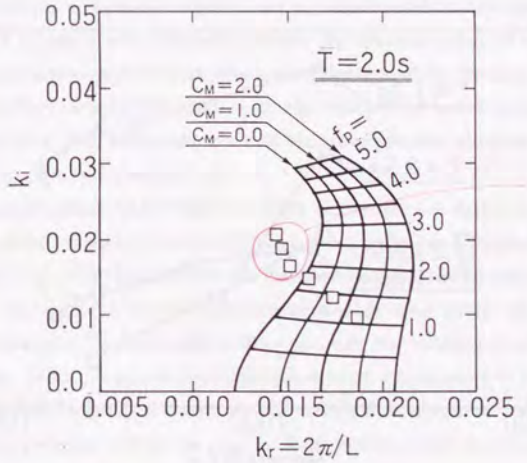

(b) T=2.0s

Fig.3.24 Comparison of experimental results of complex wave number with solutions of dispersion relation (Terapod $W = 0.45$kg,$\varepsilon = 0.50$,$h = 0.417$m)

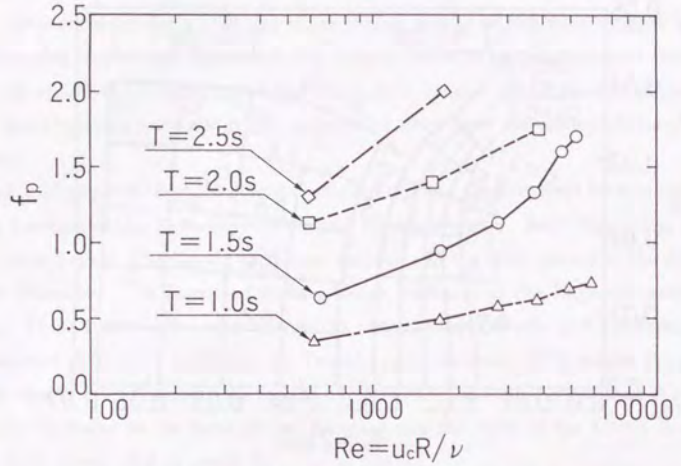

Fig.3.25 Inertia coefficient estimated by linear wave theory

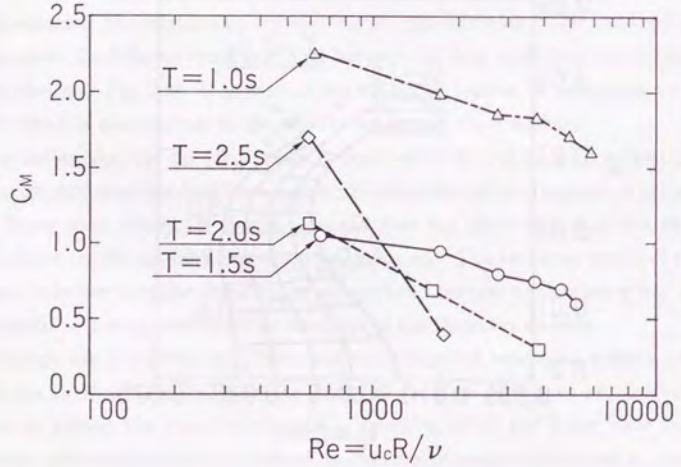

Fig.3.26 Linearized friction factor estimated by linear wave theory

Chapter 4

APPLICATION TO TRAPEZOIDAL BREAKWATERS

4.1 Introduction

Described in Chapter 3 was the numerical simulation method to compute the wave motion interacting with a permeable breakwater. The present model was verified with the simple and idealistic conditions such as the rectangular permeable breakwater on a uniform depth. The drag and inertia coefficients of the permeable breakwaters were also obtained as functions of the wave steepness for the certain limited conditions.

At a next stage, it is required to proceed to apply the present model for a realistic structure as used in a hydraulic experiment or constructed at the field. Some works were presented to apply the numerical models for the real types of breakwater: The pore pressure in rubble-mound breakwaters was investigated by Simm and Hedges(1988), Oumeraci and Partenscky(1990) relating to the stability of armor units of the rubble-mound breakwaters. It is also necessary that the wave pressure obtained in computation is checked with a hydraulic experiment.

The numerical model "HADDER" of Delft Geotechnics is rather simple one which describes the water movement in a rubble-mound breakwater (Brarends and Hölscher, 1988; Hölscher *et al.*,1988) It calculates the transient shape of the phreatic surface and the wave velocity field and the pressure inside a permeable breakwater. Sastry *et al.*(1991) applied it to evaluate the transmitted wave through the rubble-mound breakwater at Visakhapatnam, India. To reduce the transmitted wave, it is required to make the porosity of armor layer small. A group of Hannover University (Wibbeler, *et al.*,1991; Wibbeler and Oumeraci,1992) presents the similar model. Both models needs the boundary condition of the wave run-up on the seaward slope of the breakwater.

Computations using irregular waves on the basis of the long wave theory were performed by Kobayashi and Greenwald(1986) to investigate the wave run-up on a rough

impermeable mild slope. Scarlatos and Singh(1987) presented the analytical model to estimate the wave transmission though it is still based on the long-wave theory.

Wurjanto and Kobayashi(1992) also developed the one-dimensional, time-dependent numerical model based on the long wave theory to simulate the flow fields above and inside a permeable under layer for irregular waves. They showed the permeable effects resulting in the time-averaged landward mass flux above permeable under layer and the time-averaged seaward one inside it. Although the measurement in a hydraulic experiment can hardly detect the details, the mechanism of the interaction waves and permeable structures and resulting fluid motions are observed by the numerical simulation.

In this chapter, the present numerical simulation model is applied to more realistic structures (Sakakiyama *et al.*, 1991; Sakaiyama and Kajima, 1992). Two types of trapezoidal breakwaters are selected for the application of the present numerical simulation method: 1) a conventional rubble-mound breakwater and 2) a caisson breakwater covered with a filter layer of stone and armor layers of concrete blocks.

In the case of the rubble-mound breakwater, the wave run-up motion which are hardly obtained in hydraulic experiments as well as the wave reflection and transmission are calculated by the present numerical simulation model. Relating to the wave force acting on an armor unit described in section 2.3 of Chapter 2, a numerical experiment is performed to estimate the wave force action on armor units with the computed wave run-up motion.

In the case of the caisson breakwater, the low wave transmission through the rubble-mound and the wave reflection from the armor layer and the caisson are investigated both numerically and experimentally. The wave pressure acting on the caisson in the permeable structure is also estimated and is compared with the experimental result.

The scale effects on the wave reflection, transmission and the wave pressure are investigated by the experiments with large- and small-scale models of the caisson breakwater. The effects of the drag and inertia coefficients on the wave pressure are discussed with relation to the scale effects on the wave reflection and transmission.

4.2 Approximation of sloping boundary in PBM

Slope boundaries such as surfaces of a trapezoidal breakwater and configuration of sea bottom are in general contained when the wave transformation is computed for various occasions. These slopes are normally modeled with steps consisting of the rectangular

finite difference meshes in the FDM. The boundary conditions of the steps are the same ones as on an impermeable wall and at a bottom.

The approximation with respect to the slope can be improved in the PBM by considering the net volume and the net in- or out-flow areas of the meshes which contain the slope. Fig. 4.1 shows a sketch of the mesh containing the slope. The net volume for the mass and momentum in the control volume is expressed as the product of the porosity γ_{vij} and $\Delta x \times \Delta z \times$ unit length. Similarly, the net area of the in- or out-flow of the mass and momentum in the direction of x is expressed as the product of the surface permeability γ_x and $\Delta z \times$ unit length. The same is obtained in the direction of z. Note that the definition positions of the velocities are at the center of the sides of the mesh as shown in Fig. 3.3.

Fujima *et al.*(1984) applied above approximation only to the law of the mass conservation but not to that of the momentum because the description for the momentum equations are more complicated than that for the continuity equation. The governing equations of the present numerical method, the PBM are described for wide uses. It has an advantage to be applied for various purposes. The laws of the conservation of the mass and momentum in the rectangular mesh containing the slope boundary are satisfied by substituting values of the geometrical portion into the porosity and the surface permeability. The effect of the slope for both the mass and momentum can be taken into the finite difference scheme in this way.

The porosity with and the surface permeability of the side without slope are unity.

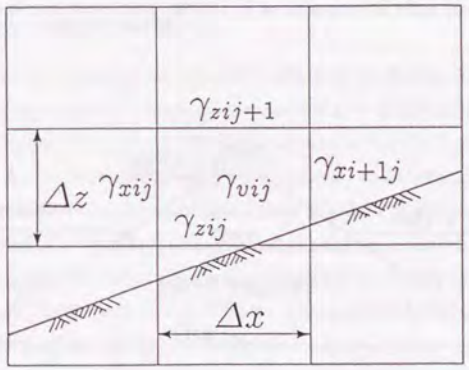

Fig.4.1 Approximation of finite difference mesh for sloping boundary

On the other hand, the porosity and the surface permeability in the meshes containing the slope in its side are less than unity. In the case of Fig. 4.1, γ_{xi+1j} and γ_{zij} are set to unity but γ_v, γ_{xij} and γ_{zij+1} less than unity.

For the meshes containing a structure with an impermeable slope, the drag and inertia coefficients are set to null. For the meshes containing the structure with a permeable slope, γ_v is replaced with the product of the porosity and the net volume rate and the surface permeability γ_x for the horizontal component is replaced with the products of the surface permeability and the ratio of the width of in- or out-flow to the side length of the mesh. The same is true for γ_z for the vertical component.

4.3 Rubble-mound breakwater

4.3.1 Experiments

Experiments were performed in the same way for the rectangular permeable breakwater described in section 3.5 in Chapter 3. The model breakwater was a conventional trapezoidal rubble-mound breakwater as shown in Fig. 4.2. The rubble-mound breakwater consists of Tetrapods of which weight is $W = 0.13$kg for the simplicity to analyze experimental results. The *In-Situ* porosity of the breakwater is $\varepsilon = 0.53$. The hydraulic radius is $R = 0.0069$m defined by Eq. (3.63). Slopes of the breakwater surface are 1 on 1.5 for both the seaward and landward side surfaces. Table 4.1 shows the experimental conditions. The model scale is supposed as $\lambda = 1/60$. The water depth at the breakwater

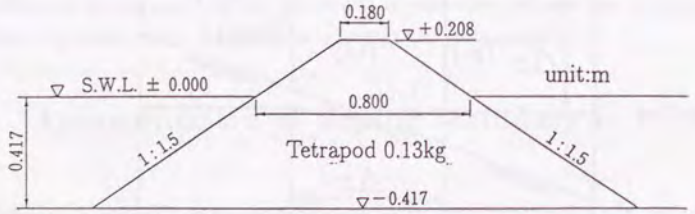

Fig.4.2 Rubble-mound breakwater($\lambda = 1/60$)

Table 4.1 Experimental conditions for rubble-mound breakwater(λ=1/60)

wave period	wave height	wave depth	Tetrapod			
T(s)	H(m)	h(m)	W(kg)	b(m)	ε	R(m)
1.00	0.011–0.097	0.417	0.13	0.059	0.53	0.0069
1.25	0.012–0.182					
1.50	0.015 -0.275					
2.00	0.018–0.294					
2.25	0.015–0.312					
2.50	0.017–0.298					

is $h = 0.417$m in the model scale and the uniform depth $h = 0.737$m. The wave periods were $T = 1.0, 1.25, 1.5, 2.0, 2.25, 2.5$s. The wave height ranges from $H \simeq 0.01$m to 0.3m. The maximum ratio of the wave height to the water depth H/h was up to about 0.7. The nonlinearity of the waves generated was remarkable but breaking wave was not included in the present experiment conditions.

The reflection and transmission coefficients were obtained for various wave conditions in the same way mentioned in Section 3.5. The reflection coefficient is estimated with the method for resolving incident and reflected waves proposed by Goda and Suzuki(1976). The displacements of the transmitted wave were measured at five locations. The averaged values of the five transmitted wave heights are used in the following analysis.

4.3.2 Experimental results

In Fig. 4.3, the experimental results of the reflection coefficient K_R and the transmission coefficient K_T are shown for various wave periods as a function of the wave steepness H/L, where L is the wave length at the breakwater($h = 0.417$m) estimated by the linear wave theory. As the wave steepness H/L increases, the transmission coefficient K_T decreases remarkably and the reflection coefficient K_R does slightly under the condition that the wave period T is constant. This trend of the experimental results agrees with that for the rectangular permeable breakwater obtained by Sollitt and Cross(1972). The calculated results by Sollitt and Cross(1972) do not agree with the relationship between the reflection coefficient and the wave steepness.

In the results of the longer wave period(T is greater than 2.0s), both K_R and K_T increase at the high wave steepness ($H/L > 0.05$ or 0.06). The increase of the transmission

coefficient is caused by the wave overtopping.

Fig. 4.4 shows the relationship between the reflection coefficient K_R and the ratio of the breadth of the trapezoidal breakwater at the still water level to the wave length B/L and that between the transmission coefficient K_T and B/L. Because the breadth B is constant($B = 0.80$m) in the experiments, these figures show the dependence of the reflection and transmission coefficients on the wave period. As the ratio of the breadth to the wave length B/L increases (the wave period decreases), the reflection coefficient K_R once decreases and has a minimum value at $B/L \simeq 0.3$ then increases slightly. The transmission coefficient K_T decreases as B/L increases.

These trends of the relationships between the wave steepness and the reflection coefficient and between the wave steepness and the transmission coefficient agree with those obtained by Kondo *et al.*(1972). They concluded that the increase of the reflection coefficient at the long wave period is due to the resonance in the permeable breakwater.

The energy dissipation rate $\Delta E = (1 - K_R^2 - K_T^2)$ is shown in Fig. 4.5 as functions of the wave steepness. As the wave steepness increases, the energy dissipation rate increases. It is because that the amount of the energy dissipation is proportional to the product of the friction factor and the velocity squared. The energy dissipation rate ΔE at the certain wave steepness decreases as the wave period increases. However, the energy dissipation rate of the results at $T = 2.25$s and 2.5s far less than those at $T \leq 2.0$s.

Basically, the wave reflection depends on the porosity and slightly on the inertial resistance. The effect of the wave period on the reflection coefficient contains the resonance in the permeable structure. The wave transmission depends on the energy dissipation in the permeable structure. The amount of the energy dissipation is proportional to the product of the friction factor and the velocity squared.

4.3.3 Simulation of wave transformation

The computation was carried out under the wave condition as shown in Table 4.2. The wave period is $T = 1.5$s and the progressive wave height at the breakwater $H = 0.15$m($H/h = 0.36$). The horizontal distance of the calculation region was $8.63 \times L_I$, where L_I is the incident wave length at the uniform depth($h_I = 0.747$m) obtained with the nonlinear wave theory. The wave lengths are $L_I = 3.20$m at the uniform depth and $L = 2.68$m at the breakwater. The cell dimensions are $\Delta x = 0.045$m($\Delta x/L_I = 1/71.1$ and $\Delta x/L = 1/58.9$) horizontally and $\Delta z = 0.03$m($\Delta z/h = 1/13.89$) vertically. The

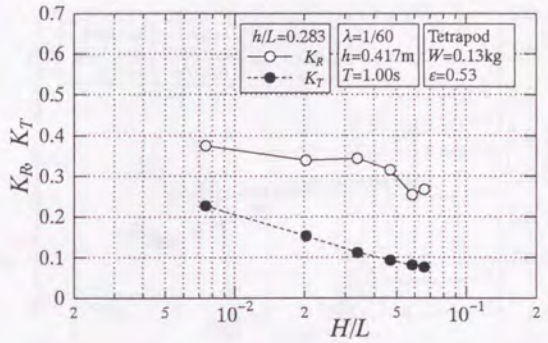

(a) $T = 1.0$s

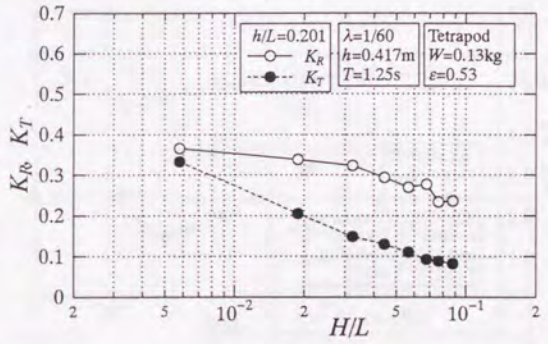

(b) $T = 1.25$s

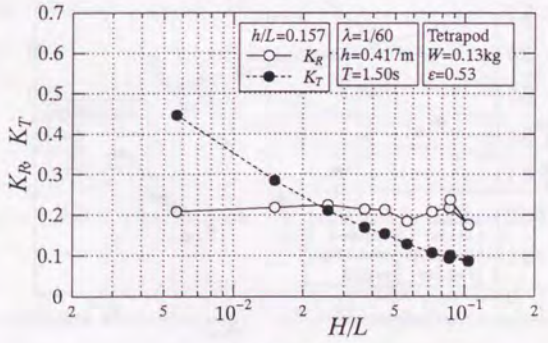

(c) $T = 1.5$s

Fig.4.3 Reflection and transmission coefficients of rubble-mound breakwater–1–

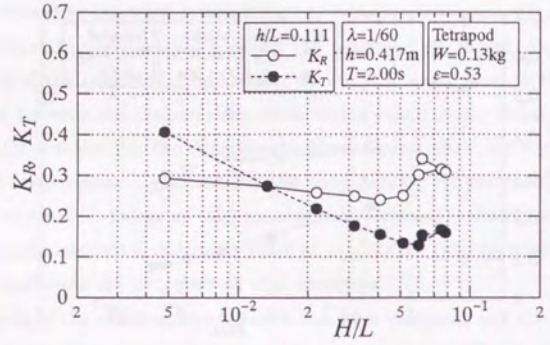

(d) $T = 2.0$s

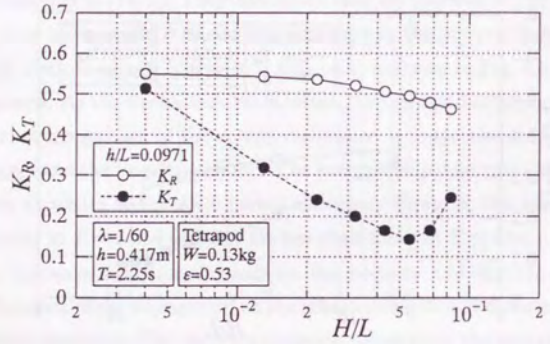

(e) $T = 2.25$s

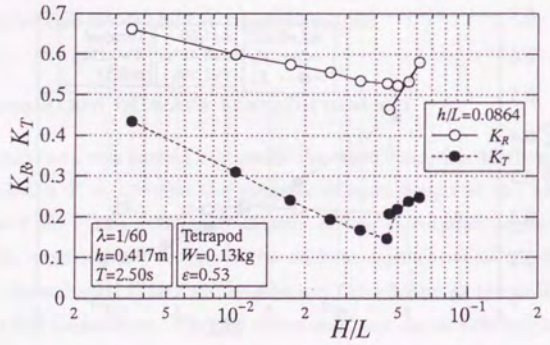

(f) $T = 2.5$s

Fig.4.3 Reflection and transmission coefficients of rubble-mound breakwater–2–

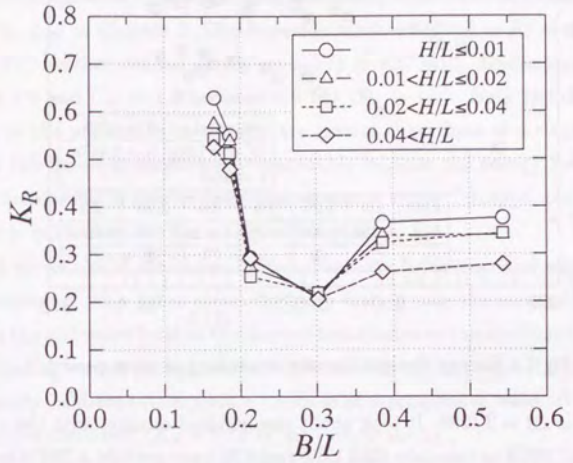

(a) Reflection coefficient

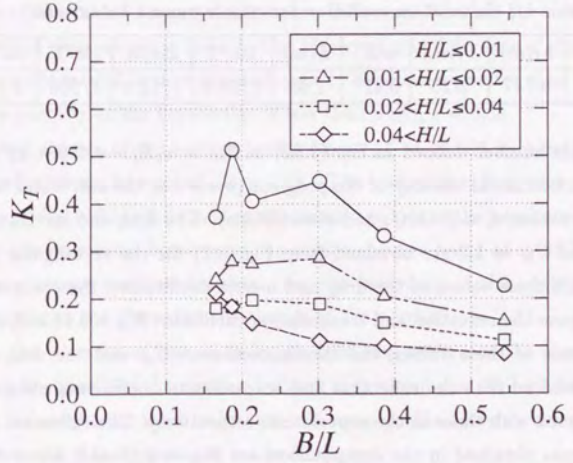

(b) Transmission coefficient

Fig.4.4 Reflection and transmission coefficients depending on relative breadth

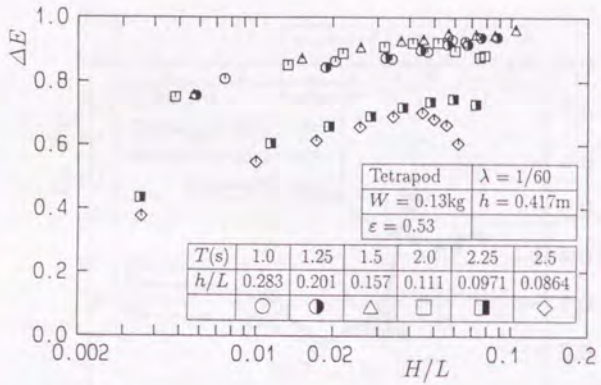

Fig.4.5 Energy dissipation rate depending in wave period

time increment is $\Delta t = T/200$. It took about one hundred minutes with the main frame computer HITAC 680H to calculate 4000 time steps(20 wave periods $\times$ 200 steps per wave period) to reach the steady state wave motion near the rubble-mound breakwater.

Table 4.2 Calculation condition for rubble-mound breakwater

H(m)	T(s)	h_I(m)	L_I(m)	h(m)	L(m)	$\Delta x/L$	$\Delta z/h$	$\Delta t/T$	cal. region
0.15	1.5	0.747	3.20	0.417	2.68	1/58.9	1/13.9	1/200	$L_I \times 8.63$

The Reynolds number defined as Eq. (3.62) is $R_{eR} = u_c R/\nu = 2.9 \times 10^3$, where u_c is the maximum horizontal velocity of the progressive wave at the still water level and R is the hydraulic radius($u_c = 0.43$m/s and R=0.0069m). The drag and inertia coefficients of $C_D = 2.0$ and $C_M = 1.7$ are obtained from Fig. 3.21 for the rectangular permeable breakwater. With these values of the drag and inertia coefficients, the computation was performed and gave the reflection and transmission coefficient $K_R = 0.15$ and $K_T = 0.11$. With the reference of these values, the inertia coefficient C_M and the drag coefficient C_D were estimated so that the reflection and transmission coefficients obtained in the computation agreed with those in the experiment, respectively. The reflection and transmission coefficients obtained in the computation are $K_R = 0.15$ and $K_T = 0.14$ which reproduced the experiment best. The corresponding experimental results are $K_R = 0.18$ and $K_T = 0.14$, respectively. The values of $C_D = 1.2$ and $C_M = 1.7$ are obtained by best fitting the computation to the experimental results.

Here we compare the drag and inertia coefficients of a single Tetrapod and the permeable breakwater obtained so far. The drag and inertia coefficients of a single Tetrapod are shown in Fig. 2.11 in Chapter 2. The Reynolds number defined as $Re = u_c b/\nu$ is R_e =2.5 $\times 10^4$ and KC number defined as $KC = u_c T/b$ is KC =12. Under this condition, we have $C_D = 1.0$ and $C_M = 1.0$(becomes 0.6 but $C_M \geq 1.0$). Both the drag and inertia coefficients of the permeable breakwater are greater than those of a single Tetrapod. It seems that this result is qualitatively reasonable because the energy dissipation in the permeable breakwater is greater than that around a single Tetrapod and the permeable breakwater is more massive than a single Tetrapod.

Fig. 4.6 shows one of the computed wave velocity fields near and within the rubble-mound breakwater. This figure shows the wave motion near the moment when the wave front passes the still water level on the slope of breakwater on the windward side. Although a partial standing wave is formed on the windward side of the breakwater, the wave profile and its velocity field are rather similar to those of a progressive wave. It is because of a small reflection coefficient ($K_R = 0.15$ in the computation).

Compared with the velocity field of the partial standing wave near $x/L_I = 6.5$, the velocity field of the wave run-up near $x/L_I = 7.25$ is deformed owing to the effect of the steep slope of the rubble-mound breakwater. Difference between the velocity inside the breakwater and that outside is remarkable. Moreover, the difference of discharge between inside the rubble-mound breakwater and outside it becomes greater than that of velocity because the porosity of the breakwater is less than unity, $\varepsilon = 0.53$.

Sequential change of the surface profile from $t/T = 18.665$ is shown in Fig. 4.7 for a half period with an interval of $\Delta t = T/8$. The partial standing wave with the small reflected wave($K_R = 0.15$) is formed on the windward side of the breakwater. As the wave approaches the permeable breakwater, its profile changes being affected by the reflected wave. Discontinuous surfaces are seen near the boundary of the onshore slope. They seems to be due to the discontinuous change of the porosity.

Within the distance of one wave-length from the surface of the breakwater on the leeward side, the profile of the number 5 shows that it contains the high frequency modes. As getting far away from the breakwater, the wave profile becomes smooth because the wave components of the evanescent mode disappear.

Fig. 4.8 shows the crest, trough and mean water levels. It shows the partial standing wave on the windward side of the breakwater and the wave attenuation in the permeable breakwater. The wave set-up is found near the still water level on the breakwater slope

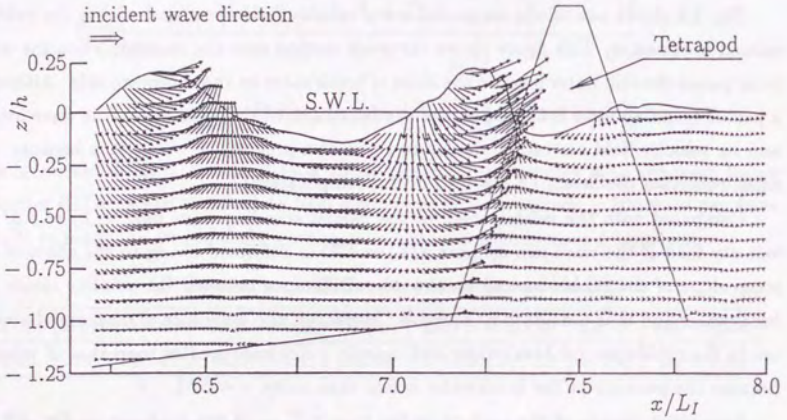

Fig.4.6 Simulated result of wave transformation due to rubble-mound breakwater

and the wave set-down in front of the position of the wave set-up. When we see the wave reflection microscopically, the wave is reflected all the position along the slope of the rubble-mound breakwater. From a macroscopic point of view, a location of the wave reflection is considered to be the still water level on the slope of the breakwater because

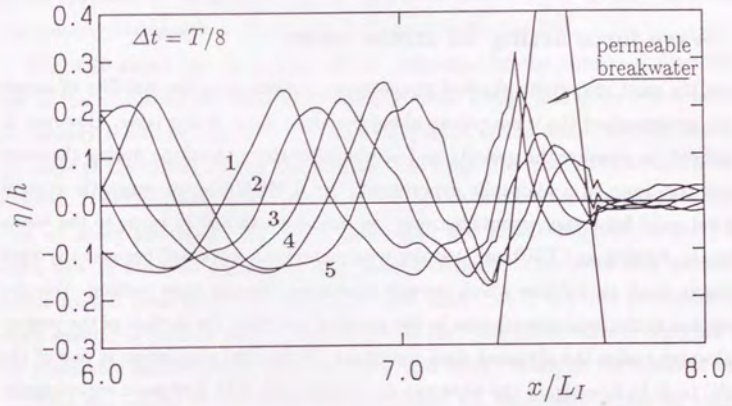

Fig.4.7 Sequential free surface displacements

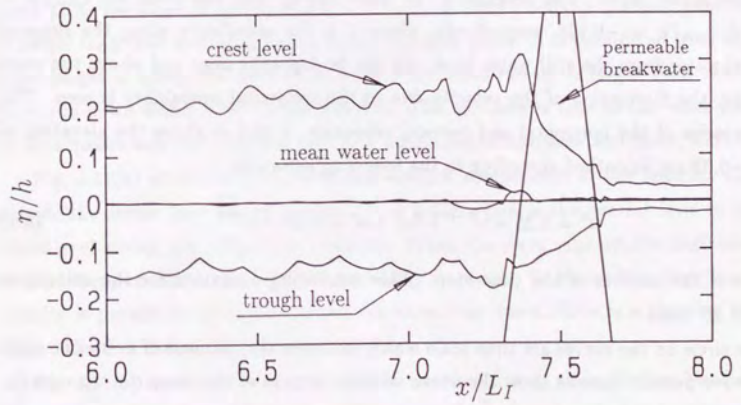

Fig.4.8 Crest, trough mean water levels in and near rubble-mound breakwater

the maximum wave height and the maximum wave set-up are found at that place from Fig. 4.8 like those of a standing wave.

It is considered from the above simulated results that the wave reflection from the permeable breakwater, the wave attenuation in it and the wave propagation through it are reasonably simulated.

4.3.4 Wave force acting on armor units

One of the most important physical phenomena to investigate the stability of armor units is the movement of the wave run-up along the slope of an armor layer. However, it is quite difficult to measure the velocity and acceleration along the slope during the wave run-up and run-down in a hydraulic experiment. An EMCM(electro magnetic current meter) is not valid for measurements because the sensor is exposed in turns to the waves and to the air. Neither an LDV(laser Doppler veocimeter) can work well because the wave front contains small air bubbles which prevent continuous signals from coming. Velocity fluctuation due to the local disturbance in the porosity and near the surface of the permeable breakwater makes the obtained data uncertain. Numerical simulation is one of the most useful tools to investigate the wave run-up cooperating with hydraulic experiments. A well-calibrated numerical simulation method helps us interpret the phenomenon.

Fig. 4.9 shows the hodographs of the wave run-up velocity at the several elevations along the armor layer. The heights of the wave run-up and run-down are $\zeta_{max}/h = 0.21$ and $\zeta_{min}/h = -0.128$, respectively, where ζ is the coordinate along the slope of the breakwater from the still water level. Of the hodographs near and above the wave run-down, the fluctuation of the velocity due to the numerical unstability is seen. The time histories of the horizontal and vertical velocities, u and w above the elevation of $\zeta/h > -0.33$ are smoothed according to the following equation:

$$u^n = 0.25 \times u^{n-1} + 0.5 \times u^n + 0.25 \times u^{n+1}, \tag{4.1}$$

where n is the number of the time step. This smoothing operation for the velocity is repeated 20 times.

The circle on the curves are time scale which indicates the moment of every one eight of the wave period. Arrows show the mean velocity vectors of the wave run-up velocity. The slope of armor layer of the breakwater is indicated with the dashed line. Above the elevation of the wave run-down, the hodographs are not closed. The direction of the flows

at $z/h = 0.187$ and $z/h = 0.043$ are into the body of the permeable breakwater. The positive(upward) velocity perpendicular to the slope of the breakwater occurred below $z/h = -0.101$. Below the level of the wave run-down, $z/h < -0.128$, velocity hodographs are closed and make ellipses in Fig. 4.9(d) $z/h < -0.200$, and the lines of apsides is parallel to the slope of the breakwater. Getting close to the bottom, the lines of the apside approach to the horizon and the ellipses of the wave run-up velocity become flat. The velocity hodograph is affected by the impermeable flat bed.

Fig. 4.10 shows the mean flow vectors estimated by the numerical simulation near and in the rubble-mound breakwater and the crest, trough and mean water levels which are already shown in Fig. 4.8. A pair of circulation of the mean flow are formed along the slope of the rubble-mound breakwater. The mean flow above the trough level directs onshore. It is the Stokes drift. From the toe of the breakwater upwards, the mean flow goes up along the breakwater slope. Wurjanto and Kobayashi(1992) showed that the mean flow in the thin permeable layer directs offshore. The mean flow pattern of the rubble-mound breakwater is more complicated than that of the thin permeable layer. A small amount of onshore mass transport due to the transmitted wave is expected through the permeable breakwater between the crest and trough levels on the windward side.

With the results of the numerical simulation, the wave force action on armor units placed on the slope of the rubble-mound breakwater is discussed here. Fig. 4.11(a) shows the time history of the wave run-up $\zeta \sin\theta$,. where ζ is the displacement of the wave front along the slope of the breakwater. The time from a zero-up crossing point to ζ_{max} is longer than that from ζ_{max} to zero-down crossing point. It is considered that when the wave height is small, the fluid resistance of the wave run-up is larger than that of the wave run-down which flows as the free fall. The opposite is true as the wave steepness H/L increases and the relative depth h/L decreases(Sakakiyama and Saito, 1988).

Fig. 4.11(b) shows the horizontal and vertical components of the velocity, u, w just outside the armor layer at the level of $z/h = 0.008$ which is the nearest level to the still water level among the calculation positions. When the wave runs up, the horizontal and vertical components of the velocity are nearly in-phase. It means the direction of the velocity is parallel to the slope. When the wave runs down, there is a time-lag between them. The flow directs into the armor layer.

Fig. 4.11(c) shows the velocity u_s and the acceleration α_s along the breakwater slope. The velocity u_s is obtained by transforming the horizontal and vertical coordinates to those of along the breakwater slope and perpendicular to that by Eq. (4.2). The acceler-

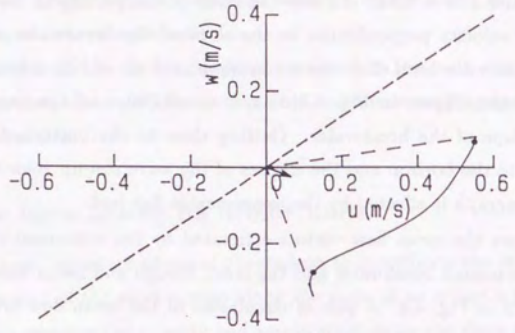

(a) $z/h = 0.187$

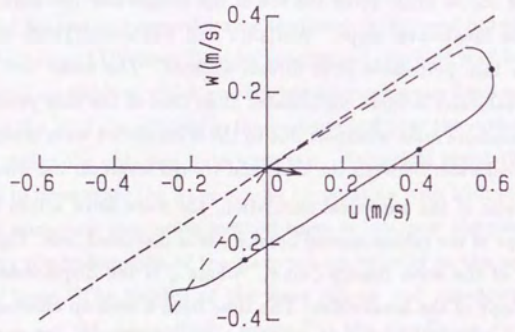

(b) $z/h = 0.043$

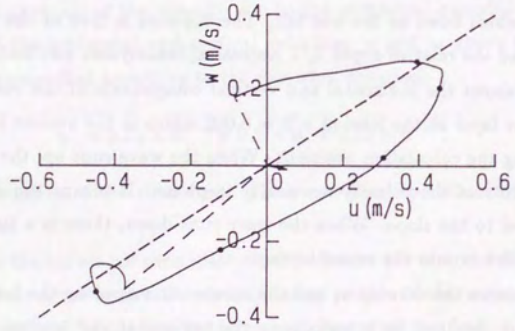

(c) $z/h = -0.101$

Fig.4.9 Velocity hodograph–1–

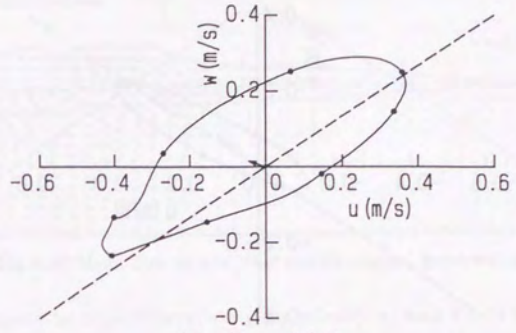

(d) $z/h = -0.245$

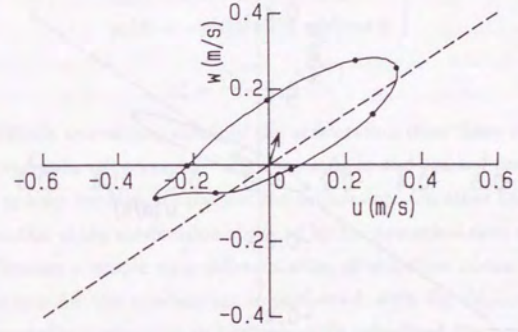

(e) $z/h = -0.388$

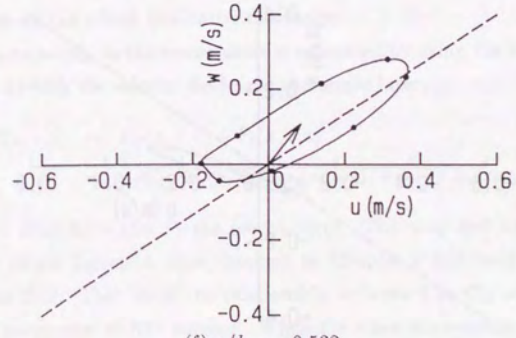

(f) $z/h = -0.532$

Fig.4.9 Velocity hodograph–2–

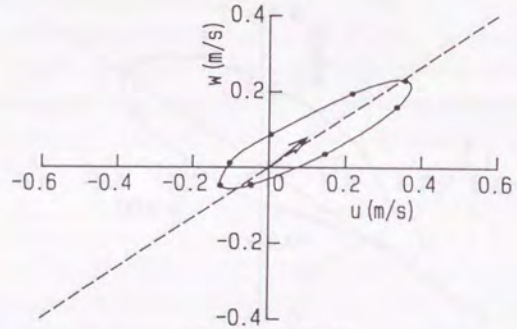

(g) $z/h = -0.676$

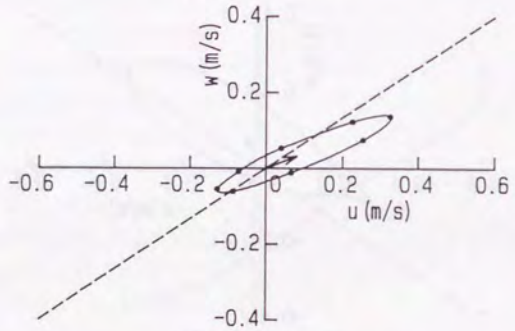

(h) $z/h = -0.820$

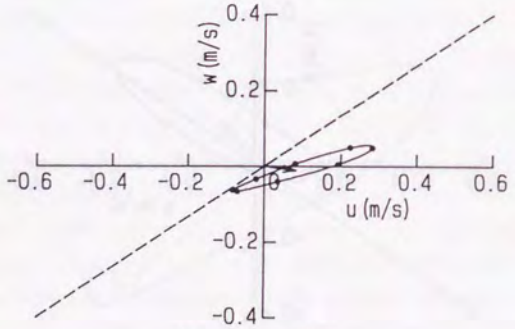

(i) $z/h = -0.964$

Fig.4.9 Velocity hodograph–3–

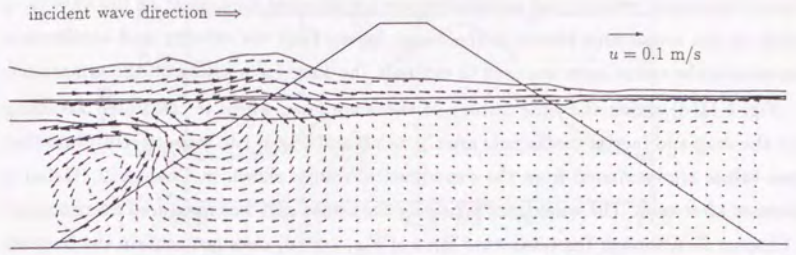

Fig.4.10 Mean flow in and near rubble-mound breakwater

ation α_s is estimated by time-differentiating the velocity u_s with Eq. (4.3):

$$\left.\begin{aligned} u_s(t) &= u(t)\cos\theta + w(t)\sin\theta \\ w_s(t) &= -u(t)\sin\theta + w(t)\cos\theta \end{aligned}\right\}, \tag{4.2}$$

$$\alpha_s^n = \frac{(u_s^{n+1} - u_s^{n-1})}{2\Delta t}. \tag{4.3}$$

It is more difficult to evaluate values of the acceleration than those of the velocity as experienced in hydraulic experiments. The time step in the present computation Δt is taken as $T/200$ to keep the high accuracy of the calculation. On other hand, too little Δt causes the fluctuation of the acceleration obtained by the numerical time differential given by Eq. (4.3). Because a simple time differentiation of velocities makes the fluctuation, smoothing operation for the acceleration is performed with Eq. (4.1). Therefore, the maximum values of the acceleration and consequently calculated the inertia forces above the level of the wave run-down are possibly controversial. With the trend of the time histories of them we can afford qualitative discussion.

The wave force acting on the armor units is estimated by using the Morison equation given by Eq. (4.4) with the velocity field near the armor layer.

$$\begin{aligned} F(x,z,t) &= F_D(x,z,t) + F_I(x,z,t) \\ &= \frac{1}{2}\rho C_D A u_s(x,z,t)|u_s(x,z,t)| + \rho C_M V \alpha_s(x,z,t) \end{aligned} \tag{4.4}$$

where F_D is the drag force and F_I the inertia force. The drag and inertia coefficients C_D, C_M of the single Tetrapod were obtained in Chapter 2 and were estimated from Figures 2.10 and 2.11. They show the relationship between C_D, C_M and the Reynolds number with a parameter of KC number. When the wave force acting on a cylinder is estimated, the environmental velocity and acceleration are used in the Morison equation.

The environmental velocity and acceleration are not obtained for evaluating the wave force acting on the armor unit placed in the armor layer. Here the velocity and acceleration just outside the armor layer are used to estimate the wave force acting on the armor unit.

Fig. 4.11(d) shows the time history of the wave force which is calculated assuming that the drag and inertia coefficients are $C_D = 1.0$ and $C_M = 1.0$, respectively. Note that these values are estimated from the experimental results shown in Chapter 2. Detail is discussed afterward. The wave force acting on the armor unit was measured as mentioned in Chapter 2. Although the total wave force of Fig. 4.11(d) does not contain the buoyant weight of the armor unit, the time history is very similar to the measured wave force as shown in Fig. 2.5 in Chapter 2. From the time history of the calculated wave force, the inertia force F_I works for a short time with a large peak behaving like a slamming force. The drag force F_D has longer duration than the inertia force. It is considered that the slamming force is not dangerous for the stability of the armor units because that force works into the body of the breakwater also as shown in Fig. 2.5 in Chapter 2. However, the breakage of slender and fragile concrete armor units is due to this type of wave force causing the armor units to be rocking (van der Meer and Heydra, 1990; Jule and Jensen, 1990; Burcharth *et al.*, 1991).

Fig. 4.12 shows the profile of the maximum velocity of the wave run-up along the slope of the armor layer on the windward side. With these values, the Reynolds number and KC number are calculated to estimate the drag and inertia coefficients from Figures 2.10 and 2.11. Fig. 4.13 shows the profiles of the drag and inertia coefficients along the slope of the armor layer. These coefficients are functions of the Reynolds and KC numbers. From the wave condition, the Reynolds number defined as $u_{smax}b/\nu$ ranges from $R_e = 1.59 \times 10^4$ at $z/h = -0.96$ to $R_e = 4.03 \times 10^4$ at $z/h = 0.043$ and KC number from $KC = 6.7$ at $z = -0.96$ to $KC = 17$ at $z/h = 0.043$. Figures 2.10 and 2.11 gives the drag and inertia coefficients under the condition KC is less than or equal to 8. The drag coefficient C_D over $KC = 8$ is extrapolated from Fig. 2.11 and varies as a function of z. On the other hand, the inertia coefficient becomes unity over the depth. If it were extrapolated literally, the inertia coefficient C_M over $KC = 8$ become less than unity. It means that the added mass becomes less than null. Mizutani(1989) obtained the inertia coefficient of submerged spheres and shows that the minimum value of the inertial coefficient is nearly unity. Therefore, it shroud be noted that the inertia coefficient C_M is 1.0 at least.

Fig. 4.14 shows the profiles of the wave force along the slope of the breakwater. The symbols indicate the peak values of the inertia, drag and total forces both during the wave

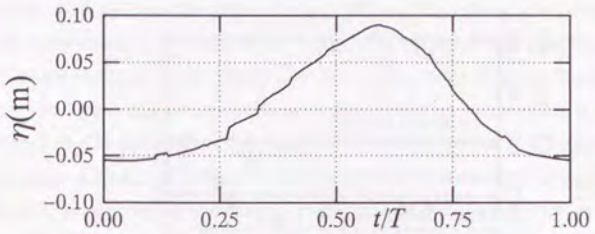

(a) Wave run-up

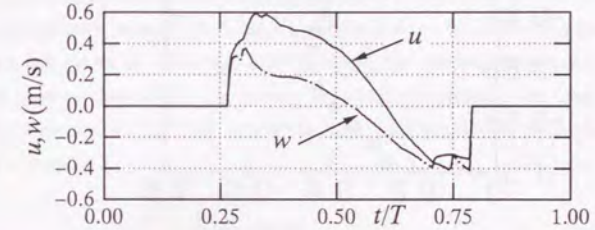

(b) Velocity u, w

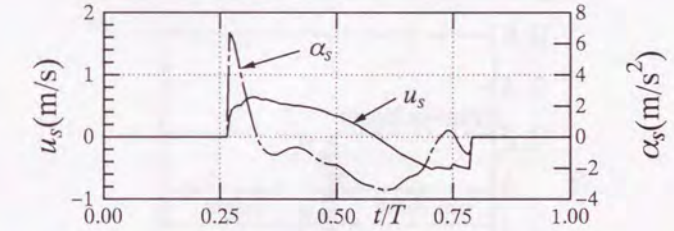

(c) Velocity u_s and acceleration α_s

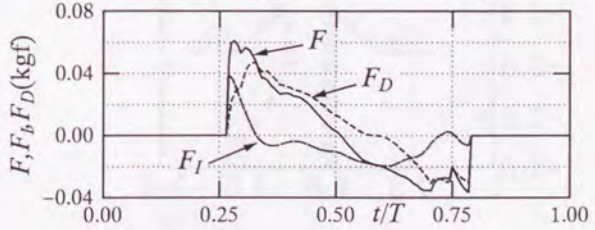

(d) Wave force(F:Total wave force, F_I:Inertia force and F_D:Drag force)

Fig.4.11 Wave run-up, velocity and wave force

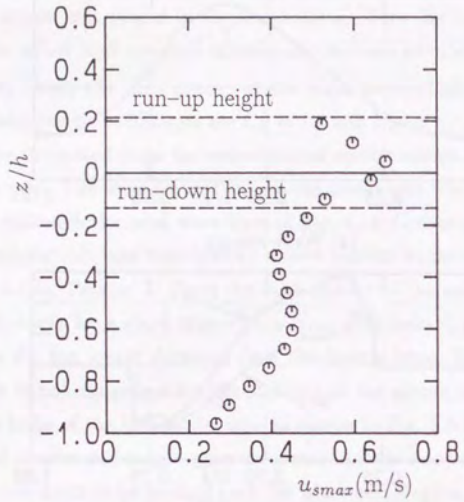

Fig.4.12 Profile of maximum velocity of wave run-up

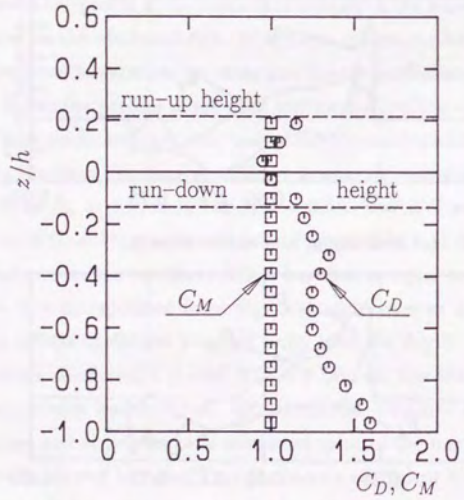

Fig.4.13 Profiles of drag and inertia coefficients used in computation

run-up in Fig. 4.14(a) and run-down in Fig. 4.14(b). The axis of abscissas indicates the ratio of the wave force to $W' \sin\theta$ which is the component of the buoyant weight of the armor unit along the breakwater slope. The ratio of the value of unity means the incipient condition of the armor unit when the friction force between armor units is neglected. The computational results shows that the profiles of the drag, inertia and total forces have the maximum values near the still water level during the wave run-up. During the wave-run down, the maximum value of the total wave force is found close to that of the drag force at $z/h \simeq -0.2$. It agrees with the fact that the armor units near the still water level are the most unstable as we have experienced in hydraulic experiments. When the velocity is small, the maximum value of the total wave force is close to that of the inertia force. On the other hand, when the velocity becomes large, the maximum value of the total wave force gets close to that of the drag force. As velocity increases, the drag force becomes predominant in comparison with the inertia force. It is consistent to the results shown in Fig. 2.8 in Chapter 2.

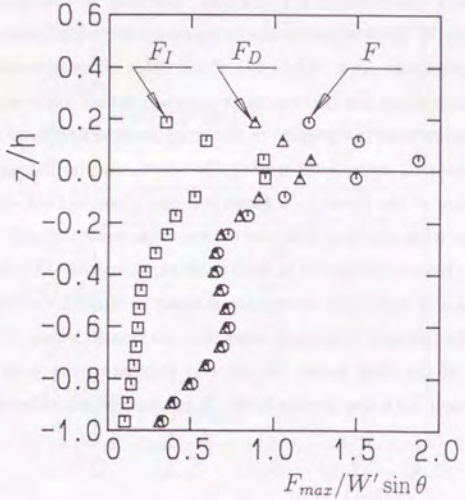

(a) During run-up

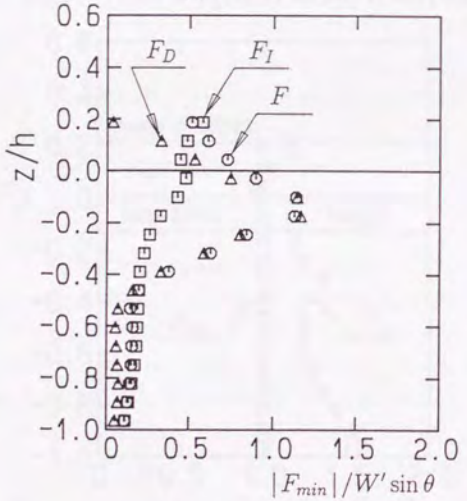

(b) During run-down

Fig.4.14 Vertical profile of wave force on armor units

4.4 Caisson breakwater covered with armor units

4.4.1 Experiments

Experiments on a caisson breakwater covered with permeable materials were performed by using both a large wave flume(205m long, 6.0m deep and 3.4m wide) and a small one(76.5m long, 1.2m deep and 0.9m wide). The model scale λ are 1/15 and 1/60, respectively. Fig. 4.15 shows the prototype breakwater of which models were used in the scale model experiments. A narrow caisson is placed in the breakwater body to reduce transmitted waves. It is not expected that this caisson resists a wave force. Armor units and stones around the breakwater support the caisson. The core material consists of stones(W = 50kg to 200kg in prototype scale) of which porosity is estimated as ε =0.4. The weights of armor units are W = 80t in the armor layer on the windward side, W = 11t in the filter layer and W = 28t in the armor layer on the leeward side. The corresponding weights of the armor units in the 1/15-scale experiment were 20kg, 6.8kg and 10.0kg. Those used in the 1/60-scale experiment were 0.37kg, 0.054kg and 0.13kg. The *In Situ* porosity of armor and filter layers in the breakwater is ε = 0.50. The armor layer at the leeward side is placed to reduce the multi-reflected waves from a floating type power plant in the basin where it is supposed to be moored. Slopes of the breakwater surface were 1 on 2 on the windward side and 1 on 1.5 at the leeward side.

Table 4.3 shows the experimental conditions indicated in equivalent prototype values. The corresponding values are shown in Tables 4.4 and 4.5 for 1/60- and 1/15-model tests, respectively. The reflection and transmission coefficients for various wave

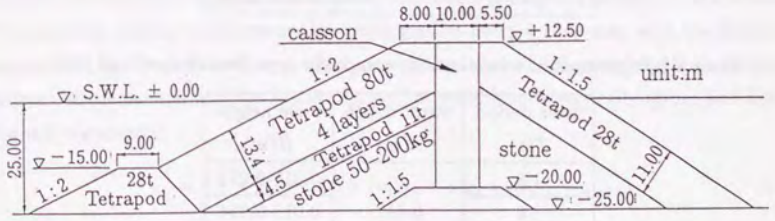

Fig.4.15 Caisson breakwater covered with armor units (λ = 1/60 and 1/15)

conditions (prototype wave conditions of incident wave height $H = 0.9$ to 17.9m, period $T = 11.6, 15.5, 19.4$s and water depth $h = 25.0$m) were obtained in the same way described above the sections concerning the experiments. The reflection coefficient is estimated by the resolving method proposed by Goda and Suzuki(1976). The displacements of a transmission wave were measured at five locations. The averaged values of the transmission wave heights obtained at five locations are used in the following analysis.

Measurements include also wave pressures on the seaward wall of the caisson covered with the permeable structures at 10 points in the large-scale experiments and at 6 points in the small-scale experiments.

The experimental results of the reflection and transmission coefficients and the wave pressure will be shown in section 4.4.4 on the scale effects on the wave transformation and the pressure.

Table 4.3 Experimental conditions for composite type breakwater in prototype

period	water depth	wave height H(m)	
T(s)	h(m)	λ =1/60	λ =1/15
11.6	25.0	0.90–16.50	0.90–16.50
15.5		1.08–17.64	1.08–16.92
19.4		1.02–17.88	1.02–17.88

Table 4.4 Experimental conditions for composite type breakwater(λ =1/15)

wave period	water depth	wave height
T(s)	h(m)	H(m)
3.0	1.667	0.060-1.100
4.0		0.072-1.128
5.0		0.068-1.192

Table 4.5 Experimental conditions for composite type breakwater(λ =1/60)

wave period	water depth	wave height
T(s)	h(m)	H(m)
1.5	0.417	0.015-0.275
2.0		0.018-0.294
2.5		0.017-0.298

4.4.2 Simulation of wave transformation

The computation was carried out under the wave conditions of the small scale-experiment such as the wave period $T = 1.5$s, the wave height at the breakwater $H = 0.15$m(the ratio of the wave height water depth is $H/h = 0.36$). Also computed for the large-scale experimental condition with respect to the equivalent corresponding wave condition, *i.e.*, the wave period $T = 3.0$s, the wave height at the breakwater $H = 0.60$m($H/h = 0.36$). Difference between the small- and large-scale conditions is the values of the inertia and drag coefficients which are functions of the Reynolds number and by which the scale effect is considered in the numerical simulation.

The computational condition is shown in Table 4.6 indicated in the prototype values. The horizontal distance of the calculation region was 8.48 $\times L_I$, where L_I is the incident wave length at the uniform depth($h_I = 44.2$m) obtained by the nonlinear wave theory. The wave lengths are $L_I = 191.24$m at the uniform depth and $L = 161.16$m at the breakwater. The cell dimensions are $\Delta x = \Delta z = 1.667$m($\Delta x/L_I = 1/114.7$ and $\Delta x/L = 1/96.7$ horizontally, $\Delta z/h = 1/15.0$ vertically). The time increment is $\Delta t = T/200$. It took about four hours with the main frame computer HITAC 680H to calculate 4000 time steps(20 wave periods $\times$ 200 steps per wave period) to gain the steady state wave motion near the caisson breakwater.

Table 4.6 Calculation condition for composite type breakwater

H(m)	T(s)	h(m)	L(m)	$\Delta x/L$	$\Delta z/h$	$\Delta t/T$	cal. region
9.00	11.6	25.0	191.24	1/96.7	1/15.0	1/200	$L_I \times 8.48$

Owing to superposition of the incident and reflected waves in front of the breakwater, the velocity field become complex. The extrapolation to estimate the velocities at free surface mentioned in Chapter 3 sometimes does not work well. Therefore, the operation of smoothing velocity and pressure are performed at every 4 time step with the following equation at the very limited area which covers the band of 1.2-wave-length horizontally in front of the caisson and the width of a half of wave height vertically above and below the still water level:

$$u_{ij} = 0.8 \times u_{ij} + 0.05 \times (u_{i-1j} + u_{i+j} + u_{ij-1} + u_{ij+1}). \tag{4.5}$$

It is confirmed that the smoothing operation does not significantly affect the reflection and transmission coefficients. The CPU time was reduced by the smoothing operation.

The iteration number for the convergence of the pressure by the SOR was reduced because the velocity and pressure become continuous.

The drag coefficient C_D and the inertia coefficient C_M were estimated so that the reflection and transmission coefficients obtained in the computation agreed with those obtained in the experiment, respectively. The reflection and transmission coefficients obtained in the calculation for the small-scale model are $K_R = 0.18$ and $K_T = 0.010$. The corresponding small-scale experimental results are $K_R = 0.21$ and $K_T = 0.015$, respectively. The computation which reproduced the experiment best gives $C_D = 0.9$ and $C_M = 1.2$. The Reynolds numbers defined with the hydraulic radius $R_{eR} = u_c R/\nu$ are $R_{eR} = 3.7 \times 10^3$ for the 1/60-scale experiment ($R = 0.0086$m for Tetrapod $W = 0.370$kg and u_c =0.43m/s). The Reynolds number for the large-scale experiment is $R_{eR} = 4.4 \times 10^4$ using Tetrapod of $W = 20$kg. The Reynolds number defined as $Re = u_c b/\nu$ of the small-scale experiment is 5.4 $\times 10^4$ and KC number defined as $KC = u_c T/b$=11.7, when $u_c = u_{smax} = 0.65$m/s, where u_{smax} is the maximum velocity of the wave run-up at the still water level in the direction of the slope of armor layer. The Reynolds number of the large-scale experiment is $Re = 4.3 \times 10^5$. The factor of model scaling according to the Froude law is 8 ($\lambda = 1/15$ and 1/60).

Fig. 4.16 shows the computed wave velocity field and the surface profile of the small-scale model when the wave runs up on the slope on the windward side of the permeable breakwater. The wave surface profile is deformed on the slope of the armor layer to have a steeper surface on the leeward side than that on the windward. The velocity of the wave front just outside the armor layer is increased according to the wave deformation. The velocity inside the armor layer is smaller and the discharge inside it also smaller than those outside the armor layer. The difference of the velocity between inside and outside the armor layer is large and the flow is concentrating to the surface of the armor layer. It is concluded that the velocity field is reasonably simulated as a whole.

Fig. 4.17 shows the sequential surface profiles near the breakwater. It is clearly found that the transmitted wave is reduced effectively by the caisson compared with the rubble-mound breakwater as previously shown in Fig. 4.2. The transmitted wave height in the permeable structure decreases as it penetrates into the structure. The transmission coefficient K_T is reduced to 0.01 (the transmitted wave height is less than 0.12m in prototype scale).

Fig. 4.18 shows the crest, trough and the mean water levels near and in the caisson breakwater covered with armor units. The mean water level rises at the two locations, on

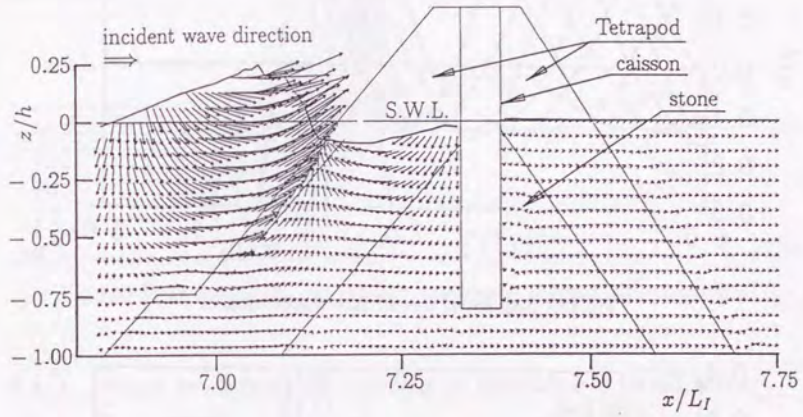

Fig.4.16 Simulated result of wave transformation due to caisson breakwater

the surface of the leeside slope of the armor layer at the still water level and on the leeside wall of the caisson. Because two components of the reflected waves from the surface of the breakwater slope and the caisson wall superimposed the location of the maximum wave height of the partial standing wave is slightly shifted from the surface of the armor layer

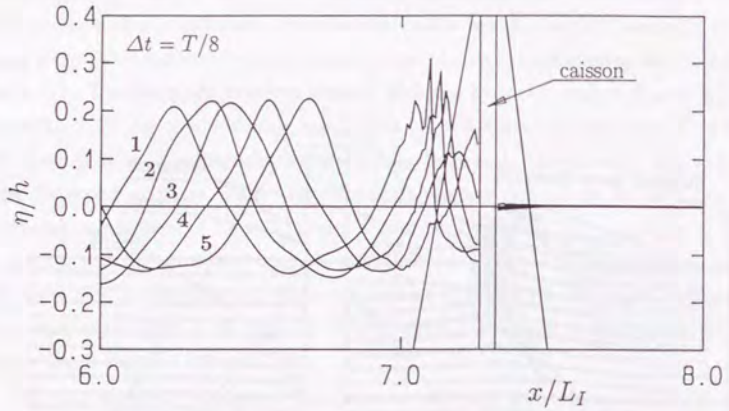

Fig.4.17 Sequential free surface displacements

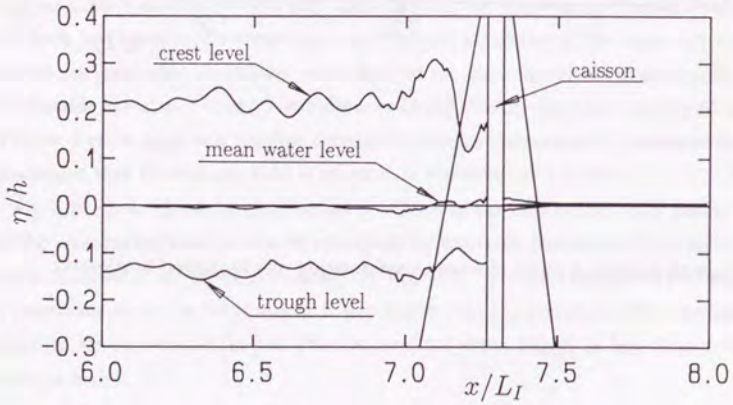

Fig.4.18 Crest, trough and mean water levels in and near caisson breakwater

at the still water level.

Fig. 4.19 shows the mean flow vectors near and in the permeable structure of the breakwater and the crest, trough and mean water levels. The mean flow field is very similar to that of the rubble-mound breakwater shown in 4.10. A pair of circulation of the mean flow are formed along the slope of the breakwater. The flow through the mound is also found and it is expected that the heel pressure on the landside of the caisson is not null. The wave reflects both from the surface of the armor layer and from the leeside wall of the caisson. According to the distribution of the wave height, the mean water level changes. The peaks of the mean water levels are seen at these two locations where the wave reflects.

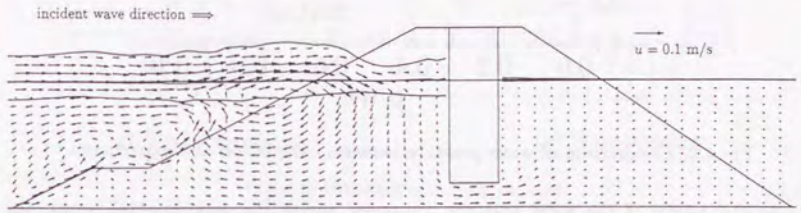

Fig.4.19 Mean flow in and near caisson breakwater covered with armor units

4.4.3 Wave pressures on caisson in permeable breakwater

The inertia and drag coefficients C_M and C_D in the computation were estimated so that the reflection and transmission coefficients obtained by the experiment agreed with the those obtained by the computation, respectively. In order to verify the present method, it is necessary to compare other values between the experiment and the computation. Here a wave-induced pore pressure is compared between the computed and measured results as shown in Fig. 4.20. The wave pressure is defined as the pressure after subtracting the hydrostatic pressure from the the computed total pressure. As shown in Fig. 4.20, the quantitative agreement of the computed pressure profile with the measured one is very good for the small-scale experiment. The large-scale experimental result is also shown in Fig. 4.20. The difference of the nondimnsional pressure between the results of small- and large-scale experiments will be discussed in subsection 4.4.4 on the scale effects of the experiments.

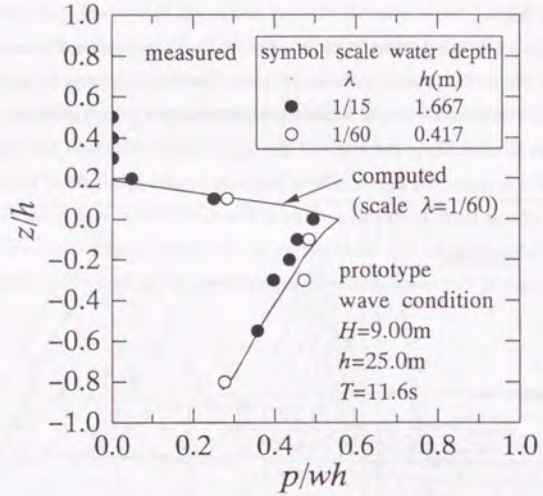

Fig.4.20 Comparison of wave pressure between calculation and experiment

As the profile of the wave pressure computed agrees the experimental result, the pressure distribution around the caisson can be investigated with the numerical result. Fig. 4.21(a) shows the total pressure distribution around the caisson and Fig. 4.21(b) that of the wave pressure. Note that the scale of the pressure in Fig. 4.21(b) is one tenth smaller than that in Fig. 4.21(b). The distributions of the total pressure acting on both the seaside and landside walls are nearly triangular and that of the uplift pressure is nearly rectangular. It means that the main portion of the total pressure is the hydrostatic pressure. Some of the wave energy is reflected from the surface of the armor layer outward and the other dissipated in the permeable structure. The rest of the wave energy becomes very small. The wave height on the wall of the caisson in the permeable structure is estimated as 0.05m($H/h = 0.12$) which is a half of the wave height of the standing wave. That of the progressive wave without the breakwater is 0.15m($H/h = 0.36$). The wave height is reduced to one third in the permeable breakwater and the wave energy is reduced to about 10%.

The velocity passing through the mound is small but not null. It yields a small transmission wave. The transmission coefficient is less than 0.05. It is equivalent to that the rate of wave energy is less than $O(10^{-3})$. The wave pressure acting on the landside

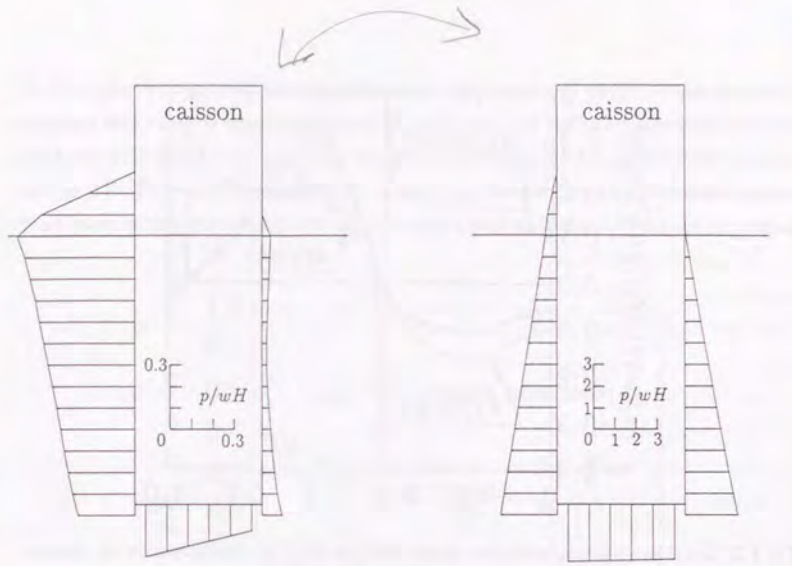

(a) Total pressure (b) Wave pressure

Fig.4.21 Pressure acting on caisson

wall is not null. The distribution of the uplift of the wave pressure shows nearly triangular and the gradient is almost linear. Goda(1985) assumes that the uplift wave pressure for the design of the caisson has a triangular distribution with a toe pressure estimated by the experimental formula and with a heel pressure of null. The gradient of the pressure distribution is assumed to be linear. The gradient of the result shown in Fig. 4.21(b) is almost linear and similar to that by Goda(1985). The heel pressure of the simulated result is not null because the caisson is narrow and the wave does not completely dissipate in the rubble-mound.

Fig. 4.22 shows the time history of the total wave force F_x acting on the caisson covered with the armor units and core materials both on windward and leeward sides and those of the lever arm length l'_z, the wave pressure moment M_y. Here l'_z is the length measured from the level of the bottom of the caisson. These time histories are phased-averaged ones for four wave period($t = 16T$ to $20T$). Comparing with the result of the wave force acting on the rectangular permeable breakwater in subsection 3.5 in Chapter 3, the wave nonlinearity appears remarkably in the wave force and moment. The maximum wave force works onshore and it is 1.5 times greater than the offshore maximum wave

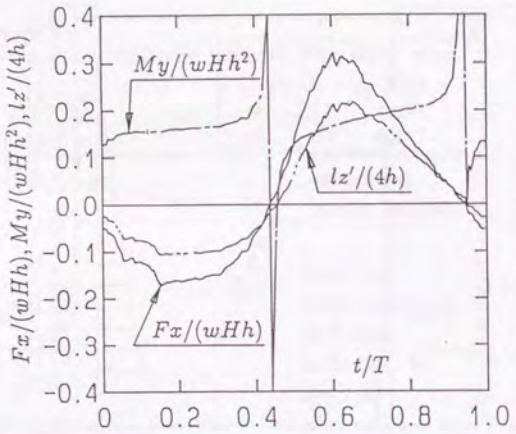

Fig.4.22 Total wave force, lever arm length and moment of wave pressure on caisson

force. The caisson of this type of structure is supported by the armor units and stones on the leeward side, the caisson will neither slide nor fall down. The above analysis can be applied for the investigation of the stability of a composite type breakwater which is normally covered with armor units only on the windward side.

Function of a permeable structure to reduce the wave energy was investigated by the previously performed hydraulic experiments. Tanimoto *et al.*(1981) proposed the concept of the reduction coefficient of wave force by armor units. It is the ratio of the total wave force acting on the caisson covered with armor units to that directly on the caisson without armor units. The latter wave force is usually estimated by integrating the wave pressure proposed by Goda(1985). The reduction coefficient of wave force is a function of the wave condition and the permeability etc. It varies roughly from 0.8 to 1.0 The value of 0.8 is usually recommended for the design. Here the effect of armor layer to reduce the wave energy is investigated with the numerical and analytical results.

Fig. 4.23 shows the profiles of pressure acting on an impermeable wall denoted by p_1 drawn with the dashed line and that on the caisson in the permeable breakwater denoted by p_2 with the solid line. The pressure p_1 is estimated with the nonlinear standing wave theory by Goda and Kakizaki(1967). The ratio of the wave-induced pressure on the impermeable wall in the armor layer to that without the armor layer denoted by p_2/p_1 is indicated with the dash-dotted line. The analytical solution was obtained under the

condition that vertical wall on the sea bottom. The numerical results obtained under the condition that there is a permeable mound under the the bottom of the caisson. Except above the still water level and near the bottom, the ratios are about 0.75. It is very close to 0.8. The reduction coefficient of the wave pressure by the permeable materials investigated with the numerical experiment agrees with that of the hydraulic experiments.

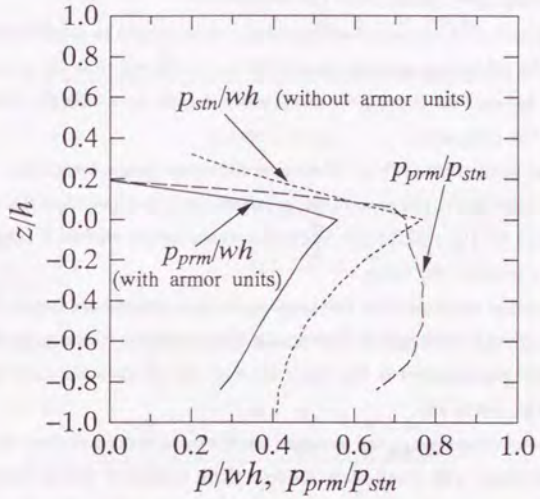

Fig.4.23 Effect of armor layer on wave pressure reduction

4.4.4 Scale effect of wave transformation and pressure

Fig. 4.24 shows the results of the reflection and transmission coefficients obtained through the large- and small-model scale experiments. The factor of according to the Froude law for scaling is 4(the large-model scale is 1/15 and the small one 1/60). It is found that the reflection coefficients of the large-scale experiment are larger than the small ones when the wave periods are $T = 11.6$s and $T = 15.5$s. This trend agrees with the result obtained by Sollitt and DeBok(1976). However, the reflection coefficient on the wave period $T = 19.4$s obtained in the small-scale experiments is greater than that obtained in the large-scale experiment when the wave steepness H/L is less than 0.04.

This is consistent with the description in Le Méhauté(1976).

It is noted that the reflection coefficient varies with the distance from a reflection wall within the distance of a wave-length. It is caused by the evanescent waves. The wave reflection measured at more than a wave-length distant from a breakwater tends to almost constant and the bottom friction is negligible to the wave reflection (Sakakiyama and Saito,1988). All the reflection coefficients of Fig. 4.24 were measured at the position more than a wave-length distant from the breakwater.

The dependency of the wave reflection on the wave period is complicated as shown in section 4.3 on the rubble-mound breakwater. It is considered that the scale effect on the wave reflection depends on the wave period which results in a change of the ratio of the inertia force to the drag force.

Because the wave period T = 19.4s is a little too large compared with normally observed ones in the fields, the present experimental results show that the wave reflection is underestimated by the small-scale hydraulic experiments within a range of the wave period which we treat in the design.

The transmission coefficients of the large-scale experiments are larger than the small-scale one, although the difference is very small. Consequently, the energy dissipation rate of the large-scale experiments is less than that of the small-scale ones when the wave period is less than about 19s.

Fig. 4.25 shows examples of the pressure profile comparing between the experimental results with the large- and small-scale models. The tendency of the scale effect on the wave pressure is opposite to that on the wave reflection. That is, the wave pressures obtained by the small-scale hydraulic experiments are larger than those by the large-scale one when the wave period is less than 19.4s The opposite is true when the wave period is 19.4s.

It is concluded from the results of the scale effects on the wave reflection and the wave pressure that the wave pressure is small when the wave reflection is large and vice versa. It is very natural and explained as follows. When the reflection coefficient is large, a small amount of wave penetrates in the permeable structure and onto the caisson. As a result, the wave pressure becomes small.

The scale effects on the wave reflection and the wave pressure mentioned above are explained with numerical experiments as follows. Fig. 4.26 shows the effect of inertia coefficient on the wave pressure, while the drag coefficient is constant at C_D=0.9. The computation are performed by varying the inertia coefficient C_M with 1.2, 1.5 and 1.7. As

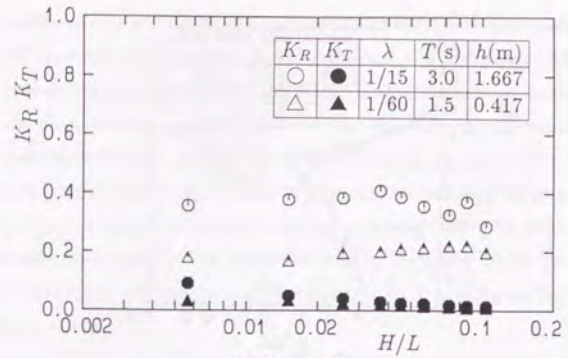

(a) T = 11.6s

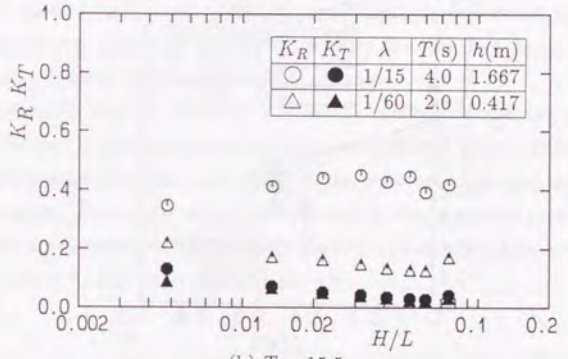

(b) T = 15.5s

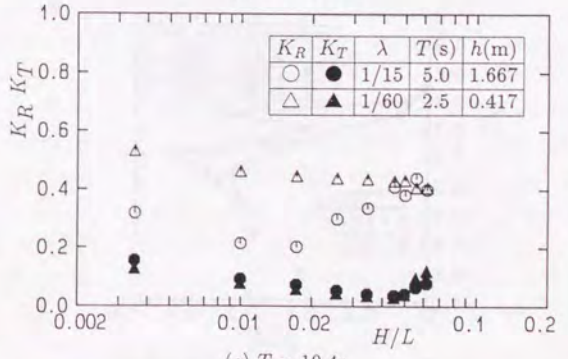

(c) T = 19.4s

Fig.4.24 Scale effect of reflection and transmission coefficients

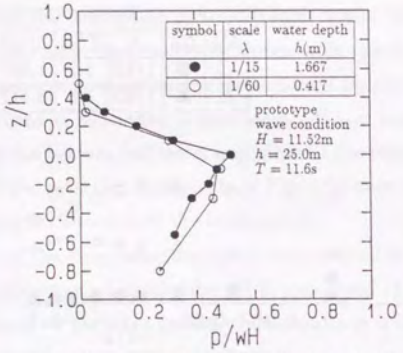

(a) $T = 11.6$s,$H = 11.5$m,$(H/h = 0.46)$

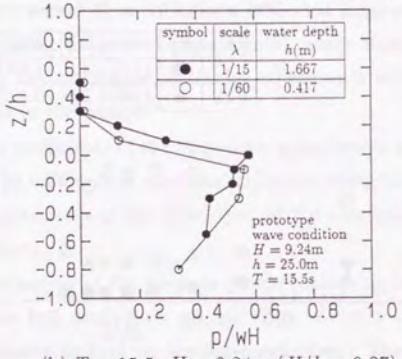

(b) $T = 15.5$s,$H = 9.24$m,$(H/h = 0.37)$

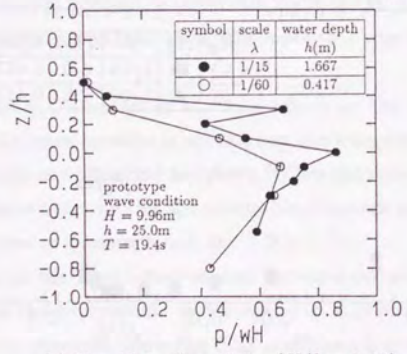

(c) $T = 19.4$s,$H = 10.0$m,$(H/h = 0.40)$

Fig.4.25 Scale effect of wave pressure on caisson in permeable structure

the inertia coefficient C_M increases, the wave pressure decreases. On the other hand, the reflection coefficient increases as the inertia coefficient C_M increases. The transmission coefficient decreases very slightly. The reflection and transmission coefficients are less sensitive to the change of the inertia coefficient C_M than the wave pressure.

As the inertial resistance described by the factor $\lambda_v = \gamma_v + (1 - \gamma_v)C_M$ defined as Eq. (3.18) increases, the wave reflection from the armor and filter layers increases. Consequently, the less part of the wave transmits through the permeable structure and the wave pressure decreases. As the Reynolds number increases under the condition that KC number is constant, the inertia coefficient increases according to the Froude law for scaling as shown Chapter 2.

Fig. 4.27 shows the effect of the drag coefficient on the wave pressure, while the inertia coefficient is constant at C_M=1.5. The drag coefficient C_D is selected as $C_D = 0.3, 0.6$ and 0.9. As the drag coefficient increases, the wave pressure decreases. It is caused by the wave energy dissipation in the permeable structure.

The relationship between the drag and inertia coefficients and the scale effects on the wave reflection, transmission and pressure are explained above. Both the drag and inertia coefficients influence the scale effect on the wave reflection and transmission also the wave pressure. These scale effects are reflected to the numerical model through C_M and C_D which are functions of the Reynolds number and of which the characteristics are investigated from Chapter 2 through Chapter 4.

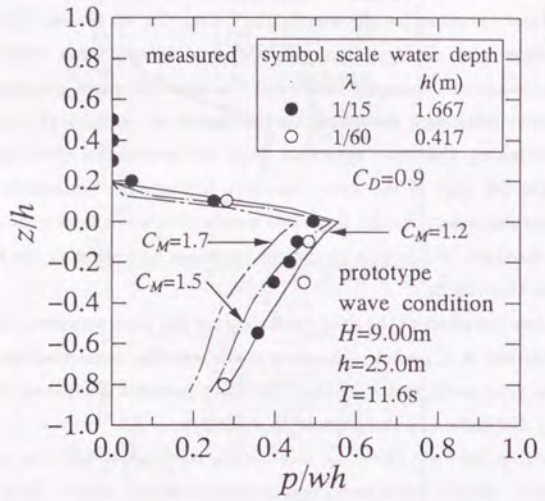

Fig.4.26 Wave pressure dependent on inertia coefficient($C_D = 0.9$)

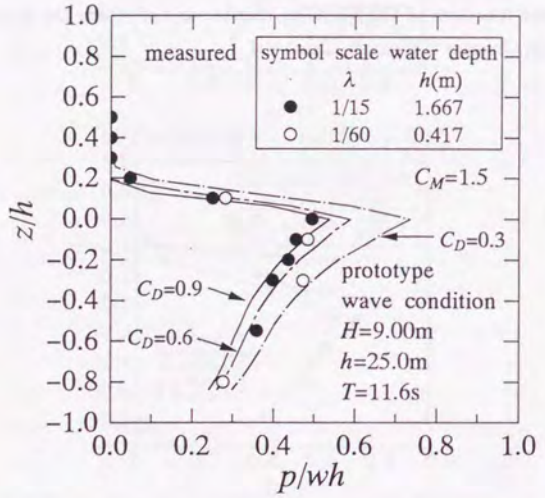

Fig.4.27 Wave pressure dependent on drag coefficient($C_M = 1.5$)

Chapter 5

WAVE TRANSFORMATION OVER SUBMERGED BREAKWATER

5.1 Introduction

The superiority of the present numerical simulation model to the other models is based on the fully nonlinear model and to include the effects of a permeable structure. Therefore, the present method can be applied to a wave field where the wave changes its period owing to the permeable breakwater as well as the wave form.

A wave field around a submerged structure such as a sand bar, submerged permeable and impermeable breakwaters, is a typical situation in which the wave disintegrates by passing the submerged structure and results in changes of its form and period.

Field observation of the wave disintegration due to a submerged bar was firstly presented by Byrne(1969) and experiments on breaking waves by a longshore bar were carried out by McNair and Sorensen(1970) and by Chandler and Sorensen(1972).

Experimental studies were also performed to investigate the efficiency of the wave decay by submerged breakwaters. Nakamura *et al.*(1966) investigated the wave energy dissipation due to the wave breaking on a rectangular impermeable submerged breakwater and Horikawa and Komori(1968) the wind wave attenuation. Tanaka(1976) examined an effect of a breadth of a submerged breakwater on the wave dissipation and the resultant sand beach deformation. Nagai *et al.*(1977) also observed the effect of a breadth of a submerged breakwater with a gentle slope on the wave transformation.

Numerical simulations were also performed: The scattering of waves by rectangular obstacles was presented by Mei and Black(1969) and the disintegration of a solitary wave by Madsen and Mei(1969). The harmonic wave to the second order solution is treated by Massel(1983). Kojima *et al.*(1991) also presented the numerical method called the method of matched eigenfunction expansions to study the interactions between Stokes-second-order waves and a rectangular impermeable structure. Ohyama and Nadaoka(1991a,

1991b) reproduced successfully the wave disintegration over an impermeable submerged breakwater using the boundary element method. These studies are based on the potential theory and restricted to the wave transformation by the impermeable structure. The wave energy dissipation due to the interaction between the structure and waves is neglected.

On the numerical simulation of the wave field where a permeable submerged breakwater exists, Isobe *et al.*(1991) derived the depth-integrated nonlinear wave equation which reduces to the Boussinesq equation for the pure wave condition without the permeable bed. However, the simulated results by the nonlinear theory correct to the first order disagree with the experimental results of the wave transformation behind the submerged breakwater.

In this chapter, the wave disintegration by passing over a two-dimensional submerged breakwater is simulated(Sakakiyama, 1992). Main purpose is concentrated on the wave transformation due to the permeable submerged breakwater. Hydraulic experiments using the small-scale experiments are performed to verify the numerical simulation model. Time histories of the surface displacements and velocities measured at several points are available to be compared directly with the numerical results.

Moreover, the effect of the permeability of the submerged breakwater on the wave transformation is investigated performing the experiments for both permeable and impermeable submerged breakwaters.

Finally, the scale effect of the permeable submerged breakwater on the wave transmission is experimentally investigated carrying out the large- and small-scale experiments. Wave motion on a submerged breakwater is much complicated from the view point of the scale effect on the wave transmission. When the wave height is relatively small compared with the water depth on the submerged breakwater, the wave passed without breaking. Under most of the wave conditions, the waves break on the submerged breakwater. The scale effect caused by the energy dissipation should be discussed in two following aspects: The wave energy dissipates in the body of permeable submerged breakwater and owing to the breaking wave. Including both nonbreaking and breaking waves on the permeable submerged breakwater, the scale effect on the transmitted wave is presented.

5.2 Experiment

Experiments were performed by using small- and large-scale models. Both permeable and impermeable submerged breakwaters were used in the small-scale experiments to

investigate an effect of the permeability on the wave disintegration. The scale effect of the permeable submerged breakwater on the transmitted waves is examined comparing between the large- and small-scale experimental results.

Fig. 5.1 shows the model submerged breakwater. The model of the submerged breakwater was $0.7h$ high, $2h$ wide at top and $2.7h$ wide at bottom, where h is the water depth at the submerged breakwater. Slopes of the submerged breakwaters were 2 on 1. The prototype water depth is assumed as $h = 10$m and the model scale of the small-scale experiment is $\lambda = 1/50$ and that of the large one $\lambda = 1/8$. The water depths are $h = 0.20$m at the small scale experiment and $h = 1.25$m at the large-scale one, respectively.

The permeable submerged breakwater consisted of 0.060-kg Tetrapod in the small-scale experiment and 20kg-Tetrapod in the large-scale one, respectively. Tetrapods were covered with wire net not to be removed by wave attacks. The porosity of the permeable submerged breakwater was $\varepsilon = 0.50$. The impermeable submerged breakwater was made of cement mortar. They were settled on a flat bottom of an impermeable mound made of cement mortar.

The small-scale experiments were carried out using the 50.0m-long, 1.5m-deep and 2.0m-wide wave flume. Fig. 5.2 shows the experimental set-up. The bottom slope was 1 on 15. The surface displacements were measured with ten capacitance type wave gages at six positions on windward side and at four positions on leeside side of the submerged breakwater. The velocity was also measured with eight electro-magnetic current meters(EMCM) in the middle of the water depth at each position where the wave gage was installed except two positions. Measurements of the surface displacements and velocities on uniform slope were carried out before the impermeable mound was constructed. The wave transformation just due to the impermeable mound was also examined by measuring the surface displacements and velocities when the submerged breakwater was removed.

Table 5.1 shows the experimental conditions for the model scale of $\lambda = 1/50$, where H_i is the wave height at the uniform depth h_i. The uniform water depth is $h_i = 0.59$m, the water depth at the submerged breakwater $h = 0.20$m and that on the top of the submerged breakwater $h_r = 0.06$m. The ratio of the width of the submerged breakwater at top B and the water depth h is B/h=2.0.

Monochromatic waves were used for a wide range of the wave heights with the wave period of $T = 1.0, 1.2, 1.5, 1.7, 2.0, 2.2$s for the permeable submerged breakwater, and $T = 1.2, 1.7, 2.2$s for the impermeable submerged breakwater. A few waves from the smallest wave height for each wave period are nonbreaking at the submerged breakwaters.

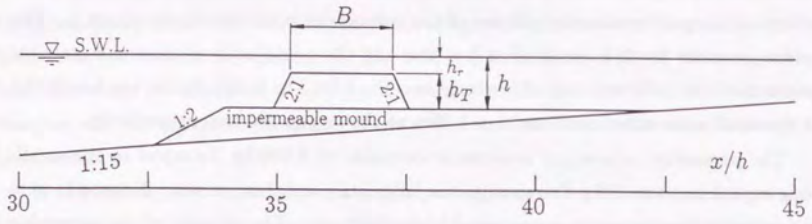

Fig.5.1 Model of submerged breakwater

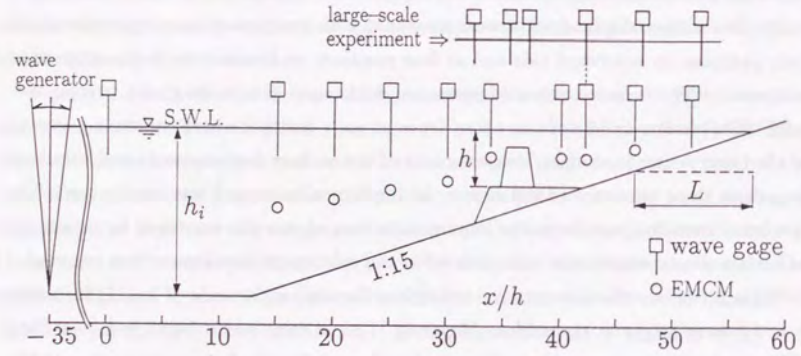

Fig.5.2 Experimental setup

Table 5.1 Experimental conditions(λ=1/50)

CASE	wave period T(s)	wave height H_i(m)	water depth h_i(m)	h(m)	h_r(m)	porosity ε
PE–12	1.2	0.044–0.215	0.59	0.20	0.06	permeable 0.53
PE–17	1.7	0.049–0.156				
PE–22	2.2	0.062–0.191				
IE–12	1.2	0.048–0.206	0.59	0.20	0.06	impermeable 0.0
IE–17	1.7	0.052–0.182				
IE–22	2.2	0.070–0.191				

Table 5.2 Experimental conditions(λ=1/8)

CASE	wave period T(s)	wave height H_i(m)	water depth h_i(m)	h(m)	h_r(m)	porosity ε
PE–30	3.01	0.397–1.460	4.25	1.25	0.375	permeable 0.53
PE–42	4.24	0.337–1.461				
PE–54	5.48	0.320–1.435				

Power spectral analyses are made of both the incident and transmitted waves to investigate the quantitatively change of the wave characteristics.

The large-scale experiments of which a model scale is $\lambda = 1/8$ were also performed using CRIEPI FLUME(205m long, 6.0m deep and 3.4m wide). Wave gages were installed at eight locations as shown in Fig. 5.2. Only one of them, the wave gage at the onshore end of the impermeable mound was set at relatively same location as the small-scale experiments. Table 5.2 shows the experimental conditions for a wide range of wave height including the nonbreaking and breaking waves on the submerged breakwater.

5.3 Numerical simulation conditions

Procedure of the numerical simulation was basically same as described in the previous chapters concerned. However, the extrapolation method to estimate the velocity at the free surface is changed when the submerged breakwater exists in the calculation region. The extrapolation method with four values proposed by Chan and Street(1970) mentioned

Table 5.3 Calculation conditions for nonbreaking waves(λ=1/50)

CASE	wave period T(s)	wave height H_i(m)	H(m)	water depth h_i(m)	h(m)	h_r(m)	porosity ε
P–10	1.0	0.047	0.035	0.59	0.20	0.14	permeable 0.53
P–12	1.2	0.045	0.038				
P–15	1.5	0.056	0.058				
P–17	1.7	0.054	0.059				
P–20	2.0	0.056	0.075				
P–22	2.2	0.065	0.089				
I–12	1.2	0.045	0.038	0.59	0.20	0.14	impermeable 0.0
I–17	1.7	0.054	0.059				
I–22	2.2	0.065	0.089				

in Chapter 3 does not work well when a velocity distribution is discontinuous. The values of velocity at the neighboring cell to the surface cell is obtained by the governing equation of the PBM and they are directly substituted into the velocities at the free surface in the region of the submerged breakwater. When a wave passes the submerged breakwater and the surface water level goes down, the number of continuous velocity values for the extrapolation is not enough. Outside this region, the extrapolation with four values of velocity is employed as same as before.

The cell dimensions are $\Delta x = 0.02$m and $\Delta z = 0.01$m for all the cases. The time increment depends on the wave period as $\Delta t = T/200$. The Courant condition for the numerical stability is satisfied with the cell dimensions and the time increments for all wave conditions. The calculation region was set as follows: The incident wave boundary was at $x = 0$m as shown in Fig. 5.2 and the out-flow boundary at the position away from a wave-length from $x = 9.3$m. A flat bottom is set in the calculation region illustrated with the dashed line in Fig. 5.2 in order to propagate the transmitted wave by applying Sommerfeld's radiation condition.

Table 5.3 shows the calculation conditions which are nonbreaking waves, where H is the wave height of the progressive wave on the impermeable mound without the submerged breakwater. The ratio of the progressive wave height H to the water depth h ranges from 0.17 to 0.45 for the wave period from $T = 1.0$s to $T = 2.2$s. They are strongly nonlinear waves. Waves break when H/h is greater than these values for each wave period on the submerged breakwaters.

Computations were performed until the steady wave motion was obtained around the submerged breakwater. The computation time depends on the wave period. When the wave period is 1.0s, the computation time was the longest, $15 \times T$ and when the wave period $T = 2.2$s, the shortest, $10 \times T$. It took about 125 minutes for $15 \times T$ and about 80 minutes for $10 \times T$ with the main frame computer HITAC 680H.

The inertia and drag coefficients were estimated with the previously obtained results of the relationships between the Reynolds number R_{eR} and the inertia and drag coefficients shown in Fig. 3.21 in Chapter 3. The Reynolds number defined as $R_{eR} = u_c R/\nu$ ranges from 7×10^2 to 2.2×10^3 for the wave conditions listed in Table 5.3. Within this range of the Reynolds number, it can be considered that both the inertia and drag coefficients are nearly constant. The values of $C_D = 0.9$ and $C_M = 1.5$ are used for the following computations in Section 5.4.

Beforehand, the effects of the inertia and drag coefficients on the wave reflection and transmission were investigated with the numerical simulation. Fig. 5.3 shows the comparison of the surface displacements when the drag coefficient were set at three values of C_D =0.9, 2.0 and 3.0 while the inertia coefficient is constant at C_M =1.5. As the drag coefficient increases, the transmitted wave height decreases but the reflected wave slightly changes. Fig. 5.4 shows the comparison when the inertia coefficient is varied at $C_M = 1.0, 1.5$ and 2.0 while the drag coefficient is constant at $C_D = 0.9$. As the inertia coefficient increases, the surface displacements of the transmitted wave changes to decline and the reflected wave is slightly changed as same as the effect of the drag coefficient.

The inertia and drag coefficients do influence the wave reflection and transmission by the permeable breakwater. However, those coefficients of the submerged breakwater have small contribution to the wave transformation compared with the rectangular and trapezoidal breakwaters. The wave motion near and above the still water level is intense. Therefore, the drag and inertia coefficients interacting with the wave motion has great influence to the wave transformation for these breakwaters.

On the other hand, the wave motion below the still water level is weak and then the effects of the drag and inertia coefficients on the wave transformation due to the permeable submerged breakwater is less sensitive than due to the permeable breakwaters. Figures 5.3 and 5.4 also shows that the wave transmission is more influenced with the drag and inertia coefficients than the wave reflection. It is concluded that the configuration condition of the submerged breakwater is more predominant to the wave disintegration than the fluid resistance.

As presented the calculation conditions in Table 5.3, the ratio of the wave height to the water depth at the submerged breakwater is up to $H/h = 0.45$ at $T = 2.2$s. The wave nonlinearity is remarkable. The previous calculation for the wave disintegration due to the impermeable submerged breakwater(Oyama and Nadaoka,1991) were weakly nonlinear, $H/h = 0.1$. Computations for the present calculation conditions of the impermeable submerged breakwater were not succeeded except for CASE I-12. It is because the vertical cell dimension $\Delta z = 0.01$m becomes relatively rough compared with the water depth when the wave runs down on the offshore slope of the impermeable breakwater. The computation of the impermeable breakwater was carried out up to $H/h = 0.15$ when the wave period is $T = 1.5$s under the condition of $\Delta z = 0.01$m. The computations on the permeable breakwater were performed for all wave conditions listed in Table 5.3.

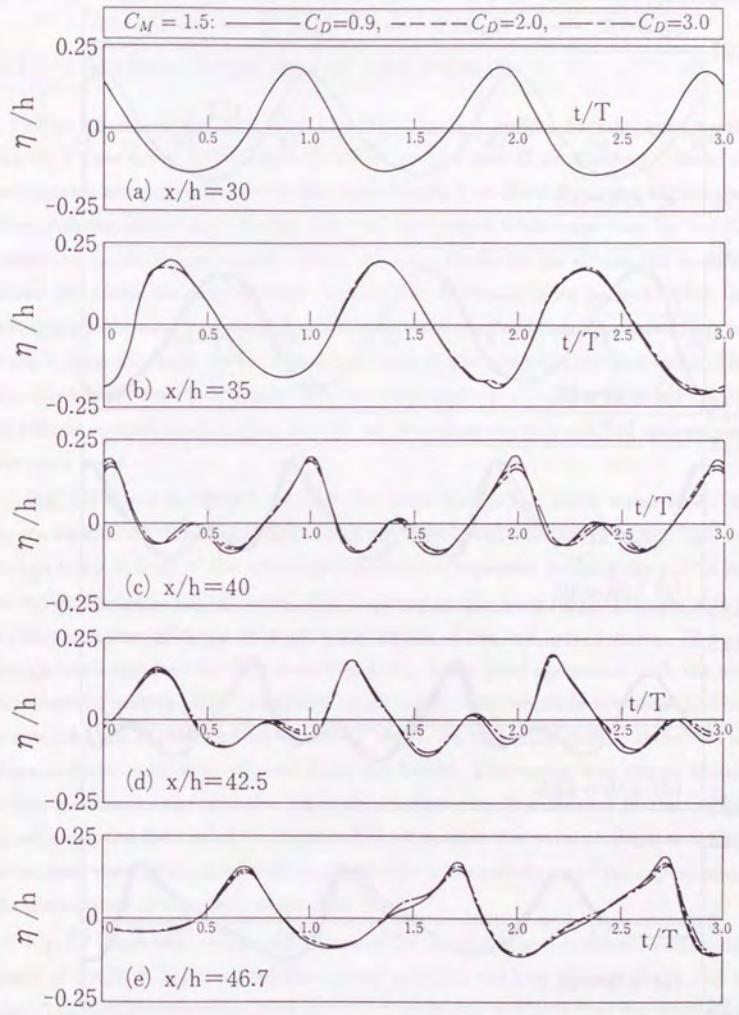

Fig.5.3 Surface displacements dependent on drag coefficient

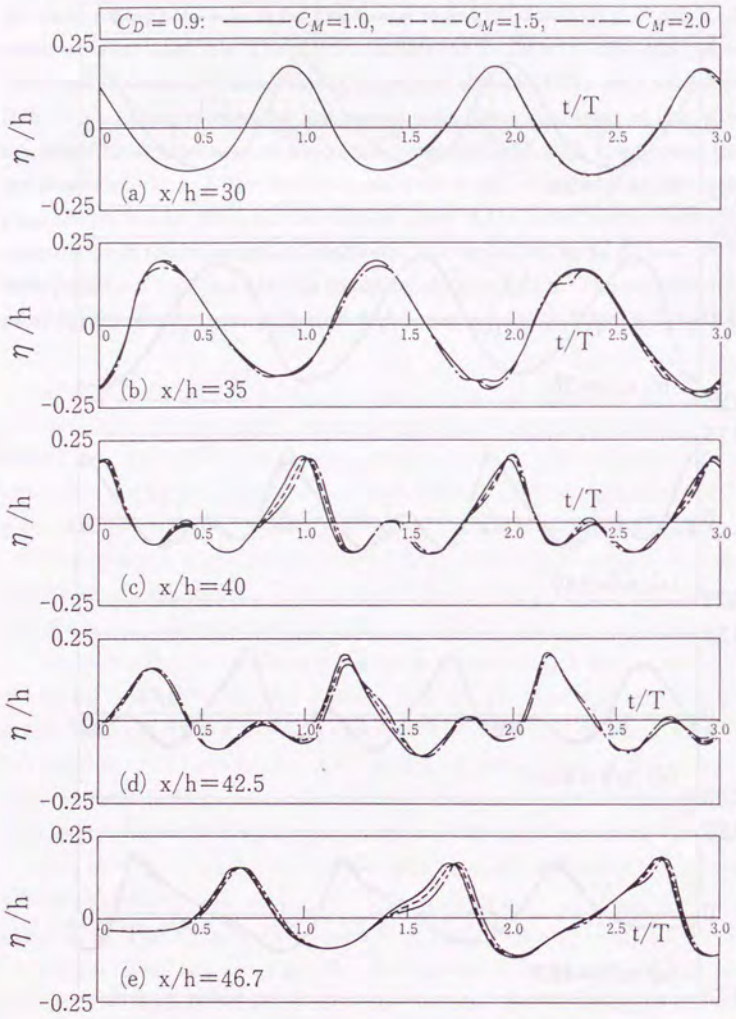

Fig.5.4 Surface displacements dependent on inertia coefficient

5.4 Numerical simulation of wave disintegration

5.4.1 Surface displacement and velocity

Fig. 5.5 shows the calculated sequential surface profiles for one wave period with the time interval of $T/8$ (CASE P–15, T = 1.5s and H = 0.058m). Both x and z coordinates are normalized with the water depth h at the submerged breakwater. The wave disintegration after passing over the submerged breakwater can be simulated as seen in an hydraulic experiment. When the wave climbs on the submerged breakwater, it shows the profile steeping the front surface and becoming more peaked. After the main wave passes the submerged breakwater, a hump of smaller height appears at the rear and trails behind the main wave. This small wave is the second-order free wave. The main wave(first-order wave) deforms as propagating onshore. The third-order wave of which amplitude is much smaller than that of the secondary wave is catched up and passed by the main wave.

Fig. 5.6 shows the distributions of the crest, trough and mean water levels obtained by the calculation. The symbols indicate the experimental results of them. The crest and trough levels in front of the submerged breakwater represent forming the partial standing wave. On the leeside of the submerged breakwater, the wave height changes as a train of waves propagates with the different wave celerity of free and locked waves. The crest and trough levels obtained by the calculation are in fairly good agreement with the hydraulic experimental results. The calculated mean water level which is the second-order value is smaller than that of the experimental result. In the experiments, there was a beach slope and the wave was reflected from the beach. The water was stored between the submerged breakwater and the beach slope. However, it is treated in the computation by adopting the flat bed at the outflow boundary that the wave propagates onshore as a permanent wave. The above difference between the calculation and the experiment causes the discrepancy of the mean water level.

Fig. 5.7 shows the comparisons between the calculated and measured surface displacements of CASE P–15(T = 1.5s) for various positions both on the windward and leeward side. The displacements obtained at x/h = 30 shown in Fig. 5.7(a) are synchronized at the time of the first crest level. Figures 5.7(a) and (b) are the surface displacements on the windward side of the permeable submerged breakwater and Figures 5.7(c) through (e) those on the leeside. It is found that on the windward side, the calculated displace-

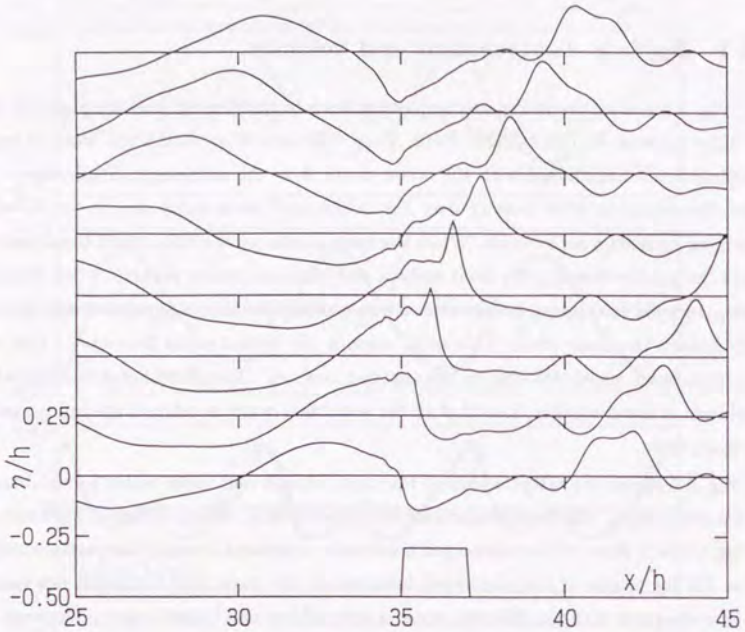

Fig.5.5 Sequential surface profiles passing over submerged breakwater

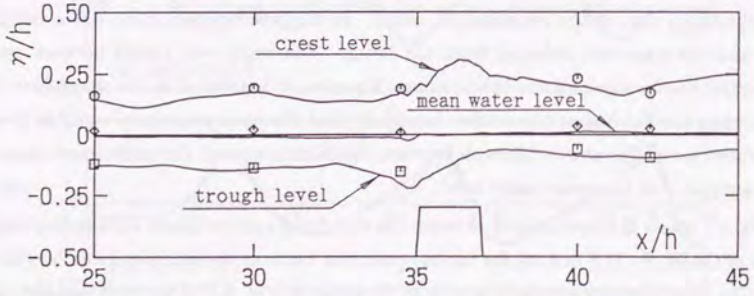

Fig.5.6 Comparison between experiment and calculation of crest, trough and mean water levels

ments are steeper than measured ones. On the leeward side, the main wave and the free waves of higher order which were provoked by the wave disintegration over the submerged breakwater propagate with each propagation velocity. Consequently, the surface displacement changes in space. Fig. 5.7(c) shows the steep wave front and the mild rear of the surface displacements. Then Fig. 5.7(d) shows the opposite. The surface displacement in Fig. 5.7(e) is similar to that of Fig. 5.7(d). The calculated surface displacements are in good agreement with the measured ones at all three positions except that the phase of the surface displacements shift slightly between them. The superposition on the main wave with the secondary and third waves causes the transient wave profiles because they propagate with each wave celerity as free waves. The distribution of the wave height is not uniform on the leeward side.

Figures 5.8 through 5.10 show the comparisons of the surface displacements between the calculation and the experiments for the other wave periods, CASE P–17, CASE P–20 and CASE P–22 at each one position on the windward and leeward sides, respectively. As the wave period increases, the number of the disintegrated wave increases. It is observed that at $T = 1.7$s the main and secondary waves are seen in Fig. 5.8 and in addition to the main and secondary wave, the third-order wave is seen at the longest wave period $T = 2.2$s in Fig. 5.10. The calculated surface displacement of the higher frequency wave is bigger than measured one. Both the surface displacement and the number of disintegrated waves in the simulation agree with the measured ones.

The agreement in the cases of the short wave such as $T = 1.0$s and $T = 1.2$s is not good compared with those of the longer wave greater than T =1.2s. Wave disintegration is not reproduced in the case of the wave period $T = 1.0$s. It is considered that numerical damping occurred owing to the cell dimensions and the wave period(Tanaka, 1978). Masamura *et al.*(1991) investigated the effect on the simulation result of the wave disintegration by the impermeable submerged breakwater with varying the size of the finite difference mesh. They also presented that as the cell dimension becomes smaller, the accuracy of the calculation is improved. By applying the present sizes of $\Delta x = 0.02$m and $\Delta z = 0.01$m, the higher frequency waves than 1.7Hz($T < 0.59$s) is influenced by the numerical dissipation. It will be improved by employing a finer cell dimension or by developing a finite deference scheme with high accuracy.

Fig. 5.11 shows the comparison between the calculated time history of the velocity and the measured one. The velocity was measured in the middle of the water depth at eight positions where the wave gages were installed. The velocity of the wave component

with the higher frequency decreases as the depth increases. The higher frequency component of velocity disappears in the time history of velocity, although that is seen in the corresponding surface displacement shown in Fig. 5.8. It is considered that the agreement of the calculated with the measured velocity is good although the difference is seen in the DC component.

Fig. 5.12 shows the calculated velocity field from $t/T = 12.75$ for one wave period with the time interval $T/8$ near the permeable submerged breakwater for CASE P–17($T = 1.70$s). Generating vortex is simulated on the leeside of the permeable submerged breakwater. By applying the potential theory to these simulation, vortex is not simulated in the calculation of the wave transformation due to the impermeable breakwater. In this calculation, the vortex generated behind the permeable submerged breakwater is caused by the velocity difference between inside the permeable structure and outside.

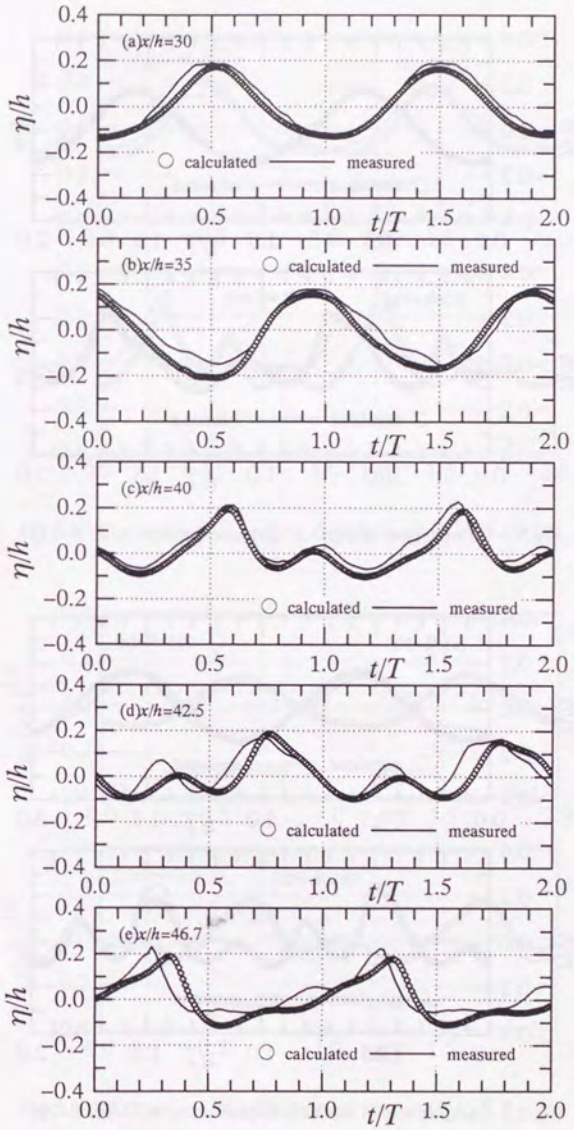

Fig.5.7 Comparison of surface displacements(CASE P–15)

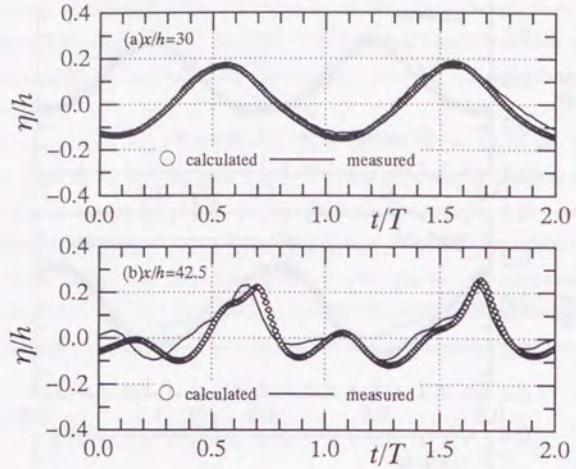

Fig.5.8 Comparison of surface displacements(CASE P-17)

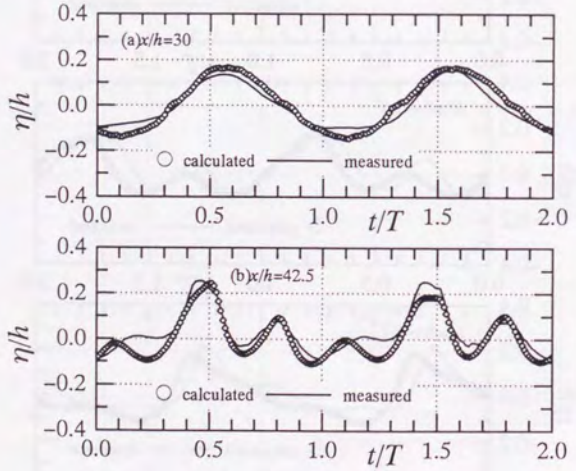

Fig.5.9 Comparison of surface displacements(CASE P-20)

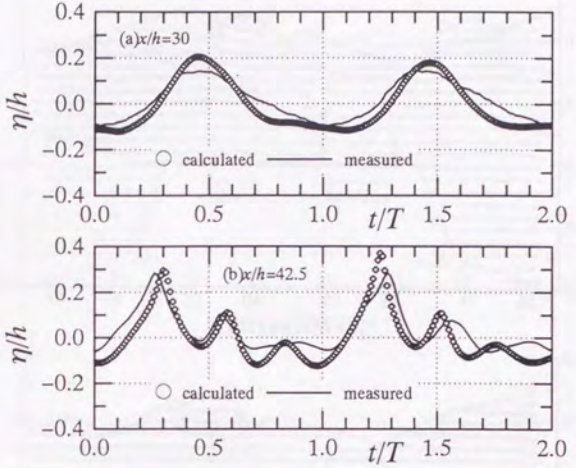

Fig.5.10 Comparison of surface displacements(CASE P-22)

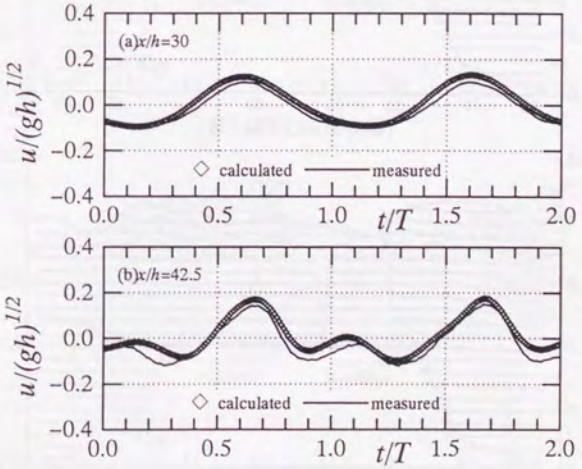

Fig.5.11 Comparison of velocity time history(CASE P-17)

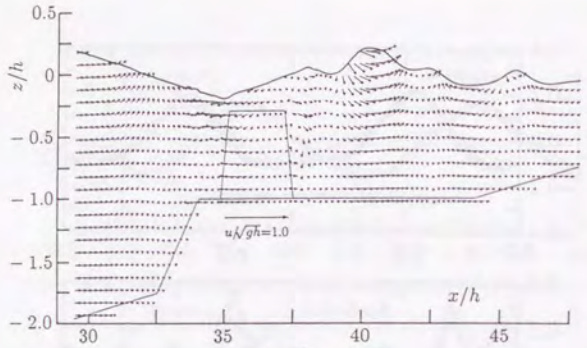

(a) t/T =12.75

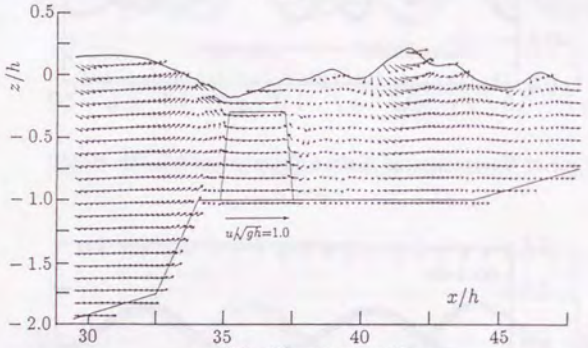

(b) t/T =12.75+1/8

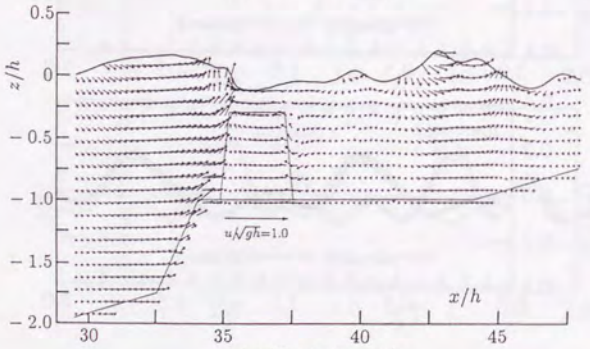

(c) t/T =12.75+2/8

Fig.5.12 Simulated results of velocity field(CASE P–17)–1–

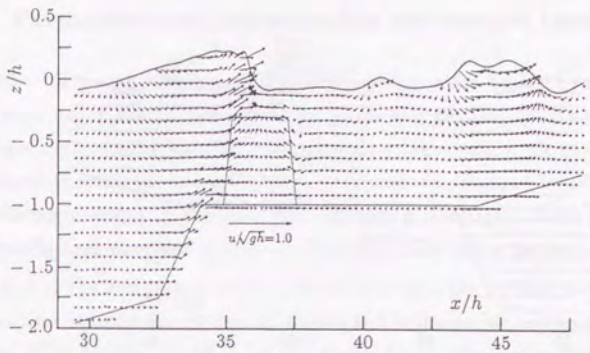

(d) t/T =12.75+3/8

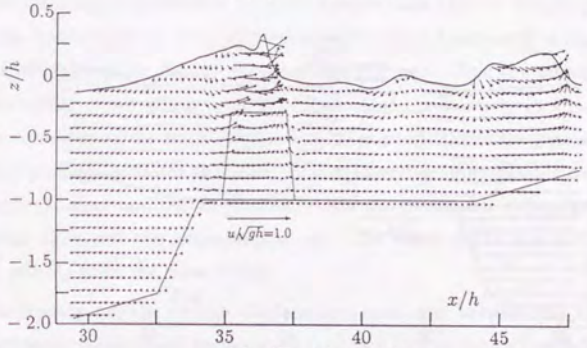

(e) t/T =12.75+4/8

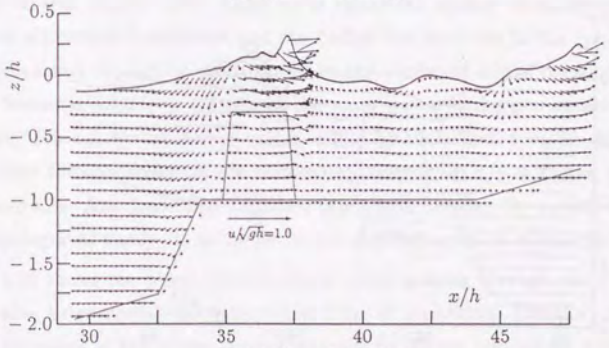

(f) t/T =12.75+5/8

Fig.5.12 Simulated results of velocity field(CASE P–17)–2–

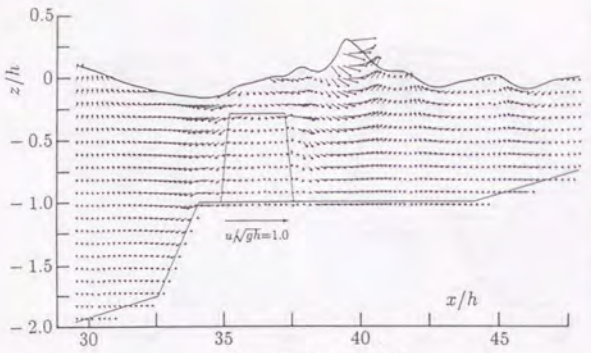

(g) t/T =12.75+6/8

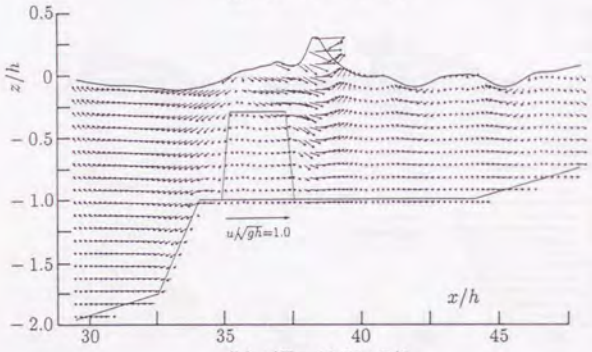

(h) t/T =12.75+7/8

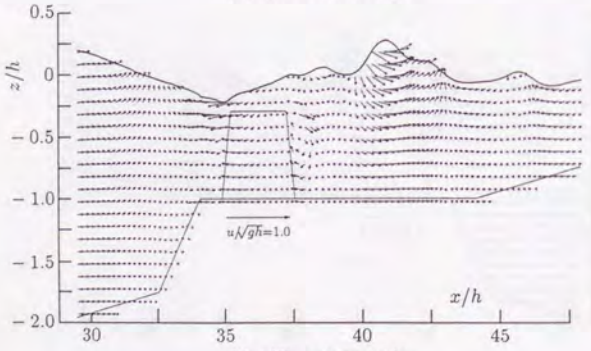

(i) t/T =12.75+8/8

Fig.5.12 Simulated results of velocity field(CASE P–17)–3–

5.4.2 Permeable and impermeable submerged breakwater

An effect of the permeability on the wave transformation behind a submerged breakwater is discussed in this section. Mitsui *et al.*(1974) presented the effect of the porosity on the wave run-up using the thin wall submerged breakwaters. However, the effect of the permeability is not investigated using a trapezoidal submerged breakwater. Here the effect of the permeability on the wave disintegration is investigated both numerically and experimentally from the point of view of the velocity field inside the permeable structure.

Fig. 5.13 is the comparison of the velocity field and the surface profile at the same calculated time between due to the permeable and impermeable submerged breakwaters (T = 1.0s, H = 0.035m, CASE P–10 and CASE I–10). The surface profile on the impermeable submerged breakwater becomes steeper than that on the permeable one. It is because the water depth on the impermeable submerged breakwater is shallow comparing with "the effective water depth" at the permeable one. Here the effective water depth means the water depth which includes an effect of the porosity in the permeable submerged breakwater on the water depth. The wave passing over the permeable submerged breakwater propagates faster than that passing over the impermeable one. The effective water depth is larger and the wave celerity over the permeable submerged breakwater is greater than that over the impermeable one. The water depth has a stronger effect on the wave celerity than the wave height.

The comparison of the surface displacement measured between due to the permeable and impermeable submerged breakwaters is shown in Fig. 5.14 (T = 2.2s, H = 0.089m, CASE P–22 and CASE I–22). Solid curve shows the surface displacement due to the permeable submerged breakwater and the dashed line that due to the impermeable one. Fig. 5.14(a) shows the surface displacement on the windward side of the submerged breakwaters. Secondary crests in troughs of the main waves of the impermeable submerged breakwater denoted by the dashed line is caused by the reflected waves. Figures 5.14(b) and (c) show the comparison of the surface displacement at $x/h = 40$ and $x/h = 42.5$ on the leeward side. Any significant difference is not seen between the surface displacements of the disintegrated waves due to the permeable and impermeable submerged breakwaters.

Fig. 5.15 shows the power spectra of the waves passing through the permeable and impermeable submerged breakwater (T = 2.2s, H = 0.089m, CASE P–22 and CASE I–22). The values of the power spectra denoted by S_n are normalized with that of the first mode S_1. The value of S_1 of the permeable submerged breakwater is larger than

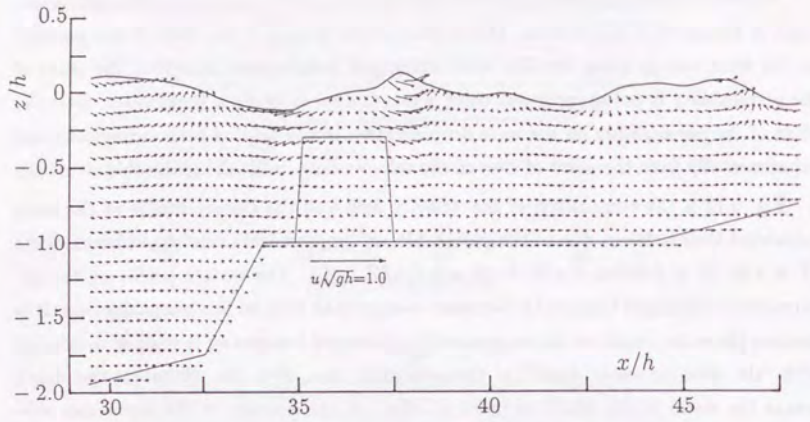

(a) Permeable breakwater(CASE P–10)

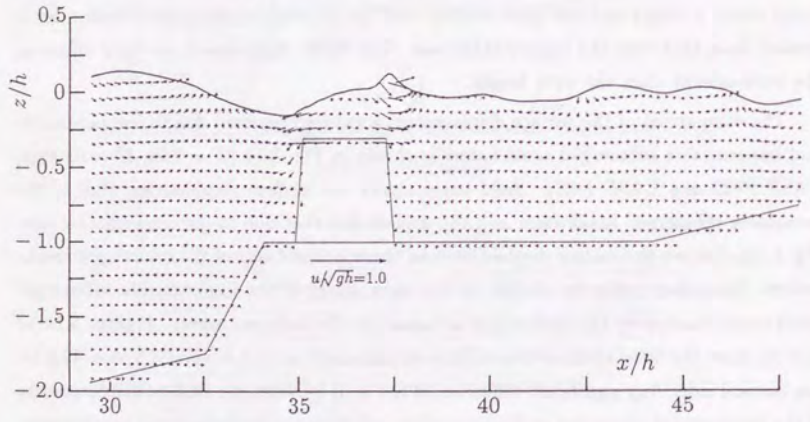

(b) Impermeable breakwater(CASE I–10)

Fig.5.13 Velocity fields around submerged breakwaters

that of the impermeable one. It is because that the wave reflection from the impermeable submerged breakwater is larger than that of permeable one with the wave attenuation in it. Although the wave energy dissipates in the permeable structure, the transmitted wave through the permeable submerged breakwater is greater than that over the impermeable one. It is because the reflected wave from the impermeable submerged breakwater is

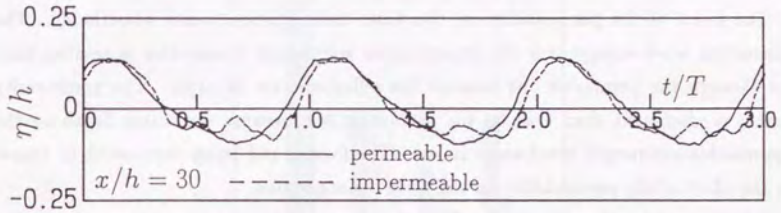

(a) On windward side of submerged breakwater at x/h =30

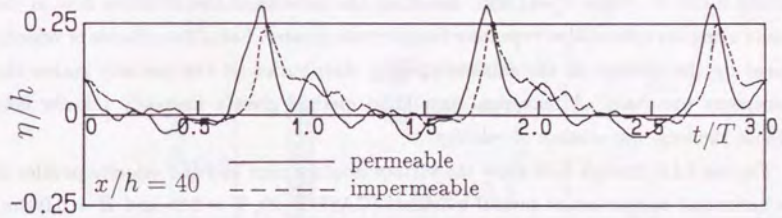

(b) On leeward side of submerged breakwater at x/h =40

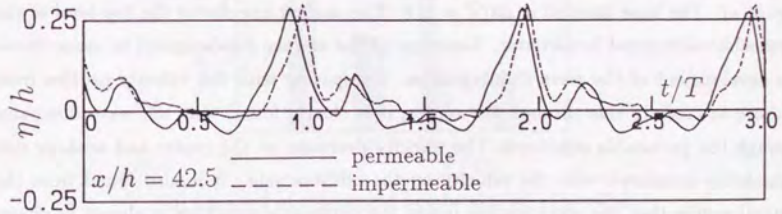

(c) On leeward side of submerged breakwater at x/h =42.5

Fig.5.14 Measured surface displacements of permeable and impermeable submerged breakwaters(CASE P–22 and I–22)

larger than that from the permeable one.

It is concluded that the significant difference is not seen between the normalized spectral values of the secondary wave S_2/S_1 of the permeable and impermeable submerged breakwaters. The following is still left to be discussed more details: the high frequency components of the locked wave are not decomposed from the free wave with the wave power spectrum analysis and the difference between the permeable and impermeable submerged breakwaters is seen in the values of third- and fourth-order of the wave spectra.

The effect of the permeability on the wave disintegration is not remarkably. The transmitted wave energy over the impermeable submerged breakwater is smaller than that through the permeable one because the reflected wave is larger. The nonlinearity is more predominant than that on the permeable one because the water depth on the impermeable submerged breakwater is less. The former and latter facts work to cancel out the effect of the permeability on the wave disintegration.

It is interesting to investigate the effect of the permeability on the wave transformation from the velocity field inside the permeable structure. However, it is difficult to measure velocity inside it. Ueno *et al.*(1989) measured the velocity of the filtration flow in the mound using the optical fiber type laser Doppler velocimeter. Local disturbance of velocity caused by the vortices in the random spacing distribution of the porosity makes the phenomena uncertain. A numerical simulation method gives a unsteady velocity field without the local disturbance of velocity.

Figures 5.16 through 5.18 show the surface displacement and the velocity profiles of the horizontal component at several moments (CASE P–22, $T = 2.2$s and $H = 0.089$m) on the offshore side, at the center and on the onshore side, respectively. Numbers added to the curves of velocity profile denote the phase time of the surface displacement in Figure(a). The time interval is $\Delta t/T = 1/8$. The dashed line shows the top level of the permeable submerged breakwater. Variation of the surface displacement in space shows the development of the wave disintegration. Comparing with the velocity profiles from offshore to onshore side through the center, it is clearly found that the wave dissipates through the permeable structure. The velocity decreases at the center and onshore side remarkably compared with the velocity on the offshore side. It is also found from the vertical profile that the wave motion inside the permeable structure is almost in-phase. Figures 5.17 and 5.18 show that the velocity inside the permeable structure is small. Consequently, the difference of the transmitted waves between through the permeable and impermeable is small.

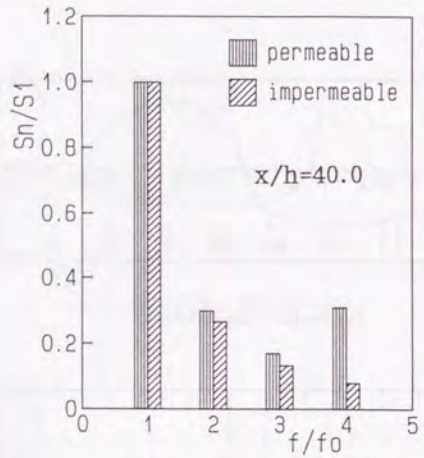

(a) Leeward of submerged breakwater at x/h =40

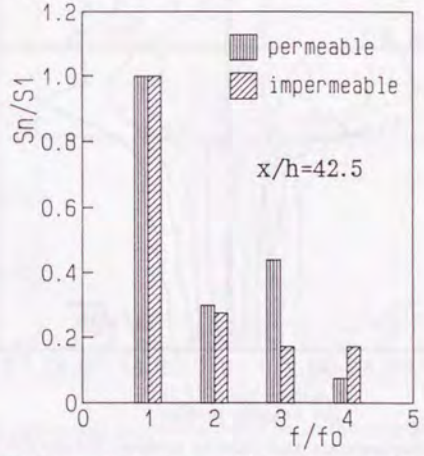

(b) Leeward of submerged breakwater at x/h =42.5

Fig.5.15 Power spectrum of waves passing through permeable and impermeable submerged breakwaters(CASE P–22 and I–22)

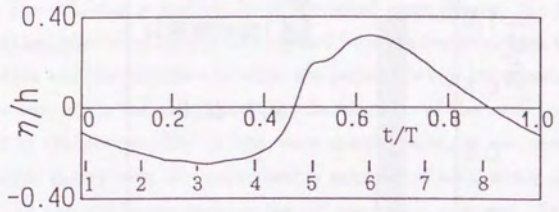

(a) Surface displacement

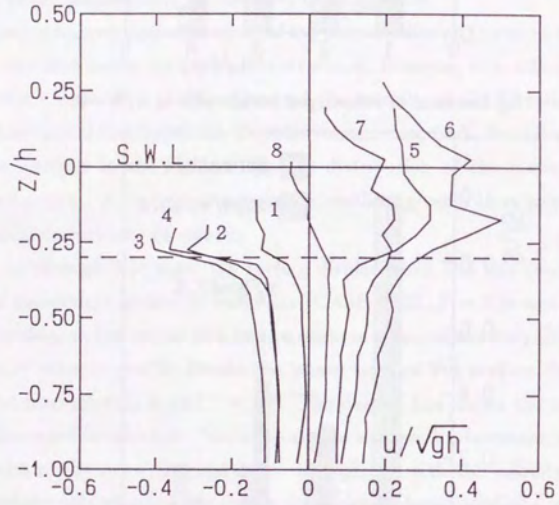

(b) Velocity profiles

Fig.5.16 Surface displacement and velocity profiles offshore(CASE P-22)

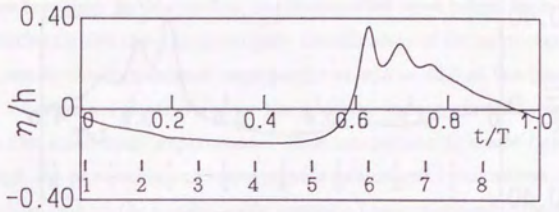

(a) Surface displacement

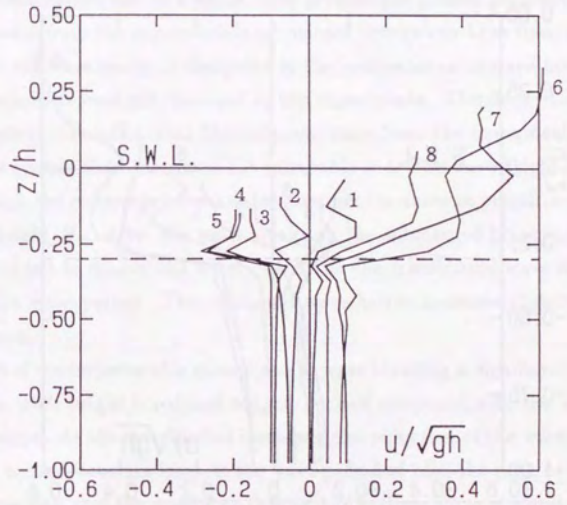

(b) Velocity profiles

Fig.5.17 Surface displacement and velocity profiles in the middle of submerged breakwater(CASE P-22)

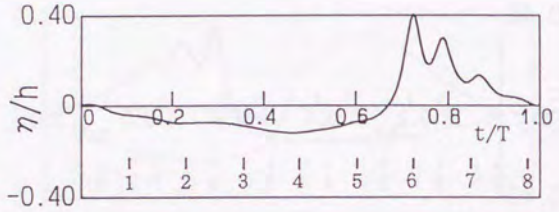

(a) Surface displacement

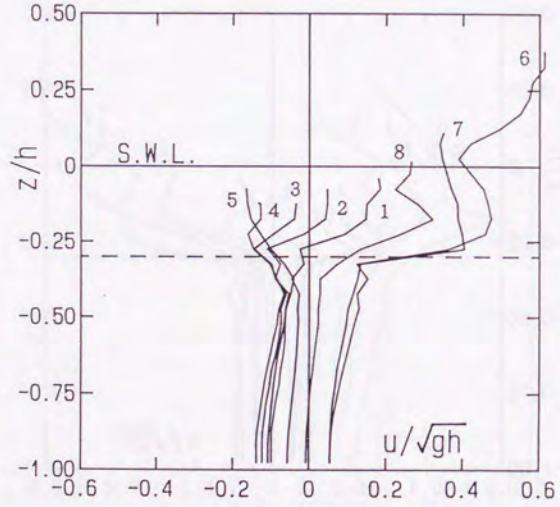

(b) Velocity profiles

Fig.5.18 Surface displacement and velocity profiles onshore(CASE P–22)

5.5 Transmitted wave heights

One main purpose for constructing the submerged breakwater is to reduce the wave height by wave breaking. In this section, the transmitted wave height from nonbreaking to breaking conditions is discussed to investigate the efficiency of the submerged breakwaters.

Fig. 5.19 shows the transmitted wave height at $x/h = 42.5$ of the fundamental wave of which the wave period is the same as the incident wave period through the different structures in the small-scale experiments. The comparison is made between the wave heights through the permeable and impermeable submerged breakwaters, in addition, on the uniform slope and on the impermeable mound. The impermeable mound plays a role of a man-made reef and it influences the wave transformation.

The results of the permeable submerged breakwater are larger than those of the impermeable submerged one as a whole. It is because the greater portion of the incident waves is reflected from the impermeable submerged breakwater than from the permeable one, although the wave energy is dissipated in the permeable submerged breakwater. The reflection coefficients were not obtained in the experiments. Therefore, it was confirmed by the numerical simulation that the reflected wave from the impermeable submerged breakwater is greater than that from the permeable one. The wave height H of the wave passing through the submerged breakwater does not increases in proportion to the deep-water wave height H_0. After the wave breaks on the submerged breakwaters, the wave height is restricted to mainly the water depth and the transmitted wave height is also a function of the wave period. The maximum wave height increases slightly as the wave period increases.

The effect of the impermeable mound on the wave breaking is significant. At $T = 1.2$s, the maximum wave height is reduced roughly by half compared with the wave height on the uniform slope. As the wave period increases, the reduction of the wave height by the impermeable mound becomes less. At the wave period of 2.2s, the ratio of the maximum wave height passing over the mound to that on the uniform slope is about two thirds.

5.6 Scale effect on transmitted waves

Experiments on the wave transformation due to the permeable submerged breakwater were performed with the large-scale model of the model scale $\lambda = 1/8$ and the small-scale model of $\lambda = 1/50$.

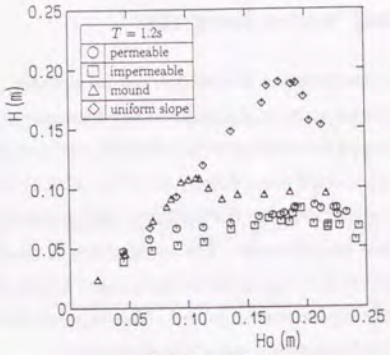

(a) $T = 1.2$s

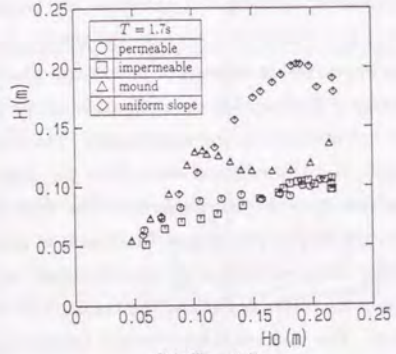

(b) $T = 1.7$s

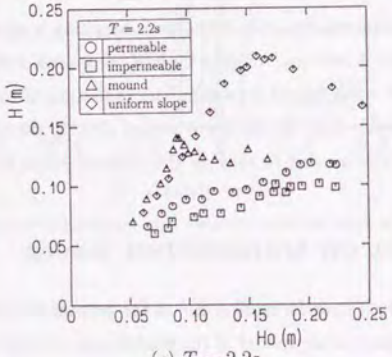

(c) $T = 2.2$s

Fig.5.19 Transmitted wave heights(λ =1/50,h = 0.20m)

Figures 5.20 through 5.22 show the scale effect of the permeable submerged breakwater on the transmitted wave. Figures(a) of each figure show the relationship between the deep-water wave steepness H_0/L_0 and a root-mean-square value of the surface displacement η_{rms} normalized by the water depth h. Solid symbols show the nonbreaking wave on the permeable submerged breakwater. Only one or two from the smallest wave height are the nonbreaking waves. Almost of them are the breaking waves on the submerged breakwaters for each wave period. Figures(b) are the comparison of the time histories of the nonbreaking wave. Figures(c) show the comparison of one of the breaking waves. Significant difference of the root-mean-square value between the large- and small-scale experimental results is not seen in Fig. 5.20 at $h/L = 0.130$. It is confirmed in the comparison of the time histories as shown in Figures 5.20(b) and (c). The same is found in Fig. 5.21 at $h/L = 0.088$. On the other hand, the result at $h/L = 0.067$ shown in Fig. 5.22 shows a significant difference between the large- and small-scale experimental results.

The scale effect of the permeable submerged breakwater on the transmitted wave is caused through the wave reflection, the energy dissipation by the drag force in the body and the breaking wave. It is considered from the numerical simulation results shown in Figures 5.3 and 5.4 that the scale effect on the wave reflection from the submerged breakwater is quite small compared with that on the wave transmission.

As the wave period increases, the velocity profile becomes vertically uniform. The effect of the submerged breakwater on the wave energy dissipation of the long wave becomes predominant compared with the short wave. When the wave height is small, the wave energy dissipates in the body of the permeable submerged breakwater. As the wave height increases, the wave breaking is predominant to the energy dissipation. However, it seems from Fig. 5.22 that the wave energy dissipation due to the drag force is not negligible in the total wave energy dissipation when the wave steepness becomes large under the long wave condition. Consequently, the difference between the large- and small-scale experimental results becomes large when the wave condition approaches the long wave one.

The scale effect on the wave breaking interacting with a permeable breakwater or a submerged breakwater is much complicated. In addition to the nonbreaking wave situation, the scale effect of the wave breaking on the energy dissipation should be investigated. Although the breaking wave can not be simulated with the numerical model at the present stage, it will be improved with a model of the wave breaking with the consideration of

experimental results.

Maruyama(1986) compared the large-scale experimental results of the wave transformation in the surf zone with the experimental formula proposed by Saeki and Sasaki(1973) and Sasaki and Saeki(1974). It was reported that the scale effect on the wave dissipation due to wave breaking is not recognized and it was concluded that the air contained does not influence the wave transformation after the wave breaking. The data with a wide range of wave periods and wave heights were used and the wave heights were normalized with the breaking wave height. However, no exact comparison using results of scale model experiments according to the Froude law is given in Maruyama(1986). Toumazis and Anastasiou(1992) presented the scale effect in breaking waves and concluded that the breaker larger than 0.5m high is independent of the surface tension effect.

Wave breaking is very unstable phenomenon and we have too little data to discuss the scale effects on the wave breaking. The experimental results on the wave breaking interacting with the permeable submerged breakwater were obtained in the present work and shown in Figures 5.20 through 5.22. The qualitative explanation was described above. It is necessary to accumulate experimental data of the scale effect on the interaction of breaking wave with a permeable breakwater in further work with our large wave flume.

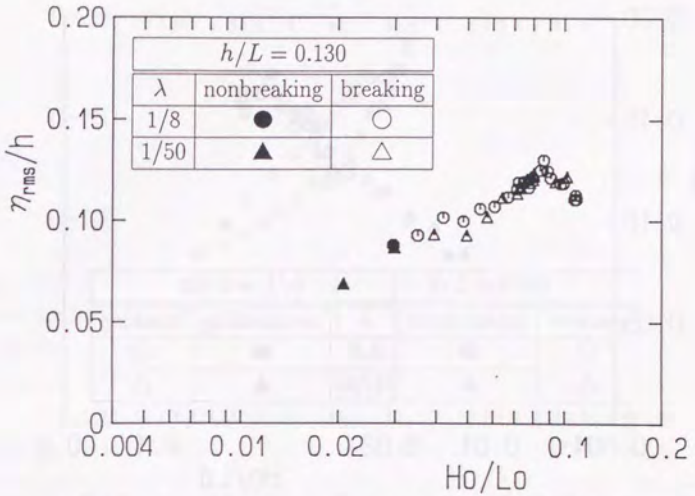

(a) Comparison of root-mean-square value of surface displacement

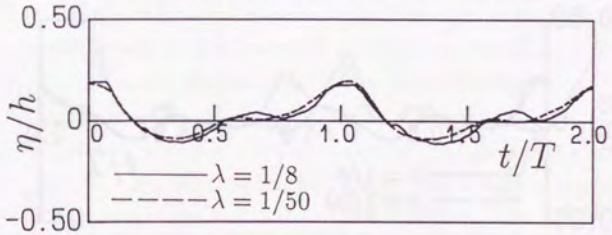

(b) Time history of nonbreaking wave($H_0/L_0 = 0.03$)

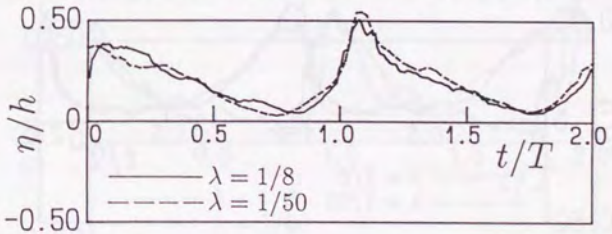

(c) Time history of breaking wave($H_0/L_0 = 0.10$)

Fig.5.20 Scale effect on transmitted wave($h/L = 0.130$)

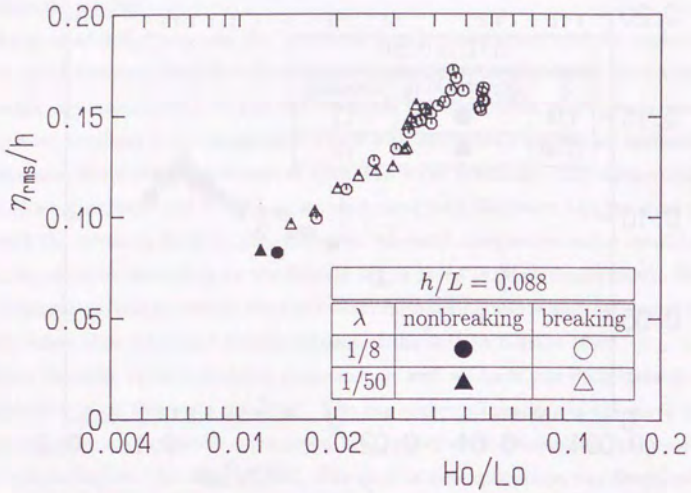

(a) Comparison of root-mean-square value of surface displacement

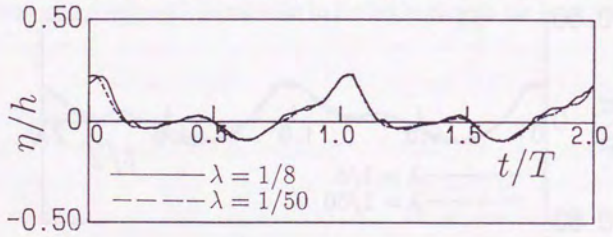

(b) Time history of nonbreaking wave($H_0/L_0 = 0.012$)

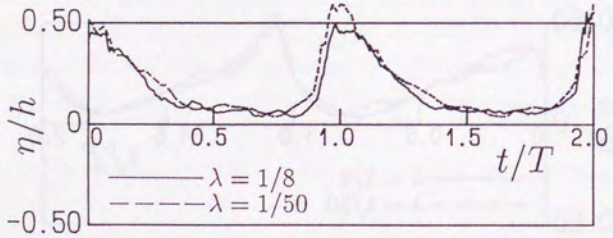

(c) Time history of breaking wave($H_0/L_0 = 0.037$)

Fig.5.21 Scale effect on transmitted wave($h/L = 0.088$)

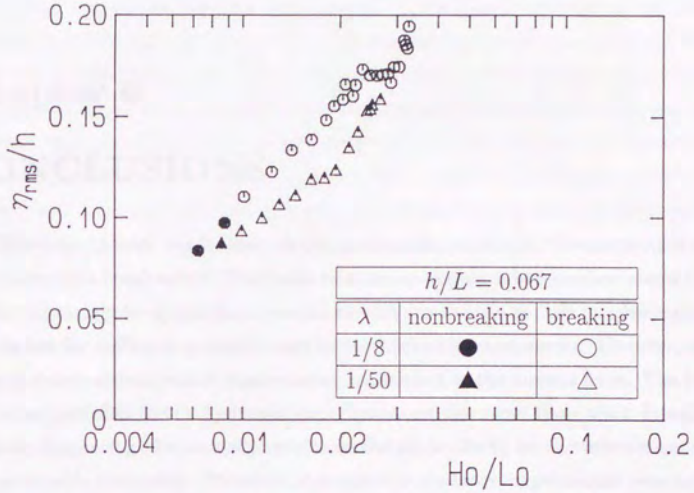

(a) Comparison of root-mean-square value of surface displacement

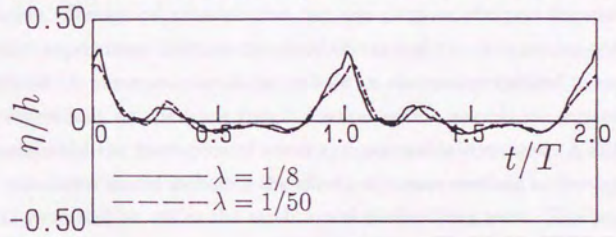

(b) Time history of nonbreaking wave($H_0/L_0 = 0.009$)

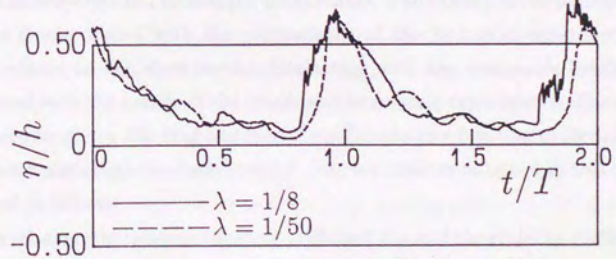

(c) Time history of breaking wave($H_0/L_0 = 0.027$)

Fig.5.22 Scale effect on transmitted wave($h/L = 0.067$)

Chapter 6

CONCLUSIONS

The present work has focused on the phenomena relating to the interaction of waves with permeable breakwaters. The tasks to examine the wave-breakwater interaction were conducted mainly by hydraulic experiments with small-scale models in a laboratory. The Froude law for scaling is normally used in the hydraulic experiments. However, the wave force, the wave reflection and transmission are subject to the viscous force. The Reynolds law is not satisfied in the hydraulic experiments at the same time when Froude law is applied. Neglecting the viscosity results in the scale effects on the interaction of waves and permeable structures. Therefore, systematic scale model experiments were performed in order to investigate the scale effects on the wave force acting on an armor unit and the wave reflection. Theoretical consideration was also given to interpret the scale effects.

Hydraulic experiments involves the scale effects and the information obtained from them is limited. A numerical simulation will be an alternative method to supersede the hydraulic experiment on the wave transformation with a permeable structure. It also helps us understand the interaction of waves and permeable structures. A fully nonlinear numerical simulation model including the effects of porous medium is developed for two-dimensional wave motion under the condition of nonbreaking wave. The present model was applied to simulate the wave motions interacting with the rectangular and trapezoidal permeable breakwaters and submerged breakwaters. The validity of the present simulation model was demonstrated with the comparisons of the hydraulic experimental results. The scale effects on the wave motion interacting with the permeable breakwater were demonstrated with the results of the small- and large-scale experiments. The scale effects are explained by giving the drag and inertia coefficients as a function of Reynolds number to the present numerical simulation model. The conclusions obtained in this research are summarized as follows:

1) The relationship between the drag coefficient C_D and the stability coefficient K_D of Hudson formula is theoretically derived to be that K_D is inversely proportional to the drag coefficient cubed under the condition that the inertia force is negligible. The relationship

is approved by the experiments.

2) The wave force acting on an armor unit in the small-scale model experiments is relatively large compared with that in the large-scale model ones. For incipient instability of armor units, The drag force is predominant to the inertia force because the wave height is normally large. It is because the drag force is nonlinear but the inertia force is linear to the wave height.

3) The scale effect on the stability of armor units can be interpreted as the scale dependent change of the relative drag force due to the neglect of the similarity of the fluid viscosity.

4) The relationship between the reflection coefficient and the wave steepness by the small-scale experiments is qualitatively same as the results of the large scale ones but the difference in quantity is confirmed. It is found that the small-scale experiments underestimate the reflection coefficients. The scale effect on the wave reflection is interpreted as the relationship between the friction factor and the Reynolds number as a parameter of the relative roughness.

5) The numerical simulation model has been developed to predict a nonlinear wave motion including the nonlinear interaction between the waves and the breakwaters. In the present method, once the parameters of the permeable structures such as the porosity, the drag and inertia coefficients are given, the computation is carried out directly without distinguishing the structure domain from the region of the pure water. The present model has been verified through the comparison with the hydraulic experiments with the rectangular permeable breakwaters. The effects of the dang and inertia coefficients on the wave reflection and transmission are examined. It is found that as the inertia coefficient increases, the reflection coefficient increases and as the drag coefficient increases, the transmission coefficient decreases.

6) The present simulation model was applied to compute the wave transformation in and near a trapezoidal rubble-mound breakwater. The wave run-up and run-down on the rubble-mound breakwater as well as the reflected and transmitted waves of the nonlinear wave can be estimated by using this model. The wave force acting on the armor units in the armor layer of the breakwater is estimated with the numerically simulated results of the wave run-up and run-down and the drag and inertia coefficients of Tetrapods.

7) The application of the present model to the computation of the wave transformation due to a caisson breakwater covered with armor units and stones was also made. The wave pressure acting on the caisson in the permeable materials was calibrated with the

results obtained in the hydraulic experiments. The numerical simulation can well reproduce the experimental results. Large-scale experiments as well as small-scale one were performed synthetically to investigate the scale effect on the wave pressure, reflection and transmission. As the model scale increases, the wave pressure decreases. It is because the wave reflection increases and the wave transmission through the permeable structure decreases. By applying the numerical simulation model to the wave transformation with the various values of the drag and inertia coefficients, the mechanism of the scale effect on the wave pressure, reflection and transmission is interpreted. As the model scale increases, the inertia coefficient of a massive structure such as a permeable breakwater increases. On the other hand, the drag coefficient decreases as the model scale increases.

8) The wave disintegration behind the permeable submerged breakwater was simulated for various wave periods within a condition of nonbreaking wave. The simulated results of the surface displacements both on the leeward and windward sides were in fairly good agreement with the experimental results. The effect of the permeability of the submerged breakwater on the wave disintegration was investigated through the comparison of the measured surface displacements and their wave spectra. The insignificant difference of the surface displacement of the disintegrate wave is seen between the permeable and impermeable breakwaters. The velocity profiles in the permeable submerged breakwater were evaluated with the present model to explain the effect of the permeability on the wave disintegration. It is found that the velocity in the permeable submerged breakwater is small and that results in the insignificant difference of the surface displacements behind the permeable and impermeable submerged breakwaters.

9) The scale effect on the interaction of the wave and permeable structure is summarized as follows: The scale effect of the permeable breakwater is subject to both the drag and inertia force, while the scale effect on the wave force acting on an armor unit is mainly caused by the drag force. The permeable breakwater is more massive than an armor unit. Therefore, the inertia force acting on the massive breakwater is not negligible compared with that on the armor unit. The scale effect of the submerged breakwater is less significant than that of the rectangular and trapezoidal permeable breakwaters. It is because that the submerged breakwater is not exposed to an intense wave motion near and above the still water level, while the rectangular and trapezoidal permeable breakwaters are.

10) It is concluded that the present numerical simulation model is applicable for the evaluation of nonbreaking wave motion near and in a permeable breakwater with an arbitrary configuration and an impermeable structure. The scale effect can be considered

into the numerical simulation by giving the drag and inertia coefficients as functions of the model scale. Although the quantitative discussion of the drag and inertia coefficients is still insufficient, the characteristic of these coefficients to reflect the scale effect is qualitatively given in the present work.

We have depended on hydraulic experiments to investigate the wave transformation by a permeable breakwater and the stability of armor units in breakwaters so far. We can become to compute the nonbreaking wave motion in and near a permeable breakwater by using the present model. Extension of the present model to three-dimensional non breaking wave field is possible, if a super computer is available. A calculation method of a free surface of discontinuous fluid motion should be conducted to simulate breaking wave. It is also necessary to involve a model of energy dissipation due to the wave breaking. Then a numerical simulation method will supersede a hydraulic experiment on the wave transformation due to a permeable structure.

REFERENCES

Amsden, A.A. and F.H.Harlow(1970): The SMAC method: A numerical Technique for calculating incompressible fluid flows, Los Alamos Scientific Laboratory of the University of California, Report LA-4370, 85p.

Brarends,F.B.J. and P.Hölscher(1988): Modelling interior process in a breakwater, *Proc. of the conference Breakwater '88*, pp.49-58.

Burcharth,H.F., G.L.Howell and Z.Liu(1991): On the determination of concrete armour unit stresses including specific results related to Dolosse, *Coastal Engineering*, 15, pp.107-165.

Byrne, R.J.(1969): Field occurences of induced multiple gravity waves, *J. Geoph. Res.*, Vol.74, No.10, pp.2590–2596.

Chan, R.K.C. and R.L. Street(1970): A computer study of finite-amplitude water waves, *J. Computational Physics*, 6, pp.68-94.

Chandler, P.L., Jr. and R.M. Sorensen(1972): Transformation of waves passing a submerged bar, *Proc. 13th Coastal Engineering Conf.*, ASCE, pp.385–404.

Dai, Y.B. and A.M. Kamel(1969): Scale effects tests for rubble mound breakwaters, U.S. Army Engineer, Waterways Experiment Station, Research Report H-69-2.

Deguchi, I., T. Sawaragi and H. Shirotani(1988): Applicability of non-linear Darcy law to the analysis of wave deformation on a permeable bed, *Proc. 35th Japanese Conf. Coastal Engineering*, JSCE, pp.487-491(in Japanese).

Delmonte, R.C.(1972): Scale effects of wave transmission through permeable structure, *Proc. 13th Coastal Engineering Conf.*, ASCE, Vol.3, pp.1867–1872.

Fan, Q., A. Watanabe and K. Horikawa(1983): Experimental study on the stability of a concrete block mound breakwater under irregular waves, *Proc. 30th Japanese Conf. Coastal Engineering*, JSCE, pp.352–356(in Japanese).

Fujima, K., T. Goto and N. Shuto(1984): Numerical investigation on validity of the equations for nonlinear dispersive waves, *Proc. 31st Japanese Conf. Coastal Engineering*,JSCE, pp.93–97(in Japanese).

Fujimoto, T., N. Abe and H. Hasegawa(1982): Experimental study on characteristics of wave dissipating concrete armor units, Report of Central Research Institute of Electric Power Industry, No.382001, 39p(in Japanese).

Goda Y. and S. Kakizaki(1966): Study on finite amplitude standing waves and their pressure upon a vertical wall, *Coastal Engineering in Japan*, Vol.13, pp.43–54. Report of

Port and Harbour Research Institute, Vol.5, No.10, 57p(in Japanese).

Goda Y. and S. Kakizaki(1967): Study on finite amplitude standing waves and their pressure upon a vertical wall, *Coastal Engineering in Japan*, Vol.10, pp.1–10.

Goda, Y.(1970): A synthesis of breaker indices, *Trans, Japan Society of Civil Engineers*, Vol.2, Part 2, pp.227–230.

Goda, Y. and Y. Suzuki(1976): Estimation of incident and reflected waves in random wave experiments, *Proc. 15th Coastal Engineering Conf.*, pp.828–845.

Goda, Y.(1985): Random seas and designs of maritime structures, University of Tokyo Press, 323p.

Günbak, A.R.(1978): Large scale model tests of placed stone breakwaters, *Proc. ASCE J. of the Waterways, Port, Coastal and Ocean Engineering Div.*, Vol.104, WW4, pp.353–355.

Hattori,M., K. Inagaki, Y. Noguchi and T. Endo(1988): Wave force on breakwaters with concrete block mound, *Proc. 21st Coastal Engineering Conf.*, pp.2144–2158.

Hino, T., H. Miyata and H. Kajitani(1983): A numerical solution method for nonlinear shallow water waves, J. Soc. Naval Arch. Japan, Vol.153, pp.1–20.

Hölscher, P., M.P. de Groot and J.W. van der Meer(1988): Simulation of internal water movement in breakwater, Modelling Soil-Water-Structure Interaction,pp.427-433.

Horikawa,K. and S.Komori(1968): On mechanism of wind waves decay due to submerged breakwater, *Proc. 15th Japanese Conf. Coastal Engineering*, JSCE, pp.340–349(in Japanese).

Hudson, R.Y.(1959): Laboratory investigation of rubble mound breakwaters. *Proc. of ASCE*, Vol.85, No.WW3.

Ippen, A.T.(1966): Estuary and coastline hydrodynamics, McGraw-Hill,744p.

Isobe,M., H.Nishimura and K.Horikawa(1978): Expressions of perturbation solutions for conservative waves by using wave height, *Proc. 33rd Annu. Conf. of JSCE*, II, pp.760–761(in Japanese).

Isobe, M., K. Shiba, C.E. Cruz and A. Watanabe(1991): Nonlinear wave transformation due to submerged breakwater, *Proc. Coastal Engineering*, JSCE, Vol.38(2), pp.551–555(in Japanese).

Izumiya, T. and M. Endo(1989): Wave reflection and transmission due to a submerged breakwater, *Proc. Coastal Engineering*, JSCE, Vol.36, pp.638–642(in Japanese).

Izumiya,T., H. Hurumata and J. Mizukami(1990): Evaluation of friction factor and local reflection coefficient for submerged structure, *Proc. Coastal Engineering*, JSCE,

Vol.37, pp.544–548(in Japanese).

Izumiya, T.(1990): Extension of mild slope equation for waves propagating over a submerged breakwater, *Proc. 22nd Coastal Engineering Conf.*, ASCE, pp.306–315.

Johnson, J.W., H. Kondo and R. Wallihan(1966): Scale effect in wave action through porous structure, *Proc. 10th Coastal Engineering Conf.*, ASCE, Vol.2, pp.1022–1024.

Jonsson, I.G.(1963): Measurements in the turbulent wave boundary layer, *10th Congress IAHR*, London, pp.85–92.

Juhl, J. and O.J. Jensen(1990): Wave forces on breakwater armor units, *Proc. 22nd Coastal Engineering Conf.*, ASCE, pp.1538–1551.

Kobayashi, N. and J.H. Greewald(1986): Prediction of wave run-up and riprap stability, *Proc.20th Coastal Engineering Conf.*, ASCE, pp.1958–1971.

Kojima, H., A. Yoshida and T. Ijima(1991): Study on nonlinear interaction between submerged plate and wave, *Proc. Coastal Engineering*, JSCE, Vol.38(2), pp.556–560(in Japanese).

Kondo, H.(1970): An analytical approach to wave transmission through permeable structures, *Coastal Engineering in Japan*, JSCE, Vol.13, pp.31–42.

Kondo,H., S.Fujima and J.Asama(1972): Hydraulic characteristic of permeable structure, *Proc.19th Japanese Coastal Engineering Conf.*, JSCE, pp.193–197(in Japanese).

Kondo, H. and H. Takeda(1981): Wave energy dissipating structure, Morikita Shuppan, 275p.(in Japanese).

Le Méhauté,B.(1976): An introduction to hydrodynamics & water waves, Springer-Verlag, 315p.

Madsen, O.M. and C.C. Mei(1969): The transformation of a solitary wave over uneven bottom, *J. Fluid Mech.*, Vol.39, pp.781–791.

Madsen, O.S. and S.M. White(1976a): Reflection and transmission characteristics of porous rubble-mound breakwaters, Miscellaneous Report No.76-5, CERC, 138p.

Madsen, O.S. and S.M. White(1976b): Energy dissipation on a rough slope, *J. Waterways, Harbour and Coastal Engineering*, ASCE, Vol.102, No.WW1, pp.31–48.

Maruyama, K.(1986): Study on wave transformations on mild slope bottom, Doctoral dissertation, The University of Tokyo, 320p(in Japanese).

Masamura, T., K. Fujima, K. Hayashi and T. Shigemura(1991): Numerical analysis on wave transformation over submerged breakwater, *Proc. 46th Annu. Conf.*, JSCE, 2, pp.962–963(in Japanese).

Massel, S.R.(1983): Harmonic generation by waves propagating over a submerged step,

Coastal Engineering, Vol.7, pp.357–380.

McNair, E.C., Jr. and R.M. Sorensen(1970): Characteristics of waves broken by a longshore bar, *Proc. 12th Coastal Engineering Conf.*, ASCE, pp.415–434.

Mei, C.C. and J.L. Black(1969): Scattering of surface waves by rectangular obstacles in waters of finite depth, *J. Fluid Mech.*, Vol.38, pp.499–511.

Mei, C.C.(1983): The applied dynamics of ocean surface waves, John Wiley & Sons, 740p.

Mitsui, H., S. Tsutsui and T. Takeuchi(1974): *Proc. 21th Japanese Coastal Engineering Conf.*, JSCE, pp.387–391(in Japanese).

Miyata, M(1986): Finite-difference simulation of breaking waves, *J. Computational Physics*, 65, pp.179–214.

Mizutani, N.(1989): Fundamental study on characteristics wave forces acting on a submerged sphere, Doctoral thesis, Nagoya University, 161p.(in Japanese).

Morison, J.R., M.P. O'Brien and J.W. Johnson(1950): The wave force exerted by surface wave on piles, *Petroleum Trans.*, AIME, Vol.189. pp.149–157.

Nagai, S., K. Kurata and K. Hasegawa(1977): Effect of breadth of submerged breakwater on wave energy dissipation, *Proc. 24th Japanese Coastal Engineering Conf.*, JSCE, pp.303–308(in Japanese).

Nakamura, M., H. Shiraishi and Y. Sasaki(1966): On wave energy dissipation due to submerged breakwater, *Proc. 13th Japanese Coastal Engineering Conf.*, JSCE, pp.76–79(in Japanese).

Nakamura, T. and T. Onozuka(1988): Mechanisms of wave attenuation due to a concrete block breakwater, *Proc. 35th Japanese Coastal Engineering Conf.*, JSCE, pp.712–716(in Japanese).

Nichols, B.D., C.W. Hirt and R.S. Hotchkiss(1980): SOLA-VOF : A solution algorithm for transient fluid flow with multiple free boundaries, Los Alamos Scientific Laboratory report, LA-8355, University of California, 119p.

Nishimura,H. and S.Wakatake(1988): Numerical analysis of two-dimensional wave motion using Lagrangian description, *Proc.JSCE*,No.393,II-9,pp.191–199(in Japanese).

Ohyama, T.(1987): A boundary element analysis for cnoidal wave run-up, *Proc. JSCE*, No.381, II-7, pp.189–198(in Japanese).

Ohyama, T and K. Nadaoka(1990): Wave-absorbing filter for open boundary in numerical wave tank, *Proc. Coastal Engineering*, Vol.37, JSCE, pp.16-20(in Japanese).

Ohyama, T and K. Nadaoka(1991a): Development of a numerical wave tank for analysis of nonlinear and irregular wave field, *Fluid Dynamics Res.*, 8, pp.231–251.

Ohyama, T. and K. Nadaoka(1991b): Analysis of wave disintegration due to submerged breakwater by using numerical wave tank, *Proc.Coastal Engineering*,JSCE,Vol.38(1), pp.16–20(in Japanese).

Oumeraci, H.(1984): Scale effects in coastal hydraulic models, IAHR, *Symp. on scale effects in modelling hydraulic structures*, pp.7.10-1–7.10-7.

Oumeraci, H. and H.W. Partenscky(1992): Wave-induced pore pressure in rubble mound breakwaters, *Proc. 22nd Coastal Engineering Conf.*, ASCE, Vol.2, pp.1334–1347.

Rojanakamthorn S., M. Isobe and A. Watanabe(1989): A mathematical model of wave transformation over a submerged breakwater, *Proc. Coastal Engineering*, JSCE, Vol.36, pp.643–647(in Japanese).

Rojanakamthorn S., M. Isobe and A. Watanabe(1990): Modeling of wave transformation on submerged breakwater, *Proc. 22nd Coastal Engineering Conf.*, Vol.1, pp.1060–1073.

Saeki, H. and M. Sasaki(1973): Study on wave transformation after wave breaking(1), *Proc. 20th Japanese Coastal Engineering Conf.*, JSCE, pp.559–564(in Japanese).

Sakakiyama, T. and S. Saito(1988) Behaviors and scale effect of wave reflection and wave run-up on armored breakwater, Report of Central Research Institute of Electric Power Industry, U88023,41p.(in Japanese).

Sakakiyama, T.(1989): Scale effect on wave reflection of breakwaters, *Proc. Civil Engineering in the Ocean*, JSCE, Vol.5,pp.279–284(in Japanese).

Sakakiyama, T. and S. Ushijima(1989): Effect of current profile on wave transformation, *Proc. 44th Annu. Conf.*, JSCE, II, pp.608–609(in Japanese).

Sakakiyama, T. and R. Kajima(1989): Scale effect of wave force on armor units, *Proc. Coastal Engineering*, Vol.36, JSCE, pp.653–657(in Japanese).

Sakakiyama, T. and R. Kajima(1990): Scale effect of wave force on armor units, *Proc. 22nd Coastal Engineering Conf.*, ASCE, Vol.2, pp.1716–1729.

Sakakiyama, T., N. Abe and R. Kajima(1990a): Porous body model analysis of nonlinear wave transformation through permeable structures, *Proc. Coastal Engineering*, JSCE, Vol.37, pp.554–558(in Japanese).

Sakakiyama, T., N. Abe and R. Kajima(1990b): Porous body model analysis of nonlinear wave transformation through permeable structures, Report of Central Research Institute of Electric Power Industry, U91048, 48p(in Japanese).

Sakakiyama, T(1991): Nonlinear-wave interaction with permeable breakwaters, *Extended Abstracts of 4th International Conference on Computing in Civil and Building Engi-*

neering, 405p.

Sakakiyama, T. and R. Kajima(1991): On dispersion relation in permeable breakwater, *Proc. 46th Annu. Conf. of JSCE*, 2, pp.868–869(in Japanese).

Sakakiyama, T., R. Kajima and N. Abe(1991): Numerical simulation of wave motion in and near trapezoidal breakwaters *Proc. Coastal Engineering*, JSCE, Vol.38(2), pp. 546–550(in Japanese).

Sakakiyama, T.(1992): Numerical analysis of wave disintegration due to submerged breakwaters, *Proc. Coastal Engineering*, JSCE, Vol.39(2), pp.625–629(in Japanese).

Sakakiyama, T. and R. Kajima(1992): Numerical simulation of nonlinear wave interacting with permeable breakwaters *Proc. 23rd Coastal Engineering Conf.*, ASCE, Vol.2, pp.1517-1530.

Sasaki, M. and H. Saeki(1974): Study on wave transformation after wave breaking(1), *Proc. 21st Japanese Coastal Engineering Conf.*, JSCE, pp.559–564(in Japanese).

Sarpkaya, T.(1976): In-line and transverse force on cylinders in oscillatory flow at high Reynolds number, *Proc. of the Offshore Technology Conference*, Vol.2, pp.95–108.

Sastry,S.V.L.N., P.Hölscher and F.B.J.Barends(1991): Numerical determination of wave transmission through a rubblemound breakwater at Visakhapatnam, India, *Coastal Engineering*, 15, pp.41–57.

Sawaragi, T., C.R. Ryu and M. Kusumi(1984): Study on design method of rubble mound breakwater against irregular waves, *Proc. 31th Japanese Conf. Coastal Engineering*, JSCE, pp.567–570(in Japanese).

Sawaragi, T. and M. Nochino(1989): Water wave breaking on uniform slope, *in Numerical Methods in Fluid Dynamics II*, pp.862–866.

Scarlatos, P.D. and V.P. Singh(1987): Long-wave transmission though porous breakwaters, *Coastal Engineering*, 11, pp.141–157.

Seiho,T., K.Fujima, K.Hayashi and T.Shigemura(1990): Numerical calculation of breaking waves using MAC method, *Proc. 45th Annu. Conf. of JSCE*, 2, pp.738–739(in Japanese).

Sha, W.T., H.M. Domanus, R.C. Schmitt, J.J. Oras and E.I.H. Lin(1978): COMMIX-1 : A three dimensional transient single-phase component computer program for thermal-hydraulic analysis, Argonne National Laboratory, NUREG/CR-0785, ANL-77-96.

Shimada,A., T.Fujimoto, S.Saito, T.Sakakiyama and H.Hirakuchi(1986): Scale effects on stability and wave reflection regarding armor units, *Proc. 20th Coastal Engineering Conf.*, ASCE, Vol.3, pp.2238–2252.

Shuto, N. and H. Hashimoto(1970): Hydraulics resistance of artificial concrete blocks, *Coastal Engineering in Japan*, Vol.13, pp.43–54.

Simm,J.D. and T.S. Hedges(1988): Pore pressure response and stability of rubble-mound breakwaters, *Proc. Conference Breakwater '88*, pp.59–69.

Sollitt, C.K. and R.H. Cross(1972): Wave transmission through permeable breakwaters, *Proc. 13th Coastal Engineering Conf.*, ASCE, pp.1823–1846.

Sollitt,C.K. and R.H. Cross(1976): Wave reflection and transmission at permeable breakwaters, CERC Technical Paper No.76-8, July, 172p.

Sollitt, C.K. and D.H. Debok(1976): Large scale model tests of placed stone breakwaters, *Proc. 15th Coastal Engineering Conf.*, ASCE, pp.2572–2588.

Tabuchi,M. and K.Takikawa(1978): Flow resistance of a permeable structure, *Proc.25th Japanese Coastal Engineering Conf.*, JSCE, pp.402–406(in Japanese).

Tadjbaksh, I. and J.B. Keller(1960): Standing surface waves of finite amplitude, *J. Fluid Mech.*, 8, p.442–451.

Takikawa, K., H. Yamada, M. Arimoto and M. Tabuchi(1991): Inner characteristics of wave breaking process on slope and its numerical analysis, *Proc. Coastal Engineering*, JSCE, Vol.38(1), pp.61–65(in Japanese).

Tanaka, N.(1978): Fundamental study on analytical method for open channel hydraulics using numerical simulation, Doctoral dissertation,Kyoto University,87p(in Japanese).

Tanimoto, K., S. Takahashi and T. Kitatani(1981): Experimental study of impact breaking wave forces on a vertical-wall caisson of composite breakwater, Report of Port and Harbour Research Institute, Vol.20, No.2, pp.3–39(in Japanese).

Thomsen, A.L., P.E. Wohlt and A.S. Harrison(1972): Riprap stability on earth embankment tested in large- and small-scale wave tanks, CERC Technical Memorandum, No.37.

Tørum ,A., B. Mathiesen and R. Escutia(1979): Scale and model effects in breakwater tests, *Proc. Port and Ocean Engineering under Arctic Conditions*, Norway, pp.1335–1350.

Toumazis, A.D. and K. Anastasiou(1992): Scale effects in breaking waves, *Proc. 22nd Coastal Engineering Conf.*, ASCE, pp.973–985.

Ueno, S., H. Koyama, K. Ishino, T. Uda and S. Murai(1989): Flow field and scouring pattern around submerged breakwater with a sloping plate, *Proc. Coastal Engineering*, JSCE, Vol.36, pp.424–428(in Japanese).

Van der Meer, J.W.(1988): Rock slopes and gravel beaches under wave attack, Doctoral

thesis, Delft University of Technology, The Netherlands, 152p.

Van der Meer, J.W. and G. Heydra(1990): Impact velocities of rocking armour units, *ASCE Proc. Seminar Stresses in Concrete Armour Units*, pp.327–343.

Welch,J.E., F.H.Harlow, J.P.Shannon and B.J.Daly(1966): The MAC method. A computing technique for solving viscous, incompressible, transient fluid-flow problems involving free surfaces, Los Alamos Scientific Laboratory of the University of California, Report LA-3425, 145p.

Wibbeler, H., Th. Hartmann and U. Meissner(1991): Numerical FEM-studies of rubble mound breakwaters – a comparison between calculated and measured data –, *Extended Abstracts of 4th International Conference on Computing in Civil and Building Engineering*, 405p.

Wibbeler, H. and H. Oumeraci(1992): Finite element simulation of wave-induced internal flow in rubble mound structures, *Proc. 23nd Coastal Engineering Conf.*, ASCE, pp.1706-1719.

Wilson, K.W. and H.R. Cross(1972): Scale effects in rubble-mound breakwaters, *Proc. 13th Coastal Engineering Conf.* ASCE, Vol.2, pp.1873–1884.

Wurjanto, A. and N. Kobayashi(1992): Irregular wave prediction and run-up on permeable slope, *J. Waterway, port, coastal and ocean Engineering*, ASCE(submitted).

Yasuda, T., M. Hara and M. Tanaka(1989): A computational method of the deformation including overturning of a solitary wave over a submerged obstacle, *in Numerical Methods in Fluid Dynamics II*, pp.919–924.

Yu, X.(1990): Study on wave transformation over submerged plate, Doctoral dissertation, The University of Tokyo, Japan, 153p.

Appendix A

RESULTS OF WAVE TRANFORMATION

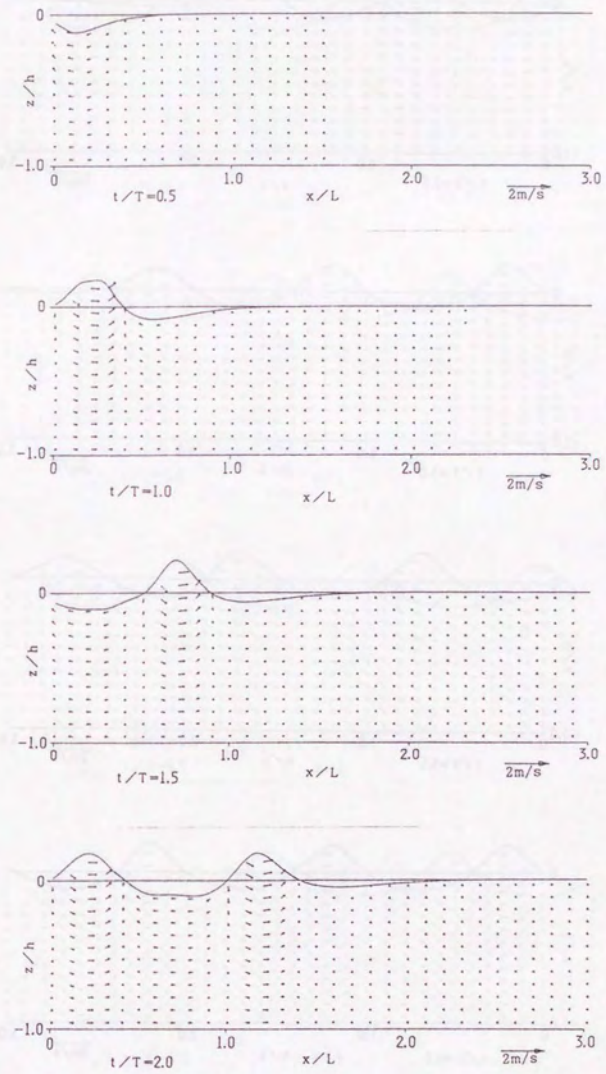

Fig.A.1 Succesive stages of progressive wave propagation from still water state –1– (Stokes wave, $H = 0.15$m, $T = 2.0$s, $h = 0.50$m)

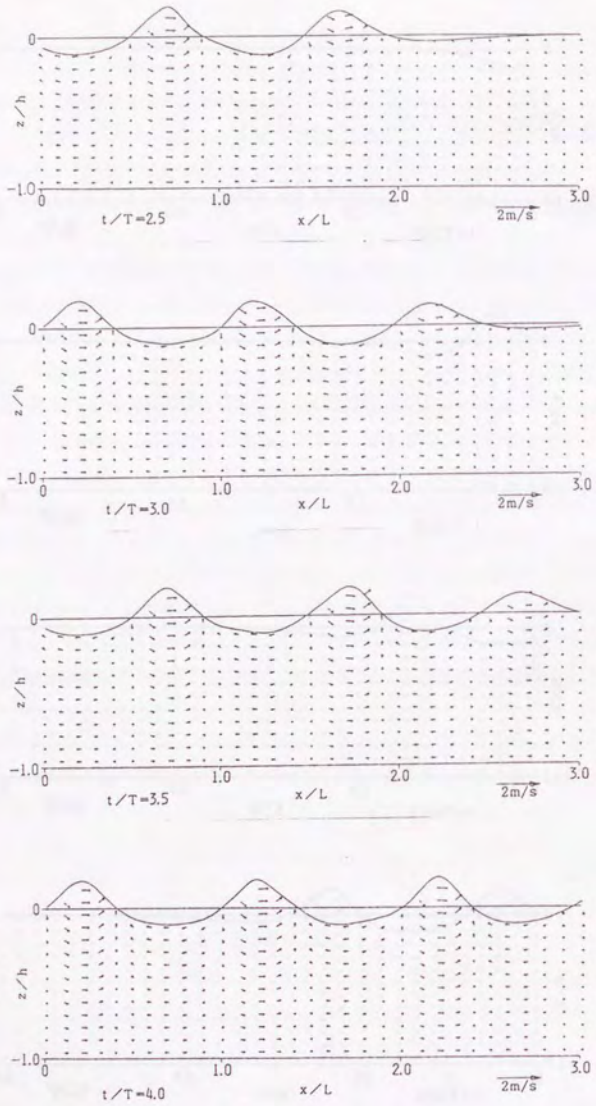

Fig.A.1 Succesive stages of progressive wave propagation from still water state –2– (Stokes wave, $H = 0.15$m, $T = 2.0$s, $h = 0.50$m)

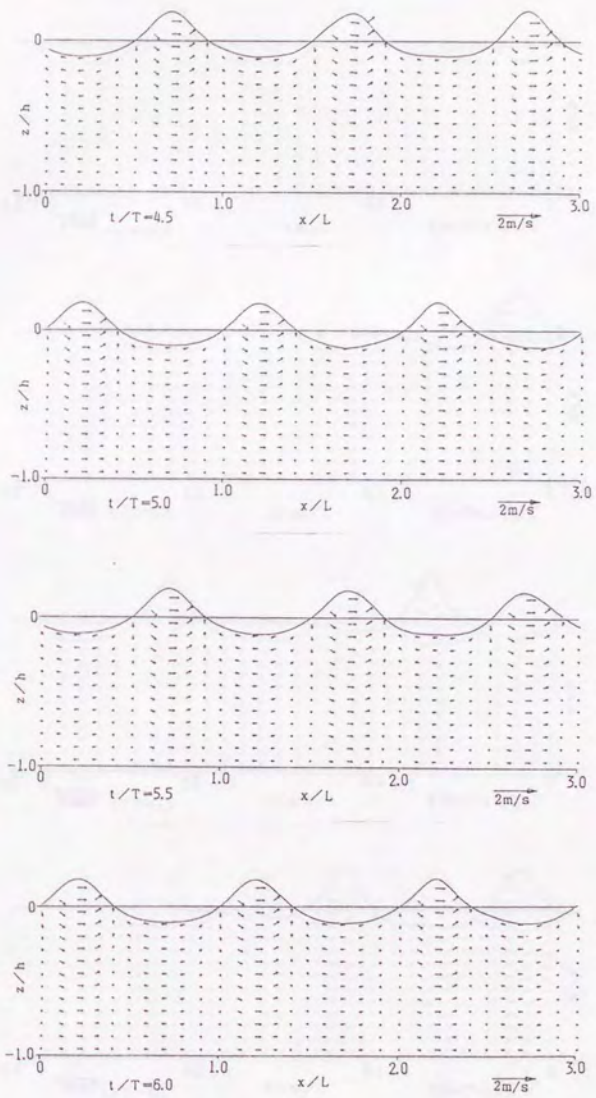

Fig.A.1 Succesive stages of progressive wave propagation from still water state –3– (Stokes wave, $H = 0.15$m, $T = 2.0$s, $h = 0.50$m)

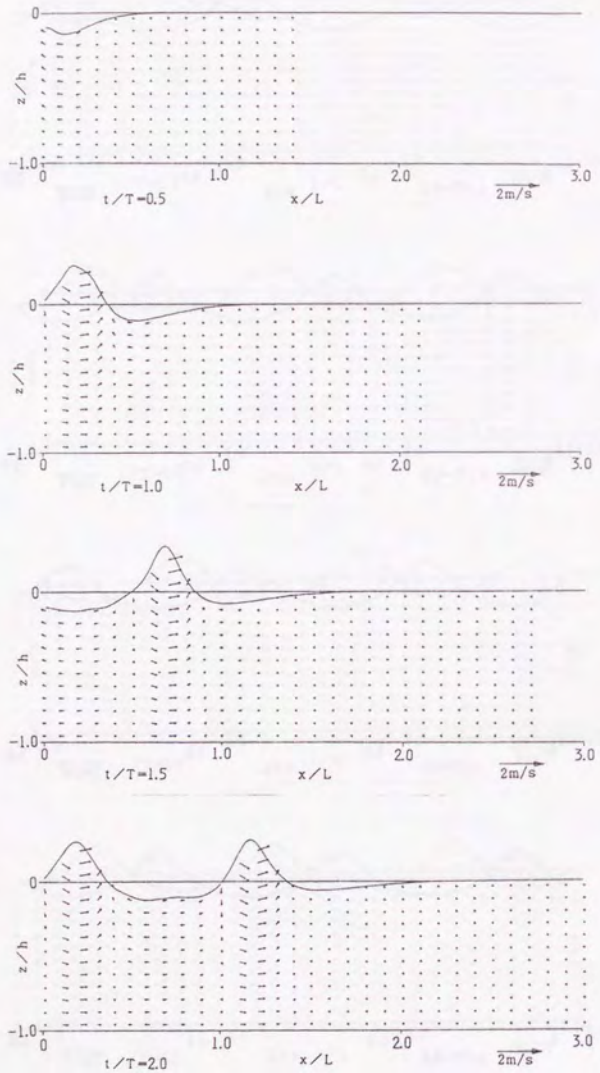

Fig.A.2 Succesive stages of progressive wave propagation from still water state –1– (cnoidal wave, $H = 0.16$m, $T = 2.0$s, $h = 0.40$m)

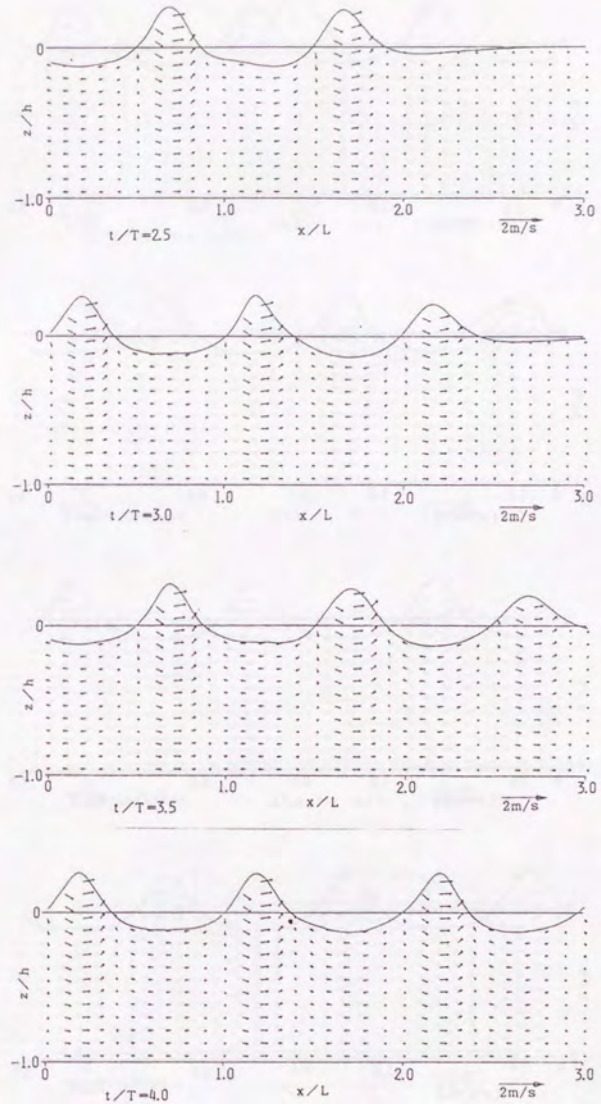

Fig.A.2 Succesive stages of progressive wave propagation from still water state –2– (cnoidal wave, $H = 0.16$m, $T = 2.0$s, $h = 0.40$m)

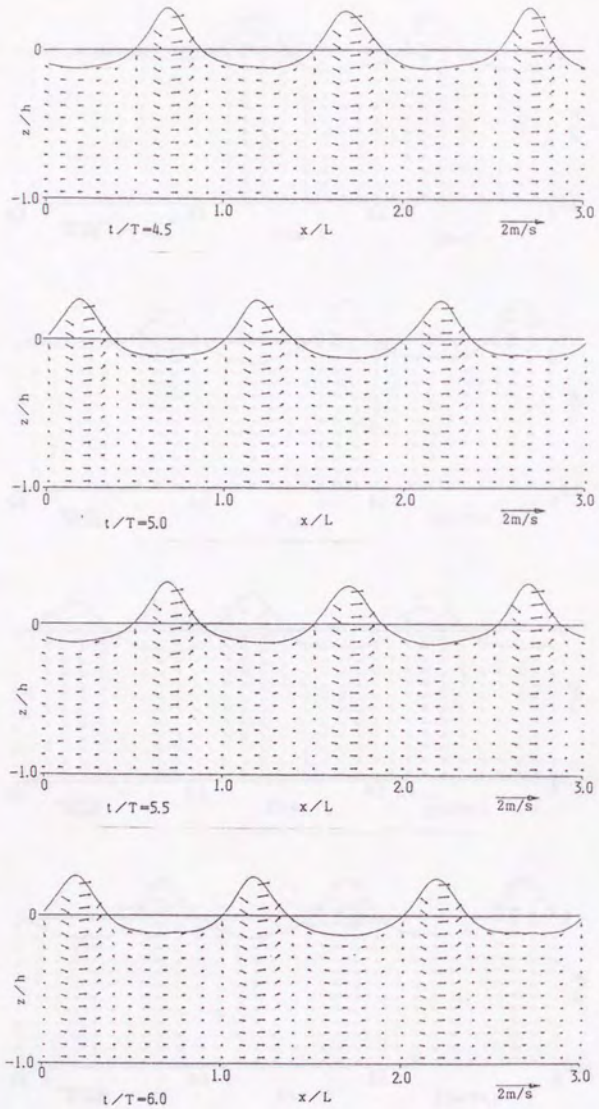

Fig.A.2 Succesive stages of progressive wave propagation from still water state –3– (cnoidal wave, $H = 0.16$m, $T = 2.0$s, $h = 0.40$m)

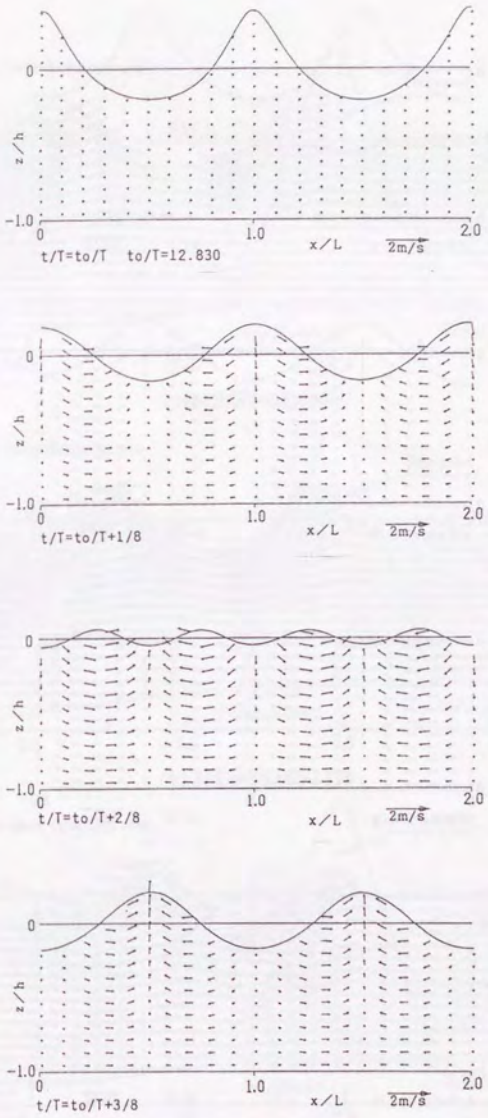

Fig.A.3 Succesive stages of standing wave –1– (Stokes wave, $H = 0.15$m, $T = 2.0$s, $h = 0.50$m)

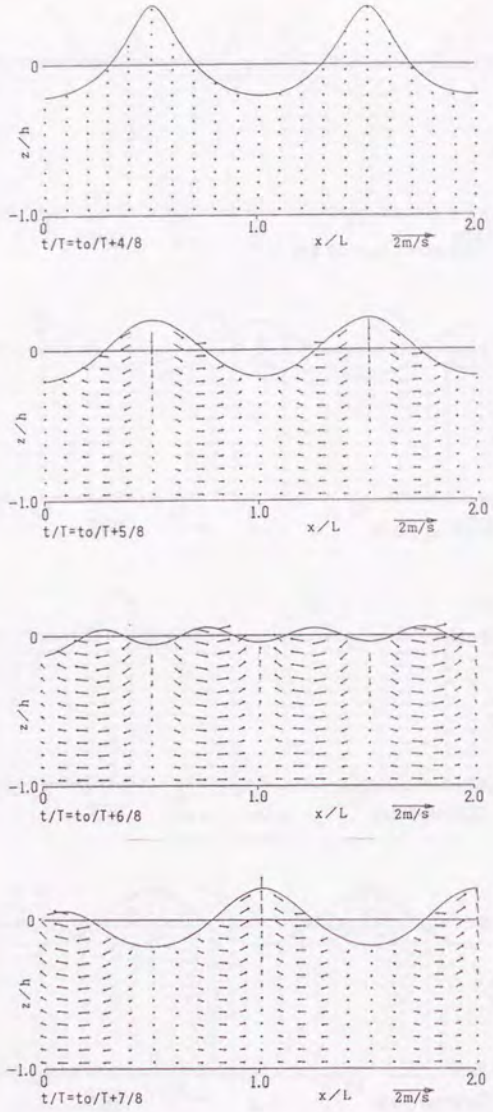

Fig.A.3 Succesive stages of standing wave -2- (Stokes wave, $H = 0.15$m, $T = 2.0$s, $h = 0.50$m)

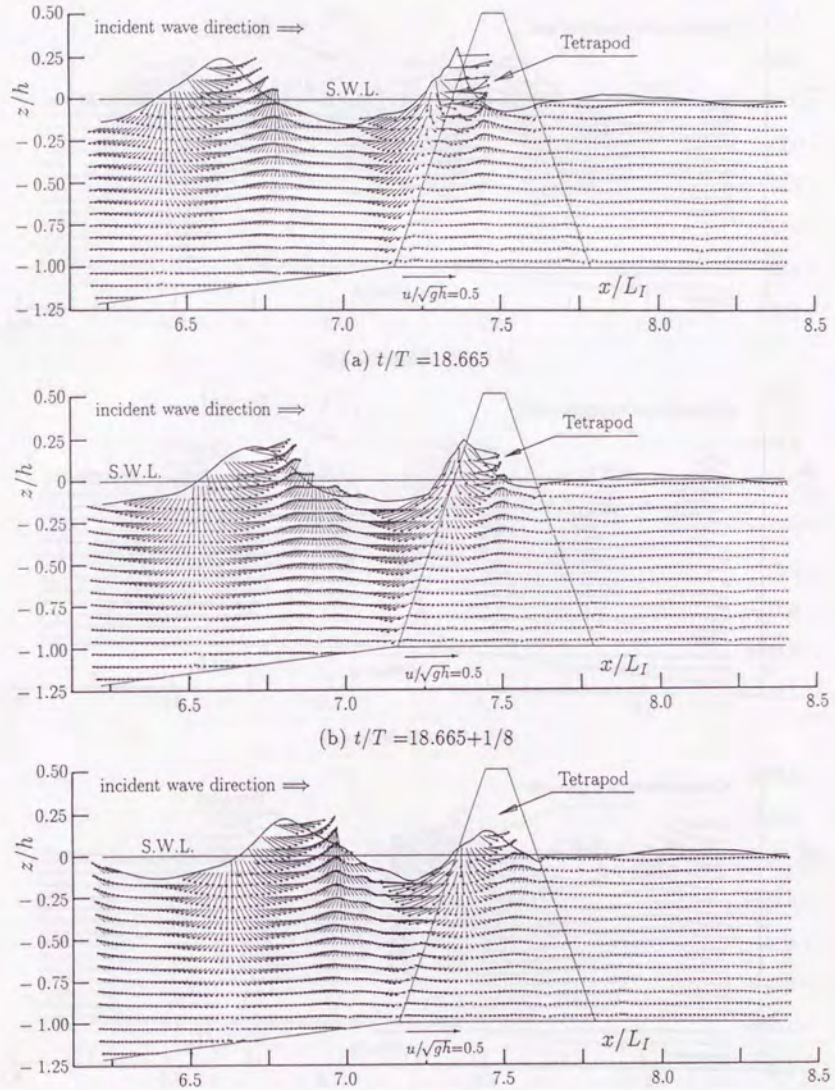

(a) t/T =18.665

(b) t/T =18.665+1/8

(c) t/T =18.665+2/8

Fig.A.4 Succesive stages of wave transformation due to rubble-mound breakwater -1- ($H = 0.15$m, $T = 1.5$s, $h = 0.417$m)

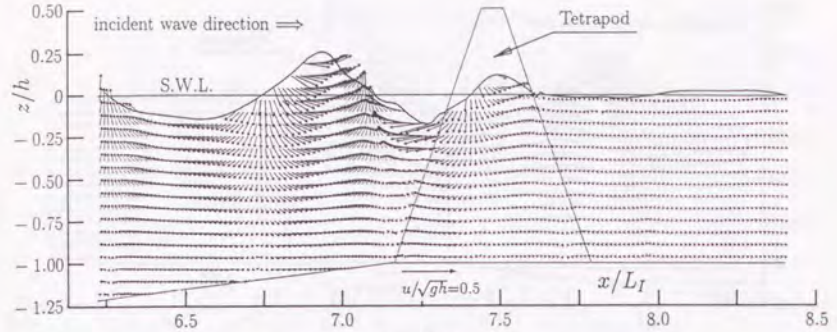

(d) t/T =18.665+3/8

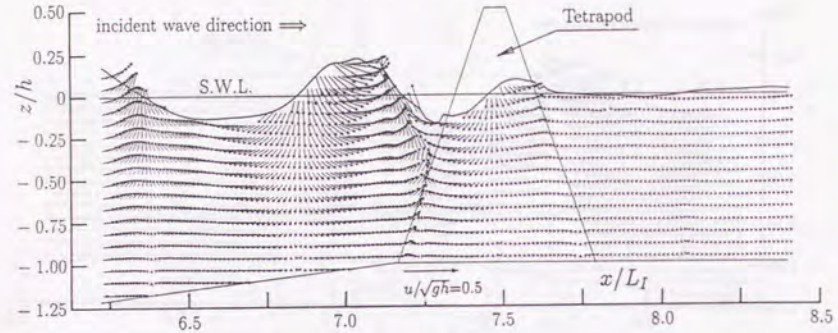

(e) t/T =18.665+4/8

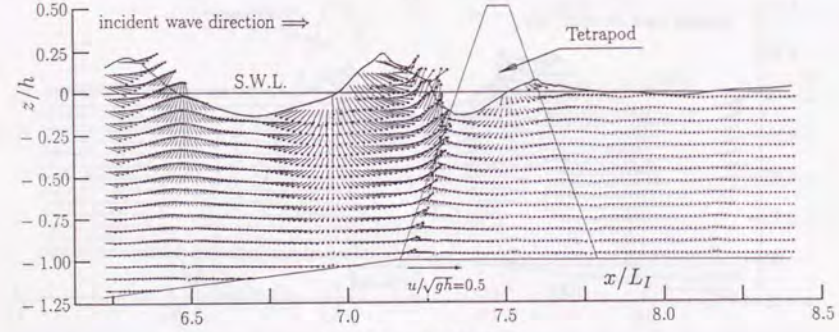

(f) t/T =18.665+5/8

Fig.A.4 Succesive stages of wave transformation due to rubble-mound breakwater -2-
(H = 0.15m, T = 1.5s, h = 0.417m)

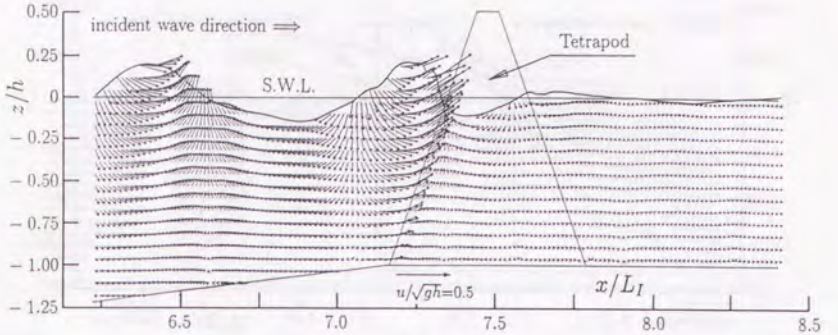

(g) t/T =18.665+6/8

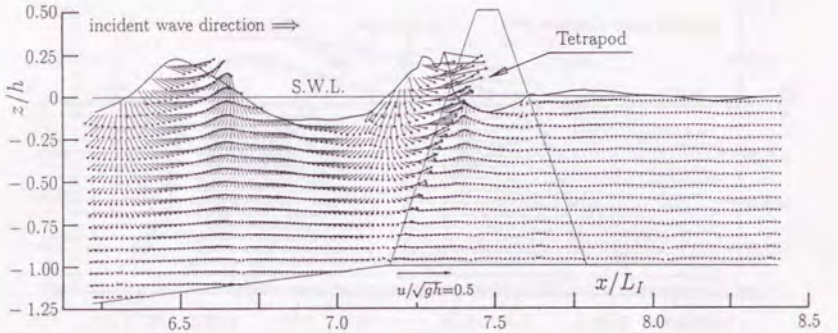

(h) t/T =18.665+7/8

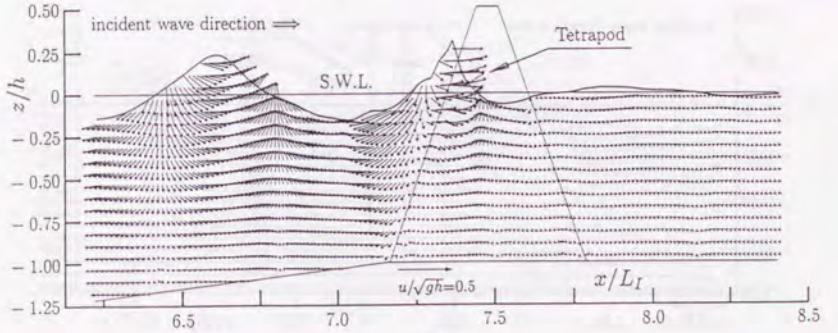

(i) t/T =18.665+8/8

Fig.A.4 Succesive stages of wave transformation due to rubble-mound breakwater -3-
(H = 0.15m, T = 1.5s, h = 0.417m)

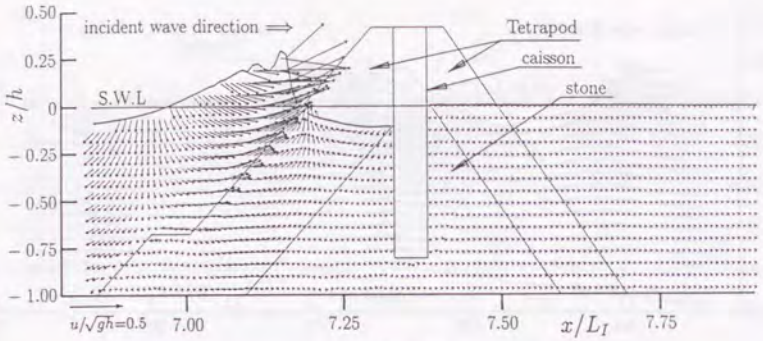

(a) t/T =18.23

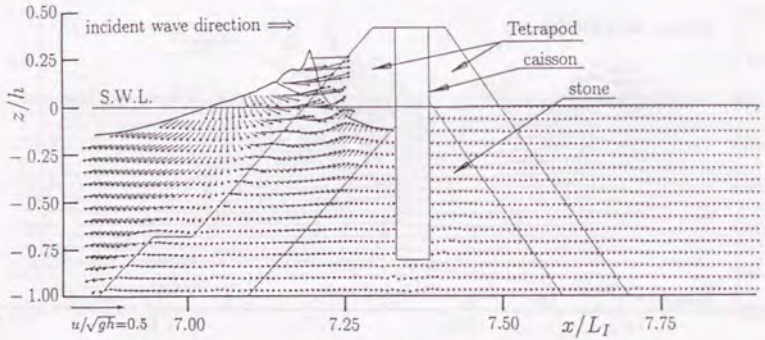

(b) t/T =18.23+1/8

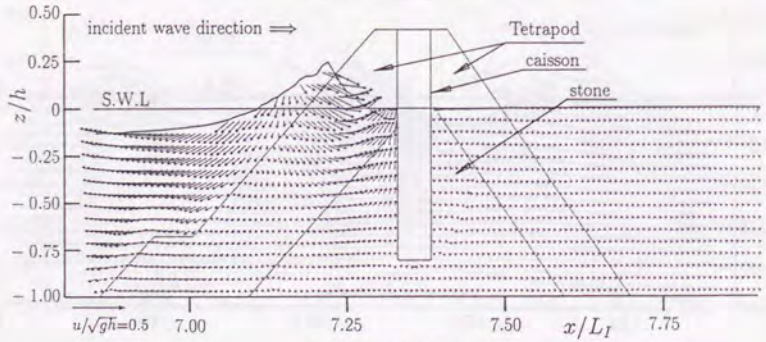

(c) t/T =18.23+2/8

Fig.A.5 Succesive stages of wave transformation due to caisson breakwater covered with armor units -1- (H = 0.15m, T = 1.5s, h = 0.417m)

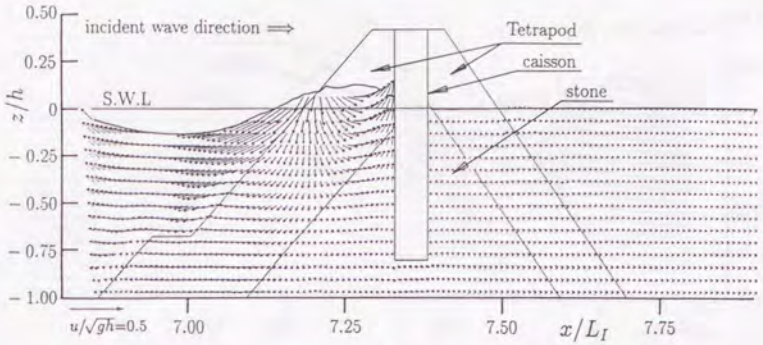

(d) t/T =18.23+3/

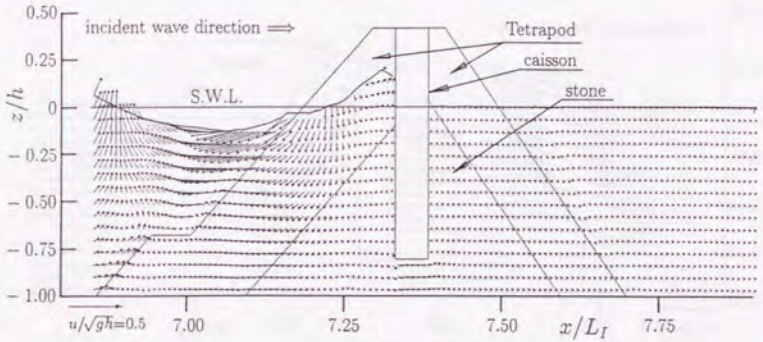

(e) t/T =18.23+4/8

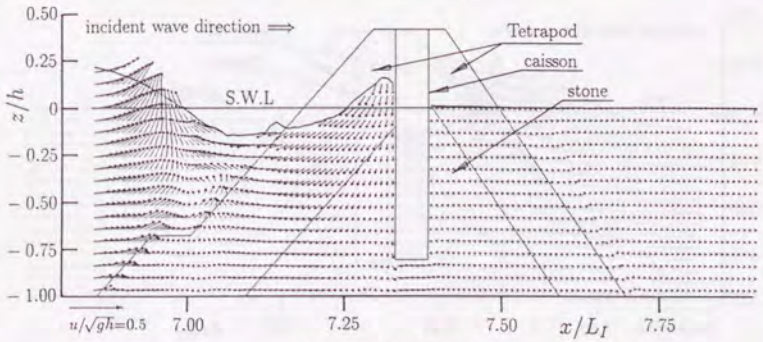

(f) t/T =18.23+5/8

Fig.A.5 Succesive stages of wave transformation due to caisson breakwater covered with armor units -2- (H = 0.15m, T = 1.5s, h = 0.417m)

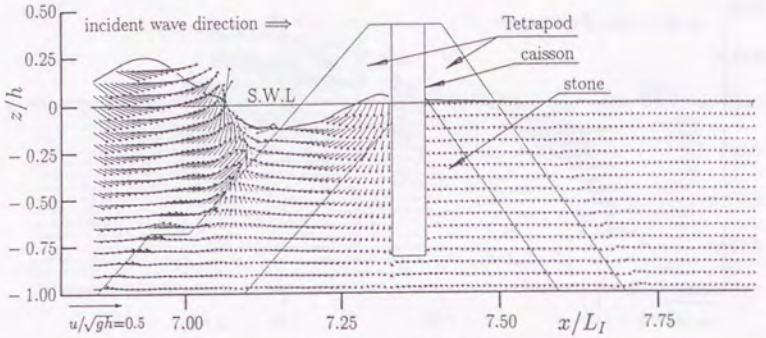

(g) t/T =18.23+6/8

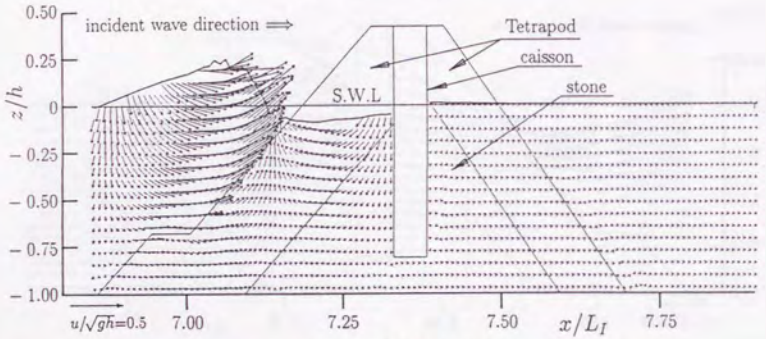

(h) t/T =18.23+7/8

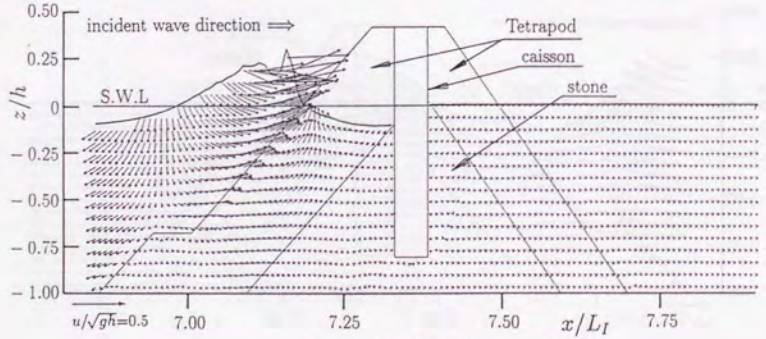

(i) t/T =18.23+8/8

Fig.A.5 Succesive stages of wave transformation due to caisson breakwater covered with armor units -3- ($H = 0.15$m, $T = 1.5$s, $h = 0.417$m)